Molecular Mode of Action and Mechanism of Resistance of the Microtubule-Stabilizing Drug Sagopilone

Dissertation
zur Erlangung des akademischen Grades des
Doktors der Naturwissenschaften (Dr. rer. nat.)

eingereicht von
Diplom-Biochemiker Sebastian Winsel
aus Berlin

am Fachbereich Biologie, Chemie, Pharmazie
der Freien Universität Berlin

April 2009

Meinen Eltern

Gutachter / Referees

1. Gutachter: Prof. Dr. Petra Knaus

2. Gutachter: Dr. Bernard Haendler

Disputation am: 02.07.2009

This work was performed between September 2005 and April 2009 at Bayer Schering Pharma, Therapeutic Research Group Oncology, Berlin.

Abstract

Microtubule-stabilizing drugs, like taxanes are frequently used in the clinic for the treatment of lung, breast, ovary, head and neck carcinomas and melanomas. However, some tumors develop resistance which impairs the success of chemotherapy. Sagopilone, a novel microtubule-stabilizing drug from the class of epothilones, was selected to overcome the limitations associated with conventional tubulin-binding agents. The aim of this study was to investigate the mode of action of sagopilone and to elucidate molecular mechanisms of resistance.

Sagopilone strongly inhibited cellular proliferation of various tumor cell lines *in vitro*. In contrast to paclitaxel, sagopilone inhibited the growth of multi drug transporter (MDR1) overexpressing cell lines, a common mechanism of resistance to paclitaxel. Depending on the drug concentration, Sagopilone mainly induced two different phenotypes. Low concentration treatment (2.5 nM) resulted in aberrant cell division, aneuploidy and cell cycle arrest in G1 whereas high concentration treatment (40 nM) led to mitotic arrest. These effects were similar to those observed with paclitaxel. However, unlike paclitaxel, sagopilone disturbed division of tumors cells already at the low concentration of 0.5 nM.

The gene expression profiles of low and high concentration phenotypes were substantially different from each other. Low concentration sagopilone led to p53 (TP53) transactivation in A549 lung cancer cells leading to cell cycle arrest. Incubation with high concentration of sagopilone was associated with upregulation of several genes involved in spindle assembly checkpoint and mitosis, indicating mitotic arrest. For both phenotypes differences in the ability to undergo apoptosis were observed. Low concentration treated A549 cells showed markedly diminished apoptosis induction capability when compared to the high concentration sagopilone-treated cells.

The knock-down of p21 (CDKN1A) and p53 in A549 cells led to abrogation of G1 arrest induced by low concentration sagopilone and to further progression of the cell cycle. This markedly increased the rate of apoptosis after low concentration sagopilone treatment. The relevance of the p53 transactivation was further

demonstrated in *in vivo* A549 xenograft tumors which only moderately responded to sagopilone. These tumors showed the low concentration gene expression pattern similar to A549 cells *in vitro* as distinguished through upregulation of p53 target genes like p21.

The gene expression of the cell cycle inhibitor p21 was induced more strongly in the four p53 wild type cell lines than the four p53 mutated cell lines. However, the p53 mutational status of the cell lines did not correlate with the sensitivity to sagopilone-induced apoptosis, indicating that additional mechanisms of resistance may exist.

Herein it was demonstrated that paclitaxel and sagopilone have a similar mechanism of action, but the efficacy of sagopilone to inhibit tumor cell proliferation was higher. Sagopilone induced aberrant cell division and G1 arrest at low concentrations and mitotic arrest at high concentrations. The upregulation of p53 target genes and the induction of G1 arrest in response to low concentrations of sagopilone, as shown in A549 cells, may represent one cellular mechanism of resistance to the drug. The presented data could provide the basis for more extensive research as to whether the p53 mutational status can be used as a stratification marker for sagopilone response in the clinic and whether targeting p53 could increase the response to sagopilone.

Zusammenfassung

Mikrotubuli-stabilisierende Substanzen, wie beispielsweise Taxane, werden in der Klink häufig zur Behandlung von Lungen-, Brust-, Ovarial-, Kopf-Hals-Karzinomen oder Melanomen eingesetzt. Unter der Behandlung mit Taxanen entwickeln einige Tumore jedoch Resistenzen gegen diese Medikamente, was den Erfolg der Chemotherapie beeinträchtigt. Sagopilone, eine neue Mikrotubuli-stabilisierende Verbindung aus der Klasse der Epothilone, wurde entwickelt, um die Nachteile herkömmlicher Tubulin-bindender Substanzen zu überwinden. In dieser Doktorarbeit sollte die Wirkungsweise von Sagopilone auf Tumorzellen aufgeklärt werden und mögliche Resistenzmechanismen der Tumorzellen gegen Sagopilone untersucht werden.

In vitro wird die Proliferation von verschiedenen Tumorzellen durch Sagopilone stark inhibiert. Im Gegensatz zu Paclitaxel hemmt Sagopilone auch die Proliferation von MDR1 (multi drug transporter) überexprimierenden Zellen, einem bekannten Resistenzmechanismus der Tumorzellen gegen Paclitaxel. Sagopilone induzierte zwei unterschiedliche Phänotypen. Geringe Konzentrationen lösten eine anomale Zellteilung aus, die zu Aneuploidie und Zellzyklusarrest in der G1 Phase führte. Hohe Konzentrationen führten zu einem Arrest des Zellzyklus in der Mitose. Diese Effekte sind denen Paclitaxels sehr ähnlich. Im Gegensatz zu Paclitaxel war bei Sagopilone jedoch schon bei sehr geringen Konzentrationen (0.5 nM) eine antiproliferative Wirkung festzustellen.

Geringe und hohe Konzentrationen Sagopilone zeigten zudem ein unterschiedliches Genexpressionsprofil. Geringe Konzentrationen Sagopilone (2.5 nM) führten in den Lungenkarzinom Zellen A549 zu einer transkriptionellen Aktivierung von p53 (TP53) kontrollierten Genen. Hohe Konzentrationen Sagopilone (40 nM) führten zu einer Hochregulation von Genen, die im spindle assembly checkpoint und der Mitose eine Rolle spielen. Diese Phänotypen zeigten eine unterschiedlich starke Apoptose-Auslösung in A549 Zellen nach Sagopilone Behandlung. A549 Zellen, die mit einer geringen Konzentration Sagopilone behandelt wurde, wiesen signifikant geringere Apoptose-Raten auf, verglichen mit A549 Zellen, die mit hohen Konzentrationen Sagopilone behandelt wurden.

Die Herunterregulation von p21 (CDKN1A) und p53 mittels shRNAs in A549 Zellen führte zur Aufhebung des G1 Zellzyklusarrests nach Behandlung mit geringen Konzentrationen Sagopilone. Dieser Effekt hatte signifikant höheren Apoptose-Raten von A549 Zellen nach der Behandlung mit geringen Konzentrationen Sagopilone zur Folge. Die Bedeutung der transkriptionellen p53 Aktivierung konnte zusätzlich an einem A549 Xenograft Mausmodell gezeigt werden, welches nur einen geringfügigen Rückgang im Tumorwachstum nach Sagopilone Gabe zeigte. Das Gen-expressionsprofil dieser Tumore entsprach dem der A549 Zellen, die *in vitro* mit geringen Konzentrationen Sagopilone behandelt wurden und eine Apoptose-Resistenz aufwiesen.

Eine unterschiedlich starke Induktion der Genexpression von p21 konnte in 4 verschieden Zelllinen mit normalem p53 im Gegensatz zu 4 Zelllinen mit mutiertem p53 festgestellt werden. Es konnte allerdings kein Zusammenhang zwischen der p21 Induktion und der Apoptose-Auslösung von p53 mutierten und normalen Zelllinen gefunden werden.

In dieser Arbeit konnte gezeigt werden, dass Sagopilone und Paclitaxel einen ähnlichen Wirkmechanismus haben, die Effizienz von Sagopilone jedoch höher ist. Sagopilone induziert eine anomale Zellteilung und G1 Arrest bei geringen Konzentrationen und mitotischen Arrest bei hohen Konzentrationen. Die transkriptionelle Aktivierung von p53 und der G1 Arrest nach geringen Sagopilone Konzentrationen stellen einen möglichen Resistenzmechanismus dar. Die gezeigten Daten bilden eine Grundlage für weitergehende Forschungen, ob der p53 Status von Tumoren als Stratifikationsmarker für die Wirkung von Sagopilone benutzt werden kann.

Abstract ..... **I**

Zusammenfassung ..... **III**

1 Introduction **1**

1.1 Cancer – some remarks 1

1.2 Structure and function of microtubule 2

1.3 Spindle assembly checkpoint 3

1.4 Microtubule-stabilizing drugs in cancer therapy 4

1.4.1 Taxanes 4

1.4.2 Epothilones 5

1.4.3 Mode of action of microtubule-stabilizing compounds 6

1.4.4 Mechanisms of drug resistance to microtubule-stabilizing compounds 7

1.5 Role of p53 9

1.5.1 p53 choice between life and death 9

1.5.2 Role of p53 mutations in response to microtubule-stabilizing drugs 11

2 Objective **12**

3 Materials and methods **13**

3.1 Cell lines and culture 13

3.2 Compounds 14

3.3 Proliferation assay 14

3.4 Cell cycle analysis 15

3.5 Immunofluorescence staining and microscopy 15

3.6 Live cell microscopy 16

3.7 Protein extraction, SDS-PAGE and Western blot 16

3.8 Apoptosis assay 17

3.9 RNA preparation and cDNA synthesis for real time PCR analysis 17

3.10 Quantitative real-time PCR 18

3.11 Drug treatments for gene expression analysis 18

3.12 RNA extraction for gene expression analysis 19

3.13 *In vitro* RNA Transcription and Hybridization to Affymetrix GeneChips.....20
3.14 Unsupervised analysis.....21
3.15 Supervised analysis.....21
3.16 *In vivo* tumor growth.....21
3.17 Cloning of shRNAs.....22
3.18 Production of lentivirus in 293FT cells 23
3.19 Lentiviral transduction of mammalian cells 23
3.20 p53 mutations in cell lines 24

4 Results 25
4.1 Proliferation assays 25
4.1.1 *In vitro* profile of sagopilone and paclitaxel in chemo-sensitive cancer cell lines 25
4.1.2 *In vitro* profile of sagopilone and paclitaxel in chemo-resistant cancer cell lines 26
4.1.3 *In vitro* profile of sagopilone, paclitaxel and ixabepilone in breast cancer cell lines 27
4.2 Cell cycle analysis of sagopilone- and paclitaxel-treated cells.....28
4.2.1 Cell cycle distribution of sagopilone-treated cells.....28
4.2.2 Cell cycle distribution of paclitaxel-treated cells.....31
4.2.3 Comparison of cell cycle effects of sagopilone- and paclitaxel -treated A549 cells 33
4.2.4 Comparison of cell cycle effects of different cell lines treated with sagopilone 34
4.3 Microscopic analysis of cells treated with sagopilone.....35
4.3.1 Live cell imaging of A549 cells treated with sagopilone 35
4.3.2 Aberrant cell division of A549 cells induced by low concentration of sagopilone 37
4.3.3 Immunofluorescence staining of MDA MB 231 cells after sagopilone treatment 39
4.4 Induction of apoptosis in A549 cells after treatment with sagopilone.....40

4.5 Genome-wide gene expression study of A549 cells treated with sagopilone and paclitaxel 42
4.5.1 Objective of the gene expression study 42
4.5.2 Unsupervised Analysis 43
4.5.3 Volcano plot 44
4.5.4 Supervised analysis 45
4.5.5 Two-Dimensional hierarchical clustering 46
4.5.6 Pathway analysis of genes regulated by paclitaxel and sagopilone 49
4.5.7 DNA damage genes regulated in response to sagopilone and paclitaxel 53
4.6 Validation of Affymetrix gene expression study results 54
4.6.1 Validation of genes differentially expressed at low concentration sagopilone and paclitaxel 54
4.6.2 Validation of genes differentially expressed at high concentration sagopilone and paclitaxel 56
4.7 *In vivo* tumor xenograft model A549 57
4.7.1 Response of A549 tumor xenograft to sagopilone 57
4.7.2 Gene expression analysis of A549 *in vivo* xenograft model 58
4.8 Contribution of the p53 status to the response to sagopilone 60
4.8.1 Changes in p21 gene expression in response to sagopilone treatment of p53 wild type and p53 mutated cell lines 60
4.8.2 Apoptosis induction of p53 wild type and p53 mutated cell lines 61
4.9 Knock-down of p53 in A549 cells 63
4.9.1 Stable short hairpin RNA knock-down of p53 in A549 cells 63
4.9.2 Cell cycle analysis of p53 shRNA knock-down cell lines 64
4.9.3 Apoptosis induction of A549 shp53 knock-down cells 66
4.10 Knock-down of p21 in A549 cells 68
4.10.1 Stable short hairpin RNA knock-down of p21 in A549 cells 68
4.10.2 Cell cycle analysis of A549 shp21 knock-down cells 69
4.10.3 Apoptosis induction of A549 shp21 knock-down cells 71
4.11 Induction of DNA damage in A549 cells after treatment with sagopilone? 72

5 Discussion **75**
5.1 Sagopilone inhibits tumor cell proliferation *in vitro* 75
5.2 Sagopilone treatment of cells results in two concentration-dependent phenotypes 76
5.3 Sagopilone-induced phenotypes differ in their gene expression profiles 78
5.4 How does p53 get activated in A549 cells after treatment with low concentration sagopilone? 79
5.5 Transactivation of p53 inhibits sagopilone-induced apoptosis in A549 cells 80
5.6 p53 transactivation in A549 xenograft tumors is associated with resistance to sagopilone 82
5.7 Knock-down of p21 in A549 cells increases apoptosis after low concentration sagopilone treatment 83
5.8 Knock-down of p53 in A549 cells increases apoptosis after low concentration sagopilone treatment 84
5.9 High concentration sagopilone upregulates DNA damage response genes and induces apoptosis 85

6 References **87**

7 List of Publications **95**

Abbreviations **96**

1 Introduction

1.1 Cancer – some remarks

13 % of all deaths are caused by cancer (WHO 2006). Cancer accounts worldwide to about 7.6 million deaths in 2007 (American Cancer Society, 2007). In Germany, 436.000 new cases of cancer are diagnosed annually and nearly 208.000 patients die from this disease each year (German Cancer Congress, 2008).

Cancer is generally characterized by uncontrolled growth of transformed cells which are capable of invasion and destruction of the adjacent tissue. Furthermore, cancer can produce metastases by spreading into other parts of the body via the lymphatic system or blood vessels.

Cancer can be caused by exogenous (e.g. chemicals, tobacco smoke, asbestos, radiation and viruses) and endogenous (e.g. genetic predisposition, immunodeficiency and chronic inflammation) factors. These factors induce changes in the genome of the cells, which are thought to be one of the main underlying reasons for cancer. More recently epigenetic changes have also been related to tumor progression.

Quite often cancer is caused by modifications leading to activation of oncogenes, thereby conferring new properties to the cells, such as hyperactive growth, enhanced cell division and inhibition of programmed cell death. Additionally, tumor suppressor genes may be inactivated, which leads to disturbance of normal cell functions such as control of cell division, cell adhesion and orientation. All these properties of cancer cells are due to defects in the regulatory circuits that control proliferation and homeostasis (Hanahan and Weinberg, 2000).

Cancer is a heterogeneous disease that makes it difficult to treat. Therefore it is necessary to understand the pathways that are disturbed in cancer cells. Targeting of multiple and specific pathways of cancer cells might lead to tailored therapies with improved outcome. For the treatment of cancer several methods have been established, including surgery, radiotherapy, hormone treatment, immunotherapy and chemotherapy, often used in combination. Chemotherapy is one of the most powerful weapons against solid tumors, especially those with metastases, and hematological malignancies. The most frequently used agents are those which interfere with spindle

microtubules that are essential for cell division. Thus, they take advantage of the higher proliferation rate of tumor cells compared to normal cells.

1.2 Structure and function of microtubule

Microtubules are important components of the cellular structure and form together with micro- and intermediate filaments the cytoskeleton of eukaryotic cells. One of the main functions of microtubules is their role in mitosis. In addition they are also involved in other cellular functions such as providing routes for the transport of molecules, organelles and vesicles, controlled by the molecular motor proteins kinesins and dyneins.

The α-,ß-tubulin heterodimer is the basic structural unit of microtubules. Both tubulins of this heterodimer bind to guanosine triphosphate (GTP). Under certain conditions ß-tubulin hydrolyzes and exchanges the GTP. The microtubules are assembled by a nucleation-elongation mechanism. Heterodimers of α-,ß-tubulin polymerize to first form a microtubule nucleus composed of short protofilaments. Thereafter, fast elongation takes place through addition of further α-,ß-tubulin dimers to both ends. 13 of these protofilaments arranged as a “hollow tube” form a microtubule. The alternating alignment of α- and ß-tubulin in the microtubules leads to a bipolar structure with a more dynamic plus end (ß-tubulin) and a less dynamic minus end (α-tubulin). The addition and loss of tubulin subunits occurs exclusively at microtubule ends and is more pronounced at the plus end. The fast and continuous exchange of tubulin subunits between the soluble phase and the filaments are the basis for normal cellular function of microtubules. The sustainable shortening and lengthening of microtubules is characterized by two principal mechanisms: dynamic instability and treadmilling. Dynamic instability is based on stochastic changes of length of the microtubules by addition and dissociation of tubulin subunits. The treadmilling mechanism refers to the growth at the plus end and concomitantly shortening at the minus end without changes of the microtubule length. In addition, some of the microtubules often dramatically shorten their length (catastrophe), a process necessary for vesicle transport.

A growing microtubule comprises GTP-containing subunits at its end (GTP cap). Hydrolyzation of the cap results in changes of linear conformation and weakens bonds in the protofilament, thereby triggering the progressive disruption of the microtubule. In addition, the dynamic instability of microtubules can also be affected by various proteins. For example catastrophin and stathmin destabilize microtubules by sequestration of free subunits. On the other hand microtubule-associated proteins (MAPs) stabilize the filaments (Halpain and Dehmelt, 2006; Bhat and Setaluri, 2007). α- und ß-tubulin molecules themselves exist in multiple isoforms in vertebrate cells. Subunits and polymers of different isotypes associate nearly equally with each other.

1.3 Spindle assembly checkpoint

One of the most important functions of microtubules is the proper segregation of sister chromatids during mitosis. The transition from metaphase to anaphase in mitosis only proceeds if the spindle microtubules are properly attached to the kinetochores of the chromosomes. This process is controlled by the spindle assembly checkpoint (SAC) by means of kinetochore associated proteins, e.g. MAD1, MAD2, MAD3, BUBR1 and BUB1, which are conserved in all eukaryotes. The proteins are active in prometaphase of mitosis. They occupy unattached kinetochores and repress the activation of a protein named cell division cycle 20 homolog (CDC20), a co-factor of the anaphase promoting complex/cyclosome (APC/C). The SAC negatively regulates (via CDC20) the ability of the APC/C to polyubiquitylate cyclin B1 and securin, thereby preventing their degradation by the 26S proteasome.

Securin is an inhibitor of the protease separase, which finally separates the sister chromatids by cleavage of the chromatid connecting cohesin. The proteolysis of cyclin B1 inactivates the master mitotic kinase (CDK1) and promotes exit from mitosis. The treatment with spindle poisons or microtubule inhibitors early during this process immediately stops proteolysis and anaphase onset. Through the control of CDC20, the SAC prolongs prometaphase of mitosis until all kinetochores of chromosomes are attached.

Once the microtubules are correctly attached, the SAC is switched off and the cell cycle proceeds to the metaphase (Fukasawa, 2007). In addition, tension between bi-

orientated sister kinetochores through attachment of spindle microtubules is important for SAC inactivation. The SAC ensures the equal distribution of the genomic material to both daughter cells (Pinsky and Biggins, 2005).

1.4 Microtubule-stabilizing drugs in cancer therapy

1.4.1 Taxanes

Paclitaxel is a naturally occurring diterpene alkaloid isolated from the bark of the Pacific yew *Taxus brevifolia* by Wall and Wani in 1967 (Wani et al., 1971). Paclitaxel was the first microtubule-stabilizing compound used in cancer therapy and has become part of the standard of care in chemotherapeutic treatment of breast, ovarian and non-small cell lung cancer. It is often used in combination with Platinum-based chemotherapy (e.g. carboplatin, cisplatin). The chemical structure of paclitaxel is shown in Figure 1.

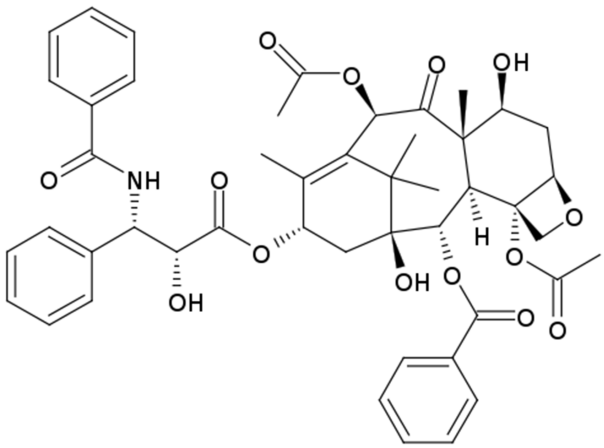

Paclitaxel

Figure 1. Chemical structure of Paclitaxel.

Docetaxel is a semi-synthetic analogue of paclitaxel which is extracted from the European yew tree and then chemically modified. It differs from paclitaxel at only two positions in its chemical structure. This leads to higher water solubility than paclitaxel. Docetaxel has also been found to have higher cellular uptake and to be

longer retained in tumor cells than paclitaxel. Docetaxel is used in the same indications as paclitaxel.

Despite some progress in the cancer chemotherapy with taxanes, this treatment is hampered by frequent side effects (e.g. allergic reactions, neuropathy, hematologic disorders and cardiovascular problems) and by the development of taxane-resistant tumors. This has raised considerable interest in other compounds with a similar mechanism of action but with more favorable pharmacochemical, pharmacokinetic and pharmacodynamic properties. Epothilones represent a new class of microtubule-stabilizing agents with promising properties. In the last few years, great efforts were made to develop semi-synthetic and synthetic epothilone analogs with improved pharmacological profiles compared to their natural counterparts (Trivedi et al., 2008).

1.4.2 Epothilones

Epothilone A and B were first purified from a culture extract of the cellulose-degrading myxobacterium *Sorangium cellulosum* by Höfle and Reichenbach in 1987 (Reichenbach and Höfle, 2008). Their structures were identified as 16-membered macrolides. Initial screening with the compounds revealed narrow antifungal activity. The scientific interest in this group of compounds was again stimulated by high-throughput screening which demonstrated a high antiproliferative activity of epothilone A and B against a range of cancer cell lines, including breast and intestinal cancer (Bollag et al., 1995). Epothilones have higher water solubility than taxanes so that solubilizing agents which can cause adverse side effects in humans are not needed. Studies in cancer cell lines indicated superior efficacy of epothilones compared to the taxanes. Moreover, epothilones showed activity in tumors which had become resistant to paclitaxel.

Epothilone B shows potent *in vitro* and *in vivo* anticancer activity. Hence, the natural epothilone B and its various analogues are currently undergoing clinical trials for treatment of various cancers. Patupilone (epothilone B) is currently being investigated in phase III clinical trials in ovarian cancer by Novartis. Ixabepilone (epothilone B analog), is the first epothilone approved in 2007 by the FDA (Food and Drug

Administration, USA) for the treatment of locally advanced or metastatic breast cancer.

Sagopilone is a synthetic epothilone analog developed by Bayer Schering Pharma, and is currently undergoing phase II clinical trials for the treatment of breast, lung, prostate and ovarian cancer. Sagopilone has been developed in order to minimize side effects and to improve pharmacokinetic and antitumor properties. From about 350 active epothilone analogs, sagopilone was chosen for development because of its promising preclinical activity (Klar et al., 2006). The chemical structure of sagopilone is depicted in Figure 2.

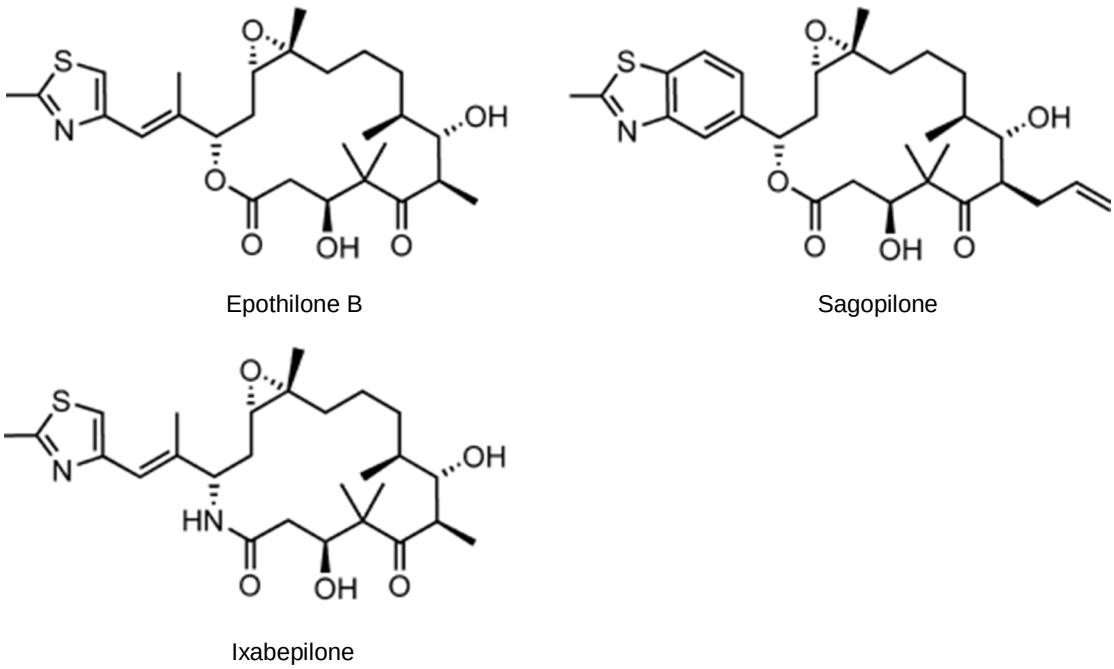

Figure 2. Chemical structures of Epothilone B, Sagopilone and Ixabepilone.

1.4.3 Mode of action of microtubule-stabilizing compounds

Taxanes and epothilones both bind to ß-tubulin, but each compound exploits the tubulin-binding pocket in a unique manner (Nettles et al., 2004). The binding to ß-tubulin results in enhanced tubulin polymerization and strong disturbance of microtubule dynamics. This microtubule stabilization causes mitotic arrest at the metaphase, followed by transient multinucleation and activation of the mitochondrial apoptotic pathway. Paclitaxel triggers apoptosis through caspase 9 activation at the

apoptosome (Janssen et al. 2007). The apoptosis of paclitaxel-treated cells is connected with the release of cytochrome c from the mitochondria, resulting in activation of caspase 9 (Kroemer et al., 2007). Further results suggest that sagopilone and paclitaxel act through a mechanism involving the Bcl-2 family of proteins. In HCT116 colon carcinoma cells knock-down of proapoptotic members of Bcl-2 family including Bax, Bak and Puma decreases sagopilone-induced rate of apoptosis, whereas the knock-down of antiapoptotic members such as Bcl-2, Bcl-X_l sensitizes cells to sagopilone-induced cell death (Hoffmann et al., 2008).

1.4.4 Mechanisms of drug resistance to microtubule-stabilizing compounds

Intrinsic and acquired drug resistance is a common feature in cancer chemotherapy. Resistance towards microtubule-stabilizing drugs includes mutations of α- and ß-tubulin, modifications in ß-tubulin isotype composition, P-glycoprotein (P-gp) over-expression and changes of microtubule dynamics by altered expression of microtubule-associated proteins (MAPs). Additionally, disorders in the spindle assembly checkpoint (SAC) and dysfunctional regulation of apoptosis contribute to chemoresistance against microtubule-stabilizing compounds (McGrogan et al., 2008).

Most tubulin mutations occur in the ßI-tubulin isotype (Berrieman et al., 2004). Mutations of ßI-tubulin weaken the binding of paclitaxel and can cause changes in microtubule dynamics and stability, leading to resistance. A connection between p53 and ßI-tubulin mutations has been proposed for the human ovarian cancer cell line 1A9 which is resistant to paclitaxel. Lack of p53 could prevent expression of the mismatch repair gene hMSH2 thus leading to a higher frequency of ßI-tubulin mutations (Warnick et al., 2001). Furthermore, A549 lung cancer cells that are highly resistant to epothilone A and B harbor ßI-tubulin mutations (He et al., 2001; Yang et al., 2005). While the role of ßI-tubulin mutations *in vitro* is well documented, their clinical implication is still controversial.

In vitro studies with purified tubulins have shown that microtubules entirely composed of ßIII-tubulin exhibit increased dynamic instability compared to other ß-tubulin isotypes (Panda et al., 1994). Upregulation of ßIII-tubulin in ovarian tumors

and in advanced breast cancers has been associated with paclitaxel resistance (Kavallaris et al., 1997; Kavallaris et al., 1999; Mozzetti et al., 2005). RNAi-mediated silencing of ßIII-tubulin in non-small cell lung cancer cell lines (NCI-H460, Calu-6) increases the sensitivity to paclitaxel (Gan et al., 2007).

Microtubule-associated proteins (MAPs) control microtubule dynamics by interacting with microtubules. MAPs play an important part in sensitivity to microtubule-interacting drugs and in the chemotherapy with paclitaxel (Orr et al., 2003). The tau protein supports tubulin assembly and microtubule stabilization (Wagner et al., 2005). Low expression of tau is associated with increased sensitivity to paclitaxel (Makrides et al., 2004). MAP4 stabilizes microtubules by increasing the rescue frequency and is involved in regulation of microtubule dynamics in mitosis (Hyman and Karsenti, 1996). Down-regulation or inactivation of MAP4 increases microtubule dynamics, which reduces the microtubule-stabilizing potency of paclitaxel (Orr et al., 2003).

Multidrug resistance (MDR) is defined as the ability of cells to develop resistance to a broad spectrum of structurally and functionally unrelated drugs. The widespread occurrence of MDR in tumor cells represents a major hurdle for successful cancer chemotherapy. The mechanism underlying MDR relates to the expression of the ATP-dependent transporter family, known as the ATP-binding cassette (ABC) transporter. Tumor cells resistant to multiple drugs express increased levels of P-glycoprotein (P-gp) encoded by the MDR-1 gene (Gottesman, 2002). The P-gp transporter binds to and pumps out drugs from cells. The relevance of MDR1/P-gp gene expression in the chemotherapy of breast cancer, non-small cell lung cancer and ovarian cancer treated with paclitaxel was documented in several studies (Tsukamoto et al., 1997, Yeh et al., 2003, Penson et al., 2004).

Differences in the expression of the spindle checkpoint proteins MAD1, MAD2, BUBR1, BUB1 and the chromosomal passenger protein survivin, aurora kinases A and B have been related to aneuploidy (Kops et al., 2005), chromosomal instability (CIN) (Cahill et al., 1998; Yoon et al., 2002; Swanton et al., 2006) and paclitaxel resistance (Masuda et al., 2003; Anand et al., 2003; Sudo et al., 2004; Swanton et al., 2007). Recently, two comprehensive overviews of this area have been published by Harrison and Swanton, 2008 and McGrogan et al., 2008.

Although no cell line with clear resistance to sagopilone could be identified in *in vitro* culture studies, a few *in vivo* xenograft models that only moderately respond to sagopilone exist. The mechanisms for this resistance to sagopilone are not known yet. Sagopilone is not a substrate of the MDR1 drug transporter and is therefore not affected by this kind of drug resistance.

1.5 Role of p53

The p53 protein is a transcription factor encoded by the TP53 gene. After its discovery in 1979 (Lane and Crawford, 1979; Linzer and Levine, 1979) p53 has been extensively studied, mainly because of its role as tumor suppressor. There is now evidence for additional functions of p53 in processes such as glycolysis, autophagy and regulation of oxidative stress (Matoba et al., 2006; Crighton et al., 2006; Bensaad and Vousden, 2005).

p53 controls the transcription of many different genes in response to stress stimuli, like DNA damage, oncogene activation, nutrient deprivation, telomere erosion or hypoxia (Vousden and Lane, 2007). This results in cell cycle arrest, DNA repair, apoptosis, autophagy, senescence, cell migration or angiogenesis (Murray-Zmijewski et al., 2008). Following DNA damage p53 regulates basic cell cycle processes including DNA repair, cell-cycle arrest, programmed cell death and senescence in order to eliminate potential harmful cells (Murray-Zmijewski et al., 2008; Riley et al., 2008; Zhivotovsky and Kroemer, 2004). Research in the last years has shown that in addition to p53 itself, two homologs named p63 and p73 also play an important role in apoptosis (Pietsch et al., 2008).

1.5.1 p53 choice between life and death

One of the most important and yet not fully understood aspect is how p53 selects between life and death, i.e. temporary growth arrest or apoptosis. Post-transcriptional modifications of p53 and interaction with co-factors influence the promoter selection of p53, which results in different gene transcription programs and therefore different cell fates (Das et al., 2008).

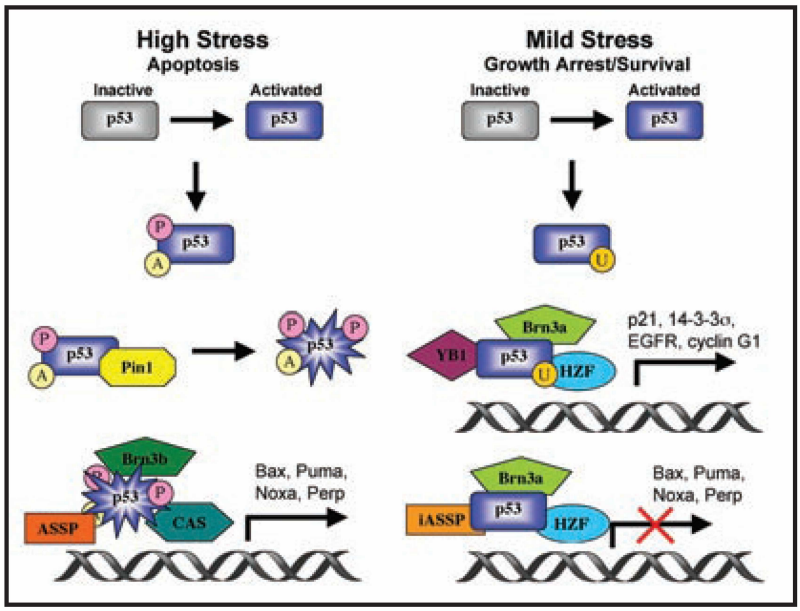

Figure 3. Transcriptional Selection of p53 Target Genes (From Das et al., 2008). In response to stress p53 is activated through post-translational modifications. Activated p53 can then be further modified to promote the transcription of apoptotic specific genes by phosphorylation at serine 46 (P) or acetylation at lysine 320 (A) or pro-arrest genes through competitive ubiquitination at lysine 320 (U). Upon severe DNA damage, increased expression of Pin1 results in p53 binding and proline-isomerization to make p53 more active on pro-apoptotic gene promoters. The binding partners Brn3b, CAS and ASSPs will then bind to p53 and trans-activate various pro-apoptotic gene promoters. Under mild stress conditions, p53 will bind to alternative proteins: YB1, Brn3a, iASSP, HZF. These binding partners will both promote the expression of pro-arrest and growth genes as well as repression of pro-apoptotic genes. For the purpose of this figure the p53 binding partners were depicted as binding to p53 simultaneously. However, it is currently unknown if the various p53 binding partners bind in consort or individually on the promoters of p53 target genes.

When p53 is bound to the promoters of pro-apoptotic genes, general transcription factors as well as histone acetyltransferases (HATs), e.g. p300, CBP (CREB-binding protein), PCAF (P300/CBP-associated factor) are recruited. The HATs acetylate lysine residues of histone tails, thereby facilitating the access of the transcriptional apparatus to chromatin. The HATs also acetylate p53 at lysine 320 and 373 (Gu and Roeder, 1997; Liu et al., 1999). Acetylation of lysine 320 of p53 by PCAF allows p53 only to bind at certain ‘high affinity’ p53 binding sites, like p21 (Di Stefano et al., 2005; Knights et al., 2006) which results in cell cycle arrest. Mutation of lysine 320 disrupts p53-mediated cell cycle arrest and raises p53-mediated apoptosis (Sakaguchi et al., 1998; Chao et al., 2006). In contrast, acetylation of lysine 373 leads to increased

phosphorylation of p53 N-terminal residues which results in enhanced interaction with ‘low affinity’ p53 binding sites, such as those of the pro-apoptotic BAX gene, leading to apoptosis (Knights et al., 2006). These findings demonstrate the importance of post-translational modifications of p53 for the promoter selection and thus for the decision between growth arrest and apoptosis.

1.5.2 Role of p53 mutations in response to microtubule-stabilizing drugs

Mutational inactivation of p53 is found in more than 50 % of all human cancers (Soussi and Lozano, 2005). Some studies suggest that mutant p53 confers increased resistance to paclitaxel. Especially, mutant p53 cannot upregulate the proapoptotic protein BAX, which results in reduced apoptosis and resistance to paclitaxel (Strobel et al. 1998). In contrast, other investigations revealed that lack of p53 activity results in increased chemosensitivity to paclitaxel (Hawkins et al. 1996; Vikhanskaya et al. 1998). To date, the importance of p53 mutational status to the response of paclitaxel remains controversial.

Some recent publications indicate an influence of the p53 status on the sensitivity to epothilones. Epothilone B-induced cytotoxicity is dependent on the p53 status as shown in prostate cells (Ioffe et al., 2004). In these investigations epothilone B showed greater cytotoxicity in p53 mutant cells compared to wild type cells (Ioffe et al., 2004). There is one report showing that epothilone B induced positive responses in glioblastoma cells with abnormal p53 status, but not in p53 wild-type cells (Quick, 2008). Altogether, these findings point to the fact that the p53 mutational status might have an influence on the sensitivity to paclitaxel and epothilones. However, the question whether the p53 mutational status influences the sensitivity to sagopilone has not been addressed to date.

2 Objective

The aim of this doctoral thesis was to investigate the molecular mode of action of sagopilone, a new microtubule binding drug under development for the treatment of cancer. It was of particular interest to analyze the antiproliferative effects of sagopilone in tumor models from different origin and to compare sagopilone with other microtubule-stabilizing drugs.

It was furthermore of interest to understand the molecular mode of action of sagopilone responsible for the improved antiproliferative activity, with a focus on the effects on the cell cycle and apoptosis. An important question was whether sagopilone induces concentration-dependent phenotypes, as has been reported for other microtubule-stabilizing drugs.

Changes in the gene expression pattern of cells after sagopilone treatment were analyzed in order to understand molecular pathways involved in the induction of apoptosis or interfering with the cell cycle program. These gene expression profiles were also used for the investigation of molecular pathways which confer resistance to sagopilone. For functional validation RNAi-mediated knock-down technology has been used to understand the impact of the regulated genes on sagopilone-induced apoptosis.

3 Materials and methods

3.1 Cell lines and culture

A549 and H460 human non small cell lung cancer cells were maintained in DMEM/HAM's F12 medium supplemented with 10% fetal bovine serum (FBS). The human non small cell lung cancer cell lines NCI-H522, NCI H23, NCI H226 and NCI H 1437 were cultured in RPMI 1640 supplemented with 10% FBS. HeLa human cervical cancer cells were grown in DMEM supplemented with 10% FBS. The human colorectal carcinomas were propagated as followed: SW480 Leibovitz's L-15 medium, HT29 McCoy's 5 A Medium modified and HCT116 DMEM/HAM's F12 medium. All media were supplemented with 10% FBS. MDA MB 231 human breast cancer cells were cultured in DMEM (Dulbecco's Modified Eagle Medium) supplemented with 10% FBS, 2 mM L-alanyl-L-glutamine and 1% nonessential amino acids. The breast cancer cell lines MDA-MB-134, ZR-75-1, T47D, MCF7, BT474, BT549 (w/o Estradiol) were grown in RPMI 1640 supplemented with 10% FBS, Insulin 10 µg/ml and 0.1 nM Estradiol. The breast cancer cell line MX-1 was cultured in RPMI 1640 supplemented with 10% FBS. The SUM 149 cell line was cultured as previously described (Forozan et al., 1999). The breast cancer cell line BT20 was propagated in DMEM/HAM's F12 medium supplemented with 10% fetal bovine serum (FBS). Hs578T cells were cultured in DMEM supplemented with 10% FBS and Insulin 10 µg/ml. The breast cancer cell lines ZR-75-30 and HCC1428 were maintained in RPMI 1640 medium supplemented with 10% fetal bovine serum, 10 mM Hepes and 1 mM Sodium pyruvate. The ovarian carcinoma cell line OVCAR-8 was grown in RPMI 1640 supplemented with 10% FBS and 10 µg/ml Insulin. NCI/Adr cells were routinely grown in RPMI 1640 supplemented with 10% FBS and 0.5 µg/ml of doxorubicin, which was omitted when cells were used for experiments. The gastric cancer cell lines EPG85-257P, EPG85-257RDB and EPG85-257RDB_shMDR1 were cultured as previously described (Lage and Dietel, 2000; Lage and Dietel, 2002). Cell lines were grown in their corresponding cell culture media as adherent monolayers in a humidified 5% CO_2 atmosphere at 37°C. The

tumor cells were harvested by using 0.05% trypsin/0.02% EDTA in PBS for five to ten minutes.

Human carcinoma cells were obtained from the American Type Culture Collection (ATCC), except for NCI/Adr (kindly provided by I. Fichtner, Max Delbrück Center, Berlin–Buch, Germany), EPG85-257P, EPG85-257RDB and EPG85-257RDB_shMDR1 (kindly provided by H. Lage, Institute of Pathology, Humboldt University Berlin, Germany), SUM149 (kindly provided by Steven Ethier, University of Michigan Medical Center, MI, USA). 293FT cells were used for lentivirus production. 293FT cells were purchased from Invitrogen and maintained in DMEM supplemented with 10% FBS, 100 U/ml penicillin, 0.1 mg/ml streptomycin and 0.1 mM non essential amino acids. All cell culture media and reagents were purchased from Biochrom, Berlin, Germany.

3.2 Compounds

Sagopilone and ixabepilone were produced at Bayer Healthcare Pharmaceuticals through total syntheses. Paclitaxel was purchased from Sigma, Deisendorf, Germany. All three chemotherapeutic compounds were solved in ethanol. The pan-caspase inhibitor ZVAD.fmk was purchased from Bachem, Heidelberg, Germany and dissolved in DMSO.

3.3 Proliferation assay

The effect of sagopilone and other anticancer agents on the proliferation of different cancer cell lines was assessed using a cell proliferation assay based on crystal violet cell staining as described before (Lichtner et al., 2001). IC50 values were calculated from three independent experiments using the SigmaPlot software (SPSS, Friedrichsdorf, Germany).

3.4 Cell cycle analysis

Fluorescence-activated cell sorter (FACS) analysis was performed to determine cell cycle kinetics. Cells were incubated with sagopilone for the indicated times, fixed with 70% ethanol, and stained with 50 µg/mL propidium iodide (PI) (Sigma-Aldrich). Cellular DNA content of 10,000 events per sample was determined by flow cytometry using the BD FACSCalibur™ (Becton, Dickinson and Company, San Jose, CA, USA) and analyzed using the CellQuest™ software (Becton, Dickinson and Company). For quantitative analysis, the histograms of DNA distribution were modeled using the ModFitLT software (Verity Software House, Topsham, USA).

3.5 Immunofluorescence staining and microscopy

Glass coverslips (Menzel, Braunschweig, Germany) were first coated with 0.01% Poly-L-lysine solution (Sigma) for five minutes and washed with PBS. Cells grown on glass coverslips were washed twice with PBS and fixed with 3.5% paraformaldehyde (Roth) for 15-20 minutes. The cells were washed twice with PBS and the cellular membranes were permeabilized with 0.25% Triton X-100 (Roth) in PBS for ten minutes, followed by two washing steps with 0.05% Triton X-100 in PBS. Unspecific binding sites were blocked with 5% NGS/1% BSA/0.05% Triton X-100 in PBS for 30 minutes. Cells were incubated with a 1:1000 dilution of a mouse anti-α-tubulin primary antibody in the above described blocking solution for one hour and washed three times with 0.05% Triton X-100, followed by a one-hour incubation with the fluorescence dye alexa fluor 488 labeled goat secondary anti-mouse antibodies 1:1500 (Invitrogen) and repeated washing with PBS. Fluorescence staining of the DNA, was achieved by incubation with DRAQ5 (1:1000 in PBS) (Biostatus, Leicestershire, UK) for ten minutes. The coverslips were mounted on glass microscope slides (Vogel, Gießen, Germany) with fluorescence mounting solution (Dako, Hamburg, Germany). Analysis of specimens was performed using the confocal laser scanning microscopy LSM 510 META (Carl Zeiss AG, Jena, Germany).

3.6 Live cell microscopy

A549 cells were seeded in a special 96-well plate with glass bottom (Greiner, Frickenhausen, Germany) and grown at 37°C for 24 hours. Before starting imaging, cells were treated with either medium containing vehicle or medium containing 2.5 nM or 40 nM sagopilone, and incubated throughout the entire observation period. The plate was placed in a 5% CO_2 and 37°C Zeiss S-M incubation chamber attached to an inverted Zeiss Axiovert 200M microscope. 14 wells were chosen for imaging and regions of interest were defined in each of these using the Zeiss AxioVision software. Cells were imaged in DIC mode in intervals of six minutes using a Zeiss AxioCam HRm CCD camera and a Zeiss Achroplan 20x/0,40 Ph2 objective lens with numerical aperture of the Nomarski filter and exposure time set to 0.16 and 65 ms, respectively. MetaXpress software (Visitron Systems, Puchheim, Germany) was used for image analysis.

3.7 Protein extraction, SDS-PAGE and Western blot

Whole cell protein was extracted from cultured A549 cells by using M-PER Mammalian Protein Extraction Reagent (Pierce, Perbio Science, Bonn, Germany) supplemented with protease inhibitors (Sigma) and phosphatase inhibitor HALT (Pierce, Perbio Science, Bonn, Germany). 200 µl extraction reagents were used for cells grown on a 6 well plate. The protein concentration of the lysates was determined by using BCA Protein Assay Kit (Pierce) according to the manufacturer's instructions.

Equal amounts of proteins were denatured in lithium dodecyl sulfate sample buffer and separated on a 4-12% Bis-Tris gel in an XCell SureLock electrophoresis cell filled with MOPS SDS running buffer. The proteins were transferred to a PVDF membrane and unspecific binding sites were blocked with a 5% solution of non-fat milk in PBS/Tween 20 for one hour. Subsequently, different antibodies (Table 1) were diluted in blocking solution and probed for one hour on the membrane. After washing three times with PBS/Tween 20 the membrane was incubated with a horseradish peroxidase-labeled secondary antibody for one hour, which was followed by washing with PBS/Tween 20. For detection ECL Plus Western Blotting Detection

Reagents (GE Healthcare, Munich, Germany) was employed. Chemiluminescence was detected on Hyperfilm ECL (GE Healthcare). If not stated otherwise all reagents and devices used for gel electrophoresis and Western blotting were purchased from Invitrogen.

Table 1. Antibody used for Western blot.

Antibody	Species	Dilution	Manufacturer	#
p21	mouse	1:100	abcam	ab16767
P21	rabbit	1:100	Santa Cruz Biotechnology	p21 (C-19) sc-397
p53	mouse	1:1000	BD Pharmingen	15801A
BUBR1	mouse	1:5000	BD Transduction Laboratories	612502
Cyclin B1	mouse	1:2000	BD Pharmingen	554176
yH2AX	mouse	1:5000	upstate	05-636
PAPRP	mouse	1:500	BD Pharmingen	551024/ clone 7D3-6
MPM2	mouse	1:500	upstate	05-368
GAPDH	mouse	1:10000	Advanced ImmunoChemical	RGM2/Clone 6C5
anti mouse HRP	goat	1:10000	Jackson ImmunoResearch Laboratories	115-035-068
anti rabbit HRP	donkey	1:5000	Amersham Bioscience	NA934

3.8 Apoptosis assay

To investigate apoptosis, cells were incubated continuously for 72 h with the indicated drug concentration of sagopilone or vehicle, trypsinized and stained with 3,3'-dihexyloxacarbocyanine iodide (DiOC6(3) (Invitrogen, Karlsruhe, Germany) and propidium iodide as described before (Castedo et al., 2002).

3.9 RNA preparation and cDNA synthesis for real time PCR analysis

The cells were seeded in 96-well plates and treated with the indicated compound or vehicle. RNA preparation and cDNA synthesis were performed in a two-step reaction using Cells-to-cDNA II Kit (Ambion, Austin, USA) according to the manufacturer’s instructions. The obtained cDNA was directly used for qRT-PCR.

In case of mammalian tissue, tumors were homogenized using stainless steel beads and the TissueLyser Adapter Set according to the manufacturer’s recommendations (Qiagen, Hilden, Germany). Total RNA was extracted using the RNeasy Mini Kit

(Qiagen, Hilden, Germany) according to the manufacturer's recommendations including a DNase I (Qiagen) step to digest genomic DNA. To synthesize double-stranded cDNA from RNA, SuperScript III First-Strand Synthesis System for qRT-PCR (Invitrogen, Karlsruhe, Germany) was used according to the manufacturer's instructions. The reaction was primed with random hexamer primers.

3.10 Quantitative real-time PCR

All used TaqMan assays (Table 2) and TaqMan Universal PCR Master Mixes were purchased from Applied Biosystems (Foster City, USA). qRT-PCR was performed according to the manufacturer's instructions. The amounts of cDNA equivalent to 10 – 30 ng RNA were used for the PCR reaction. Human endogenous control plate (Applied Biosystems) was previously used for selection of an optimal internal reference gene which was unchanged during the treatment with sagopilone and paclitaxel. All experiments were performed in triplicates. Quantification of cDNA was achieved by dilution series of cDNA from human placenta (BioCAT, Heidelberg, Germany). The assay was performed with the 7500 Fast Real-Time PCR System (Applied Biosystems).

Table 2. TaqMan® Assay-On-Demand -human; Applied Biosystems (Foster City, USA).

Gene name	Gene symbol	Assay ID
p21	CDKN1A	Hs00355782_m1
p53	TP53	Hs00153340_m1
Cyclin B1	CCNB1	Hs00259126_m1
BUBR1	BUB1B	Hs00176169_m1
FAS	FAS	Hs00163653_m1
GADD45A	GADD45A	Hs00169255_m1
MDM2	MDM2	Hs00242813_m1
HPRT (endog.control)	HPRT	# 4326321E

3.11 Drug treatments for gene expression analysis

A549 cells were seeded in 10 cm cell culture plates and allowed to attach overnight. The cells were then treated with normal growth medium or medium containing either vehicle (ethanol), 2.5 nM sagopilone, 40 nM sagopilone, 4 nM paclitaxel or 40 nM

paclitaxel, respectively for 18 hours. Thereafter the cells were subjected to RNA extraction.

3.12 RNA extraction for gene expression analysis

Total RNA was extracted using the RNeasy Mini Kit (Qiagen, Hilden, Germany) according to the manufacturer's recommendations including a DNase I (Qiagen) step to digest genomic DNA. Total RNA was checked for integrity using the RNA LabChips on the Agilent Bioanalyzer 2100 (Agilent Technologies Inc., Palo Alto, CA, USA) and the concentration was determined on a Nanodrop spectrophotometer (Peqlab, Erlangen, Germany).

Table 3. RNA quality control.

Sample No.	Set	Treatment	Concentration [nM]	Agilent RIN	RNA ratio (28S/18S)	RNA conc. [ng/µl] NanoDrop
1	1	/	untreated	9.5	1.5	287.3
2	1	Ethanol (vehicle)	Ethanol (vehicle)	9.5	1.7	701.9
3	1	Paclitaxel	4	9.4	1.8	784.0
4	1	Paclitaxel	40	9.5	1.6	822.4
5	1	Sagopilone	2.5	9.5	1.5	872.4
6	1	Sagopilone	40	9.5	1.9	910.5
7	2	/	untreated	9.8	1.9	776.4
8	2	Ethanol (vehicle)	Ethanol (vehicle)	9.8	1.8	846.1
9	2	Paclitaxel	4	9.8	2.0	712.6
10	2	Paclitaxel	40	9.8	1.9	721.1
11	2	Sagopilone	2.5	9.9	1.9	675.1
12	2	Sagopilone	40	9.8	1.9	719.8
13	3	/	untreated	9.8	1.9	811.8
14	3	Ethanol (vehicle)	Ethanol (vehicle)	9.9	2.0	917.0
15	3	Paclitaxel	4	9.8	2.0	960.8
16	3	Paclitaxel	40	9.8	2.0	830.5
17	3	Sagopilone	2.5	9.9	2.0	766.3
18	3	Sagopilone	40	9.9	2.1	665.3
19	4	/	untreated	9.7	2.0	780.7
20	4	Ethanol (vehicle)	Ethanol (vehicle)	9.7	2.0	776.2
21	4	Paclitaxel	4	9.7	2.0	982.9
22	4	Paclitaxel	40	9.7	1.9	979.3
23	4	Sagopilone	2.5	9.7	2.0	806.8
24	4	Sagopilone	40	9.6	1.9	804.3
25	5	/	untreated	9.8	2.0	943.1
26	5	Ethanol (vehicle)	Ethanol (vehicle)	9.8	2.2	993.8
27	5	Paclitaxel	4	9.7	2.1	961.2
28	5	Paclitaxel	40	9.7	2.3	879.6
29	5	Sagopilone	2.5	9.7	2.0	1017.2
30	5	Sagopilone	40	9.7	2.3	935.8

RIN - RNA integrity number (Schroeder et al., 2006)

3.13 In vitro *RNA Transcription and Hybridization to Affymetrix GeneChips*

The One-Cycle Eukaryotic Target Labeling Kit (Affymetrix Inc., Santa Clara, CA, USA) was used according to the manufacturer's instructions. Briefly, 2 µg of high quality total RNA were reverse-transcribed using a T7 tagged oligo-dT primer for the first-strand cDNA synthesis reaction. After RNase H-mediated second-strand cDNA synthesis, the double-stranded cDNA was purified and served as template for the subsequent *in vitro* transcription reaction which generates biotin-labeled complementary RNA (cRNA). The biotinylated cRNA was then cleaned up, fragmented and hybridized to GeneChip HGU133Plus2.0 expression arrays (Affymetrix, Inc., Santa Clara, CA, USA.), which contain 54675 probe sets. The GeneChips were washed and stained with streptavidin-phycoerythrin on a GeneChip Fluidics Station 450 (Affymetrix). After washing, the arrays were scanned on an Affymetrix GeneChip 3000 scanner with autoloader and barcode reader. A total of 30 HGU133Plus2.0 arrays were processed (biological replicates for all treatments and vehicles n = 5).

The primary outcome of Affymetrix analyses is the intensity of cRNA hybridization to respective complementary probe sets indicating the expression level. Probe sets are a combination of 25mer probes representing the most optimal balance between sensitivity and specificity to determine whether or not the complementary sequence of cRNA or cDNA is present in the sample. Expression analyses were performed using the Expressionist Pro 4.0 software (Genedata AG, Basel, CH). The quality of the data files (CEL format) containing probe level expression data was checked and refined using the Expressionist Refiner software (Genedata AG). The refiner process was performed by clustering of samples on feature intensity level. This allows the identification of possible outliers on feature intensity level. Subsequently, refined CEL files were condensed with MAS5.0 (Affymetrix) and LOWESS normalized using all experiments as a reference. The normalized expression data sets were loaded into the CoBi database (Genedata, Basel, Switzerland) and analyzed with the Genedata Expressionist software.

3.14 Unsupervised analysis

Principle Component Analysis (PCA) showing the relationships between individual samples was performed using the Expressionist Analyst Pro 4.0 software (Genedata AG, Basel, Switzerland).

3.15 Supervised analysis

A valid value proportion analysis was performed for each group (4 of 5 probe sets must show a signal) and the resultant probe sets were united. These data were subjected to a number of pairwise comparisons using the Expressionist Analyst Pro 4.0 software (Genedata AG, Basel, Switzerland).

Statistical analyses included pairwise comparisons between control samples treated with vehicle (Ethanol) and compound treated samples. Probe sets were considered to be regulated if they were outside of the ellipsoid region in the Volcano plot. Venn intersection analyses for significantly regulated or counter-regulated genes were conducted to identify regulatory overlaps using the Expressionist Analyst Pro 4.0 software.

Hierarchical clustering analysis was performed on the combined list of 990 genes significantly regulated by sagopilone (sag) and paclitaxel (pac) (Volcano plot: >5x-fold change and p-value <1x10-5 from T-test for 40 nM sag and pac; for 2.5 nM sag and 4 nM pac >3-fold change and p-value <5x10-3) using the Expressionist Analyst Pro 4.0. Pathway analyses were performed with the GeneGo Metacore database and software tools.

3.16 In vivo *tumor growth*

The in vivo efficacy of sagopilone was assessed in the A549 human non small cell lung cancer xenograft. All animal experiments were conducted in accordance with the United Kingdom Coordinating Committee for Cancer Research (UKCCCR) regulations for the welfare of animals and the German animal protection law, after approval by the local authorities (internal BSP animal protection officer and the animal protection commission from the government of Berlin LaGeSo). Female

NMRI athymic nude mice with a body weight of approximately 20 g (Bayer Schering Pharma, animal facilities) were fed with Altromin R (Altromin, Lage, Germany) diets and autoclaved water provided ad libitum. Mice were caged in Macrolon type III wire mesh–bottom cages (10 mice per cage) under low-germ conditions at room temperature (22 °C) and 50%–60% relative humidity, with a daily light cycle of 10 hours dark/14 hours light. A549 tumor cells grown in cell culture were suspended in Matrigel (Becton Dickinson, Heidelberg, Germany) and transplanted by a single subcutaneous injection ($3x10^6$ cells) into the left flank of nude mice. After tumors had reached approximately 25 mm^2,in size, mice were randomly assigned to the control group or one of the two treatment groups (short term and long term treatment). The control group was given only vehicle whereas the treatment groups received 10 mg/kg sagopilone intravenously once. Tumor growth was assessed by determining tumor area (product of the longest diameter and its perpendicular) with calipers twice weekly. Control and treatment groups were removed from the experiment when, after progression, tumor size reached a median value of at least 100 mm^2. The data are presented as group tumor growth curves showing medians and interquartile ranges for each observation time point.

3.17 Cloning of shRNAs

To design shRNAs the BLOCK-iT™ RNAi Designer software (Invitrogen) was used. Oligonucleotides (Table 4) were purchased from TIB MOLBIOL (Berlin, Germany). Plasmids used for gene silencing via short hairpin (sh) RNA were generated using Gateway Cloning (BLOCK-iT U6 RNAi Entry Vector Kit and BLOCK-iT Lentiviral RNAi Expression System; Invitrogen) according to the manufacturer’s recommendations. Sequence analysis of pENTR and pGT-396_hygro was performed by Martin Meixner (SMB, Services in Molecular Biology, Berlin).

Table 4. Oligonucleotides for cloning of shRNAs into pGT-396_hygro.

Oligo	Sequence
shDharmacon2	CACCGTAAGGCTATGAAGAGATACTTCAAGAGAGTATCTCTTCATAGCCTTA
shQiagen	CACCGTTCTCCGAACGTGTCACGTTTCAAGAGAACGTGACACGTTCGGAGAA
shp53_3	CACCGCATCTTATCCGAGTGGAAGGTTCAAGAGACCTTCCACTCGGATAAGATGC
shp53_4	CACCGACTCCAGTGGTAATCTACTTCAAGAGAGTAGATTACCACTGGAGTC
shp53_5	CACCGCGCACAGAGGAAGAGAATCTTTCAAGAGAAGATTCTCTTCCTCTGTGCGC
shp21_1	CACCGCTTCGACTTTGTCACCGAGATTCAAGAGATCTCGGTGACAAAGTCGAAG
shp21_2	CACCGGTGACTTCGCCTGGGAGCGTTTCAAGAGAACGCTCCCAGGCGAAGTCACC
shp21_3	CACCGGAGTCAGACATTTTAAGATTTTCAAGAGAAATCTTAAAATGTCTGACTCC
shp21_4	CACCGCCTAGACTGTAAACCTCTCTTTTCAAGAGAAAGAGAGGTTTACAGTCTAGG
shp21_5	CACCGGGAAGGGACACACAAGAAGATTCAAGAGATCTTCTTGTGTGTCCCTTCCC
shp21_6	CACCGCACTGAAGTGCTTAGTGTACTTCAAGAGAGTACACTAAGCACTTCAGTGC

3.18 Production of lentivirus in 293FT cells

6-well plates were coated with collagen and 1.5 Mio. 293FT cells were seeded in their culture medium (3.1) in each well and allowed to attach overnight. On the day of transfection, medium was removed and replaced with 2 ml of growth medium containing serum, but with no antibiotics. Complexes from packaging mix, pLenti-plasmid (pGT-396_hygro) and Lipofectamine 2000 were prepared as recommended by the manufacturer (Invitrogen, Karlsruhe, Germany). In the evening, medium was removed and 2 ml of culture medium were added. The next day, the virus-containing supernatants were collected. To remove cellular debris the viral supernatants were filtered through a sterile 0.45 µm low protein binding filter.

3.19 Lentiviral transduction of mammalian cells

A549 cells (150,000 pro well) were seeded onto 6-well plates and allowed to attach overnight. On the day of transduction, culture medium was removed, virus-containing medium (2ml) was prepared as recommended by the manufacturer (Invitrogen) and added to cells. Cells were incubated at 37°C for 3 hours. Virus-containing medium was then removed, replaced with 2 ml of fresh, complete culture medium and cells were again incubated at 37°C overnight. Cells were replated into larger-sized tissue culture formats and after 48 hours the medium was replaced for medium containing

Hygromycin B (Roche, Mannheim, Germany) in order to select for stably transduced cells.

3.20 p53 mutations in cell lines

Table 5. Description of p53 mutations of cell lines.

Name	Topography	Morphology	TP53 status	Exon	Mutation	Protein change	Reference
H460	LUNG	Large cell carcinoma	WT	--	--	--	O'Connor et al., 1997
MCF-7	BREAST	Adenocarcinoma	WT	--	--	--	Concin et al., 2003
A375	SKIN	Malignant melanoma	WT	--	--	--	Bamford et al., 2004
HCT-116	COLON	Carcinoma	WT	--	--	--	O'Connor et al., 1997
MDA-MB-231	BREAST	Adenocarcinoma	MUT	8-exon	c.839G>A	p.R280K	Bartek et al., 1990
NCI-H1437	LUNG	Adenocarcinoma	MUT	8-exon	c.800G>C	p.R267P	Mitsudomi et al., 1992
T47D	BREAST	Infiltrating duct carcinoma	MUT	6-exon	c.580C>T	p.L194F	Nigro et al., 1989
SK-BR3	BREAST	Carcinoma	MUT	5-exon	c.524G>A	p.R175H	Kovach et al., 1991

Mutations were located in the DNA-binding domain of TP53 (amino acids 98-309)

Source: The International Agency for Research on Cancer (IARC)
http://www-p53.iarc.fr/

4 Results

4.1 Proliferation assays

4.1.1 *In vitro* profile of sagopilone and paclitaxel in chemo-sensitive cancer cell lines

The activities of sagopilone and paclitaxel were examined in 15 cancer cell lines by *in vitro* proliferation assays. Lung, cervix, colon and breast cancer cell lines were incubated continuously for 72 hours with 0.01 to 100 nM sagopilone or paclitaxel. Cell number was then determined using the crystal violet proliferation assay and IC50 values were calculated.

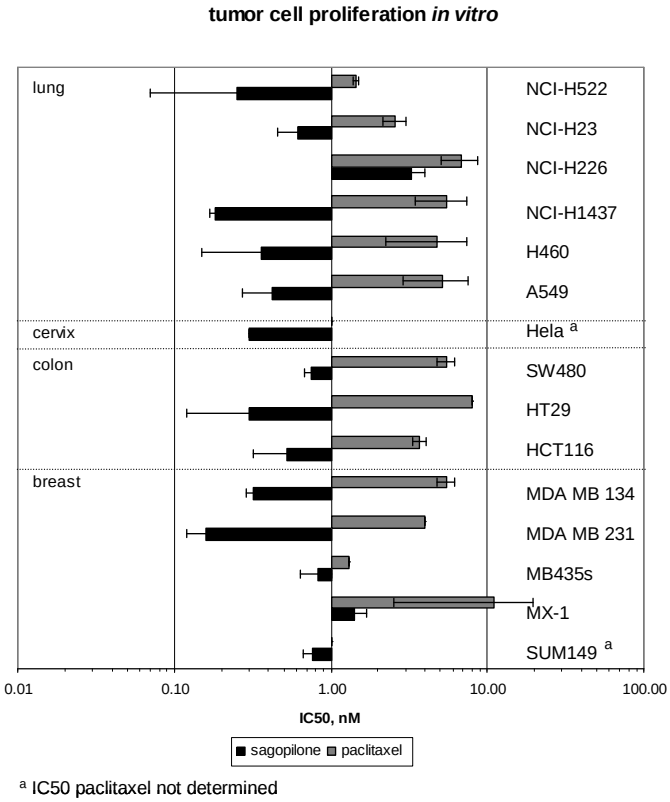

Figure 2. Inhibition of tumor cell proliferation *in vitro*. Cell lines were incubated continuously with 0.01 to 100 nM sagopilone or paclitaxel for 72 hours. Subsequently, the cells were submitted to crystal violet proliferation assay and IC50 was determined. IC50 values are mean ± standard deviations calculated from three independent experiments. Bars without standard deviation result from one representative experiment.

Figure 2 shows IC50 values determined for a panel of different cell lines. Sagopilone inhibited tumor cell proliferation in all cell lines with IC50 values ranging from 0.2 to 3.3 nM and was effective at subnanomolar concentrations in the majority (13 of 15) of all cell lines. In all assays where the antiproliferative activity of paclitaxel was also measured, sagopilone was consistently more effective than paclitaxel. Paclitaxel inhibited cell proliferation with IC50 values between 1.3-11.0 nM.

4.1.2 *In vitro* profile of sagopilone and paclitaxel in chemo-resistant cancer cell lines

Since the emergence of chemoresistance represents one of the major obstacles in cancer therapy, we have analyzed the antiproliferative activity of sagopilone and paclitaxel on multidrug resistant human cancer cell lines characterized by overexpression of the multidrug resistance gene (MDR1) in comparison to their drug-sensitive counterparts.

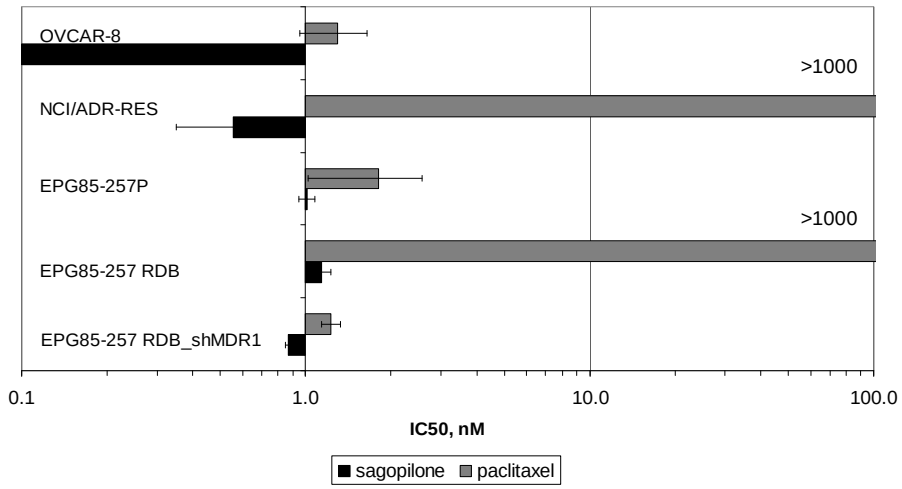

Figure 3. Sagopilone inhibited tumor cell proliferation of chemoresistant cell lines. Inhibition of tumor proliferation *in vitro* was measured after continuous incubation with growth medium containing 0.01 to 100 nM sagopilone or paclitaxel for 72 hours. The cells were fixed and cell growth was determined by performing a crystal violet proliferation assay. IC50 values were calculated from the ovarian cancer cell line OVCAR-8 and their adriamycin-resistent subclone NCI/ADR-RES characterized by MDR1 overexpression, the gastric cancer cell lines EPG85-257P, the daunorubicin-selected MDR1 overexpressing subline (EPG85-257RDB) and the EPG85-257RDB cell line with short-hairpin RNA-mediated selective knockdown of MDR1 (EPG85-257RDB_shMDR1).

As shown in Figure 3, Sagopilone and paclitaxel inhibited cell proliferation in both parental tumor cell lines (OVCAR-8, EPG85-257P). Sagopilone showed a slightly lower IC50 than paclitaxel. In contrast, only sagopilone inhibited the proliferation of MDR1 over-expressing cell lines (NCI/ADR-RES, EPG85-257RDB) with IC50 values comparable to those seen for their parental counterparts. Paclitaxel was fully ineffective as documented by a strongly increased IC50 (>1000 nM). The sensitivity to paclitaxel could be restored through stable transfection with shRNA targeting MDR1 (EPG85-257RDB_shMDR1). Thus, in contrast to paclitaxel, which only showed antiproliferative activity in chemosensitive cell lines, nanomolar concentrations of sagopilone inhibited cell proliferation of chemosensitive as well as of chemoresistant cell lines overexpressing the MDR1 drug transporter.

4.1.3 *In vitro* profile of sagopilone, paclitaxel and ixabepilone in breast cancer cell lines

As breast cancer is sensitive to microtubule targeting drugs, Sagopilone was compared to paclitaxel and ixabepilone, in different estrogen receptor (ER)-positive and ER-negative breast cancer models. Sagopilone strongly inhibited the growth of 6 ER-positive (mean IC50 1.2 nM ± 0.9) and 3 ER-negative (mean IC50 0.9 nM ± 0.4) breast cancer cell lines (Figure 4). Ixabepilone was less active than sagopilone in these cell lines, having mean IC50 values of 7.9 nM ± 6.0 in the ER-positive and 3.9 nM ± 1.7 in the ER-negative cell lines. In the instances where antiproliferative assays were additionally performed, the inhibition by sagopilone was consistently stronger than of paclitaxel. Paclitaxel inhibited cell proliferation with mean IC50 values of 3.4 nM ± 3.0 in the ER-positive and 3.4 nM ± 1.7 in the ER-negative cell lines.

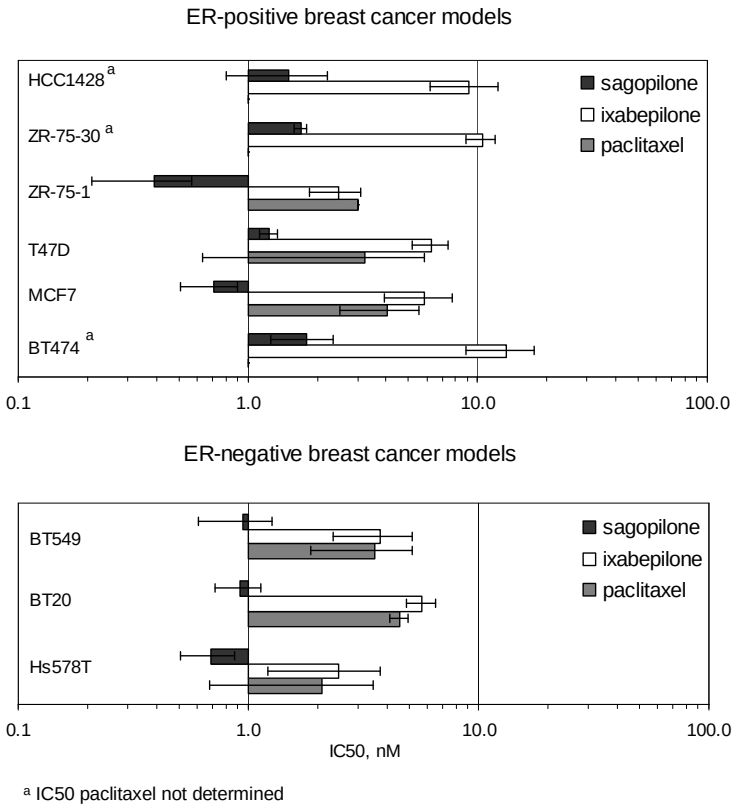

Figure 4. Inhibition of tumor cell growth in estrogen receptor-positive and -negative breast cancer cell lines. Cell lines were incubated continuously with 0.01 to 100 nM ixabepilone, sagopilone or paclitaxel for 72 hours. The cells were fixed and cell growth was determined by performing a crystal violet proliferation assay. IC50 values are mean ± standard deviations calculated from three independent experiments. Bars without standard deviation result from one representative experiment.

4.2 Cell cycle analysis of sagopilone- and paclitaxel-treated cells

Due to the interference of microtubule-stabilizing drugs with the mitotic spindle apparatus, effects on the cell cycle distribution are expected. To examine these, A549 cells were treated for 18 hours with a range of sagopilone and paclitaxel concentrations. They were then subjected to propidium iodide staining. The DNA content of the cells was measured by flow cytometry.

4.2.1 Cell cycle distribution of sagopilone-treated cells

Vehicle-treated A549 cells (Figure 5) displayed the cell cycle distribution typical of a proliferating population of cells. The most prominent peak consists of G0/G1 (2N)

cells. The smaller peak is composed of G2/M (4N) cells. The area between these peaks consists of cells in the S phase of the cell cycle.

Changes of cell cycle distribution were observed in cells treated with 2.5 nM sagopilone for 18 hours (Figure 5). The amount of cells with a relative DNA content of 2N (G0/G1) decrease from 56.7 % ± 1.6 to 14.4 % ± 3.7. Concomitantly, two new peaks appeared in the vicinity of the G0/G1 cell population, one with fluorescence intensities lower than G0/G1 cells (hypodiploid cells) and another with a greater fluorescence which overlays the S phase cell population (hyperdiploid cells). Taken together this aneuploid population of cells accounts for 54.2 % ± 2.8 of all cells. Furthermore, the number of G2/M cells increased from 10.1 % ± 1.7 to 24.8 % ± 2.3. From 10 nM sagopilone upwards, the cell cycle profile significantly changed. For example, the treatment with 40 nM sagopilone led to a dramatic increase in the number of G2/M cells to 87.2 % ± 0.9. On the other hand the number of G0/G1 cells decreased to 6.8 % ± 0.9. Additionally, compared to the 0.5 - 5 nM sagopilone-treated A549 cells, the aneuploid cell population almost completely disappeared.

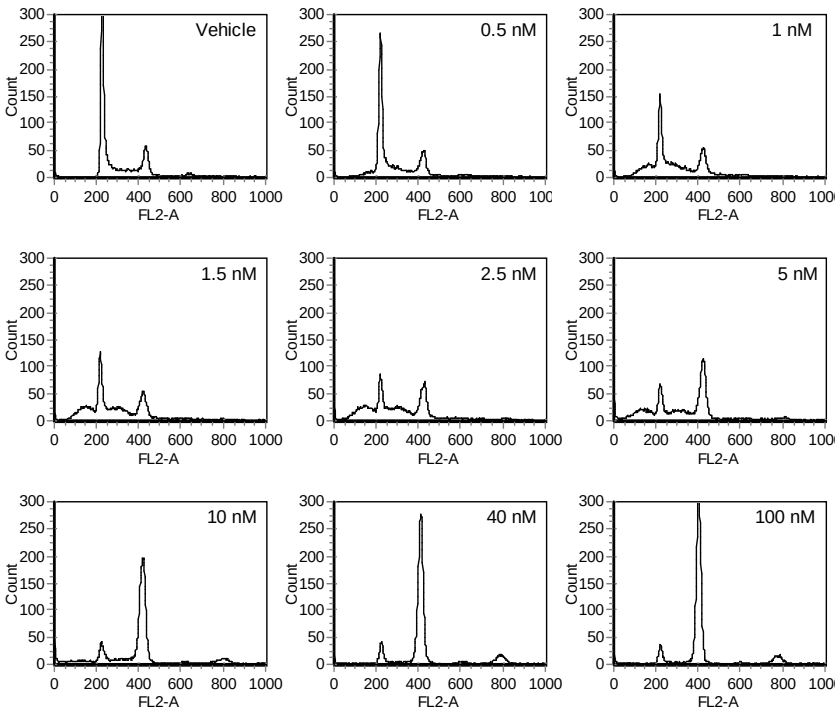

Figure 5. Cell cycle analysis of A549 cells treated with sagopilone. Cells were incubated with growth medium containing either vehicle or 0.5 to 100 nM sagopilone for 18 hours, followed by fixation and incubation with propidium iodide. DNA content was determined by flow cytometry.

Cells which possess a DNA content greater than 2N (hypodiploid cells) have the same fluorescence intensities than S phase cells and are therefore difficult to quantify. The software ModFitLT (Verity Software House) allows modeling of flow cytometry histograms and was used for quantification. Figure 6 shows a modeled cell cycle histogram of vehicle-treated and sagopilone-treated (2.5 nM and 40 nM) A549 cells. The histogram of DNA distribution was modeled as the sum of G0/G1, G2/M, S phases, and two aneuploid populations.

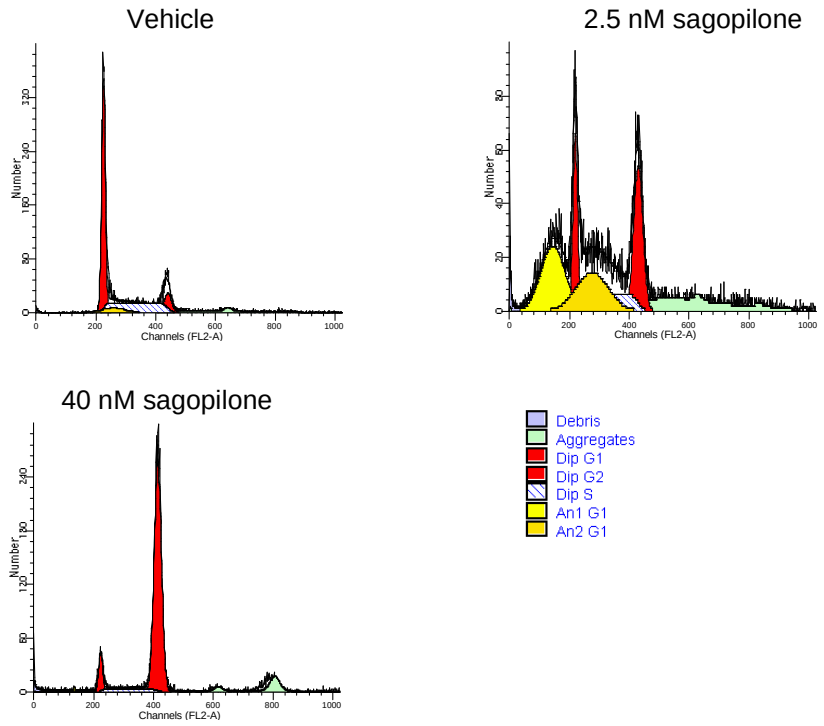

Figure 6. Cell cycle histogram modeling. Histograms of cell cycle distribution of A549 cells treated with increasing concentrations of sagopilone were modeled as a sum of G0/G1 (Dip G1), G2/M (Dip G2), S phase (Dip S), and two aneuploid populations (An1 G1, An2 G1) close to the G0/G1 peak, by using the ModFitLT software.

The changes in the cell cycle distribution depending on the sagopilone concentration are shown in Figure 7 which depicts the percentage of the aneuploid, G0/G1 and G2/M cell populations obtained from the modeled cell cycle histograms. For a better overview, the S phase cells were excluded from the diagram. At low sagopilone concentrations (0.5 to 10 nM) an increase of the aneuploid cell population was detected and was accompanied by a decrease of the 2N G0/G1 cells. The population

of aneuploid cells completely disappeared at drug concentrations exceeding 10 nM. Concomitantly starting from concentrations of 2.5 nM sagopilone, a rapid rise of the G2/M cell population was observed, which culminated at 10 nM sagopilone, indicating that the mitotic block suppressed the induction of aneuploidy. At drug concentrations which exceeded 20 nM sagopilone, no further changes in cell cycle distribution were observed.

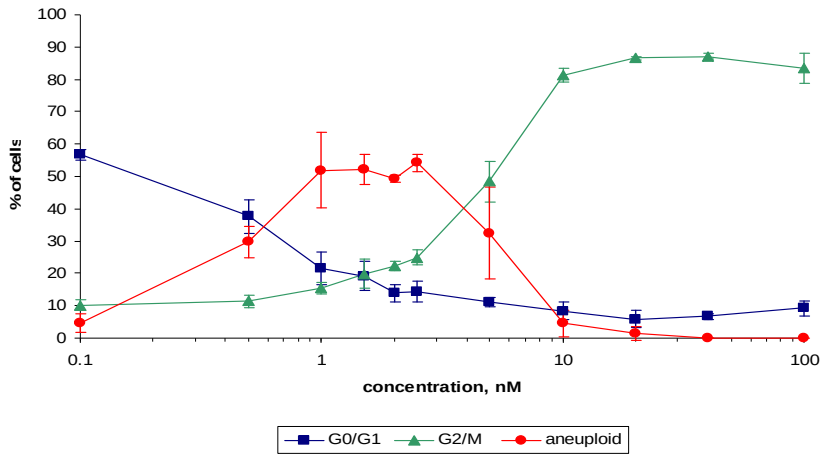

Figure 7. Cell cycle analysis of A549 cells treated with increasing concentrations of sagopilone. A549 cells were incubated with medium containing 0 to 100 nM sagopilone for 18 hours. The cells were fixed and stained with propidium iodide. Cellular DNA content was determined by flow cytometry. Cell cycle histograms were modeled using the ModFitLT software. The amounts of cells constituting the aneuploid, G0/G1 and G2/M populations were determined and plotted against the drug concentration. Shown is the average of three independent experiments and standard deviations.

4.2.2 Cell cycle distribution of paclitaxel-treated cells

The cell cycle analysis of A549 cells treated with 4 nM paclitaxel for 18 hours (Figure 8) revealed an identical cell cycle distribution as the 2.5 nM sagopilone-treated cells (Figure 5). Compared to the vehicle-treated A549 cells the number of G0/G1 cells was considerably diminished to 13.2 % ± 5.4. Furthermore, like in the 2.5 nM sagopilone-treated cells, an aneuploid cell population appeared accounting for 55.7 % ± 3.9. The number of G2/M cells was found to be increased (24.7 % ± 7.1 %).

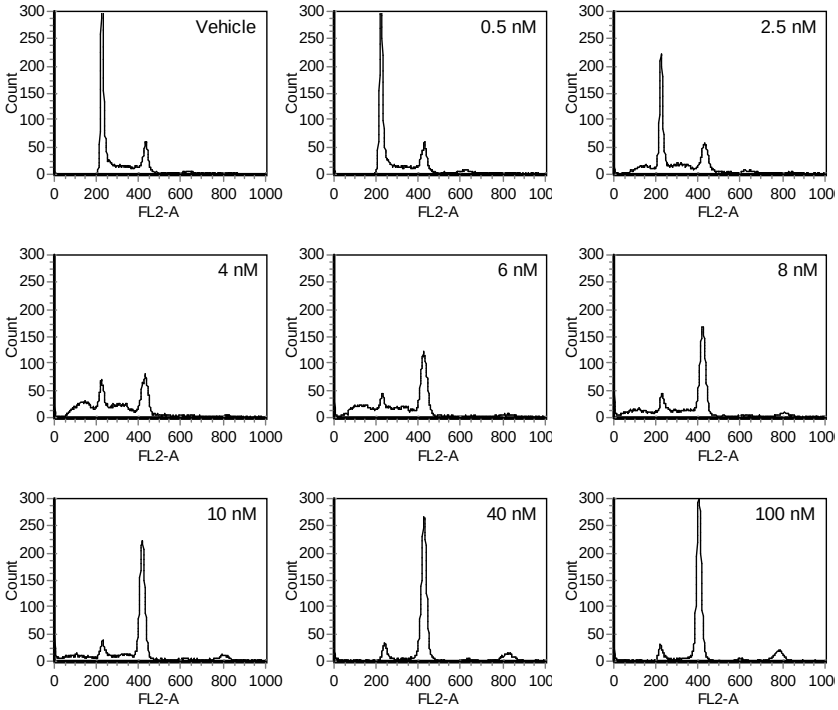

Figure 8. Cell cycle analysis of A549 cells treated with paclitaxel. Cells were incubated with growth medium containing either vehicle or 0.5 to 100 nM paclitaxel for 18 hours, followed by fixation and incubation with propidium iodide. DNA content was determined by flow cytometry.

A549 cells treated with 40 nM paclitaxel possessed an increased number of G2/M cells (82.7 % ± 3.6). Concomitantly, the number of G0/G1 cells decreased to 6.8 % ± 0.9. Additionally, compared to the 4 nM paclitaxel-treated A549 cells, the aneuploid cell population almost completely disappeared.

Figure 9 shows a cell cycle concentration response curve of A549 cells treated with paclitaxel for 18 hours. At low paclitaxel concentrations (1 to 10 nM) an increase of the aneuploid cell population and concomitantly a decrease of the G0/G1 cells population were observed. Simultaneously, starting at the 6 nM paclitaxel concentration an increase of G2/M cells was measured. The effect was highest at 10 nM and remained almost unchanged up to 100 nM. At the concentration of 10 nM paclitaxel the amount of aneuploid cells fell to 0.1 % ± 0.1.

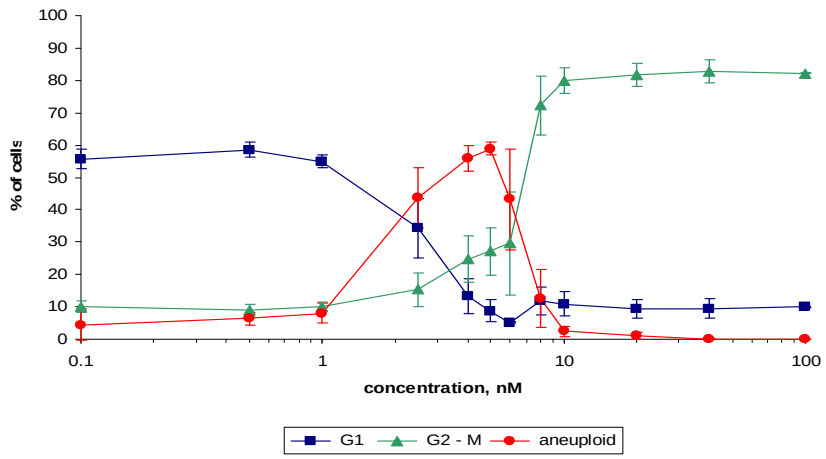

Figure 9. Cell cycle analysis of A549 cells treated with increasing concentrations paclitaxel. A549 cells were incubated with medium containing 0 to 100 nM paclitaxel for 18 hours. The cells were fixed and stained with propidium iodide. Cellular DNA content was determined by flow cytometry. Cell cycle histograms were modeled by using the ModFitLT software. The amounts of cells constituting the aneuploid, G0/G1 and G2/M populations were determined and plotted against the drug concentration. Shown is the average of three independent experiments and standard deviation.

4.2.3 Comparison of cell cycle effects of sagopilone- and paclitaxel -treated A549 cells

The cell cycle distribution plots of A549 cells treated with sagopilone and paclitaxel showed similar curve shapes (Figure 7, 9). However, important differences were found in the occurrence of the aneuploid cell population. Table 6 shows the IC50 values of G0/G1 decrease and the EC50 of the aneuploid cells population for both compounds. The half-maximal induction of the aneuploid cell populations (EC50 aneuploid cell) was calculated to be 0.4 nM ± 0.2 for sagopilone and 2.1 nM ± 0.1 for paclitaxel, indicating a higher potency of sagopilone to disturb the cell cycle of cancer cells. The EC50 of the aneuploid cell population was identical to the IC50 calculated from proliferation assays. This indicates that the induction of aneuploidy at concentrations under 1 nM is the main reason for the high antiproliferative activity of sagopilone.

Both compounds displayed relatively similar EC50 G2/M increase values of 4.3 nM ± 0.3 and 5.9 nM ± 0.4 for sagopilone and paclitaxel, respectively. This strongly suggests a similar mechanism of mitotic arrest. At concentrations of 20 nM and

higher, no dramatic differences were found in the cell cycle distribution of A549 cells treated with sagopilone or with paclitaxel. Based on cell cycle data, equivalent drug concentrations for further analysis were defined as 2.5 nM sagopilone and 4 nM paclitaxel (termed low concentration), corresponding to the maxima of the aneuploid cells and 40 nM for both compounds, representing the almost maximal amount of G2/M cells (termed high concentration).

Table 6. Comparison of antiproliferative and cell cycle effects of sagopilone and paclitaxel on A549 cells. Cells were treated as previously described (Figure 2, 5, 8). IC50 values are mean ± standard deviations calculated from three independent experiments. Additionally, IC50 of G0/G1 decrease, EC50 of G2/M increase and EC50 of aneuploid cells were calculated from cell cycle plots of A549 cells treated with sagopilone and paclitaxel (Figure 7, 9).

Compound	IC50 proliferation [#]	IC50 G0/G1 decrease [*, #]	EC50 G2/M increase [*, #]	EC50 aneuploid cells [*, #]
sagopilone	0.4 ± 0.2	0.8 ± 0.1	4.3 ± 0.3	0.4 ± 0.2
paclitaxel	5.2 ± 2.3	2.5 ± 0.3	5.9 ± 0.4	2.1± 0.1

[*] calculated from cell cycle plots
[#] nM (mean ± SD)

4.2.4 Comparison of cell cycle effects of different cell lines treated with sagopilone

The effects of sagopilone on the cell cycle were additionally analyzed in other cell lines. Table 7 shows cell cycle data calculated from 7 different cell lines. At very low concentrations (≤ 1.3 nM) the formation of aneuploid cells reached their half maximal induction in all cell lines. This led to a decrease of the G0/G1 cell population with normal 2N DNA content. Higher concentrations of sagopilone caused mitotic arrest.

The results indicate a similar and concentration-dependent effect of sagopilone on the cell cycle of different cell lines. Sagopilone possessed a biphasic mode of action for the different cell lines, with induction of aneuploidy at low concentration followed by mitotic arrest at higher concentrations.

Table 7. Comparison cell cycle effects of sagopilone-treated cell lines. IC50 of G0/G1 decrease, EC50 of G2/M increase and EC50 of sub G1 cells were calculated from cell cycle plots of the indicated cell lines treated with sagopilone for 18 hours. Values are the mean ± standard deviations calculated from three independent experiments.

Cell line	EC50 sub G1 cells #	IC50 G0/G1 decrease #	EC50 G2/M increase #
MDA MB 231	1.0 ± 0.2	2.4 ± 0.4	5.5 ± 0.6
T47D	0.5 ± 0.3	0.8 ± 0.2	5.7 ± 0.7
MCF7	1.3 ± 0.4	2.4 ± 0.3	11.2 ± 1.3
Hela	0.2 ± 0.1	0.7 ± 0.3	5.0 ± 0.3
NCI-H1437	0.3 ± 0.1	1.3 ± 0.3	1.6 ± 0.3
NCI-H23	1.4 ± 0.4	4.8 ± 0.5	8.4 ± 0.5
HCT116	1.1 ± 0.3	7.9 ± 1.0	13.8 ± 1.8

nM (mean ± SD)

4.3 Microscopic analysis of cells treated with sagopilone

4.3.1 Live cell imaging of A549 cells treated with sagopilone

To verify the order of events leading to the variations in cell cycle distribution seen in Figure 5, live cell imaging (LCI) was applied to examine the fate of single cells in a time frame of approximately 26 hours. Using LCI we analyzed A549 cells that were treated either with drug-free medium or with medium containing 2.5 nM or 40 nM sagopilone. Differential interference contrast images were taken in intervals of six minutes (in collaboration with Dr. Stefan Prechtl, Lead Discovery Screening Berlin, Bayer Schering Pharma and Kevin Mittelstaedt, TRG Oncology, Bayer Schering Pharma). Figure 10 A shows the cell division of normal, untreated A549 cells. Most of them exhibit a normal cell division into two daughter cells of similar size within a time period of approximately 3 hours from the first signs of cell rounding to flattened daughter cells. However, few cells showed normal division only at the first glance. The potential progeny cells fused again shortly before completing cell division and appeared as flattened interphase cell. After that, the cell rounded again and attempted to divide a second time. This observation reveals that untreated A549 cells occasionally require more than one attempt to accomplish cell division. In comparison to untreated cells, the incubation with 2.5 nM sagopilone led to markedly delayed

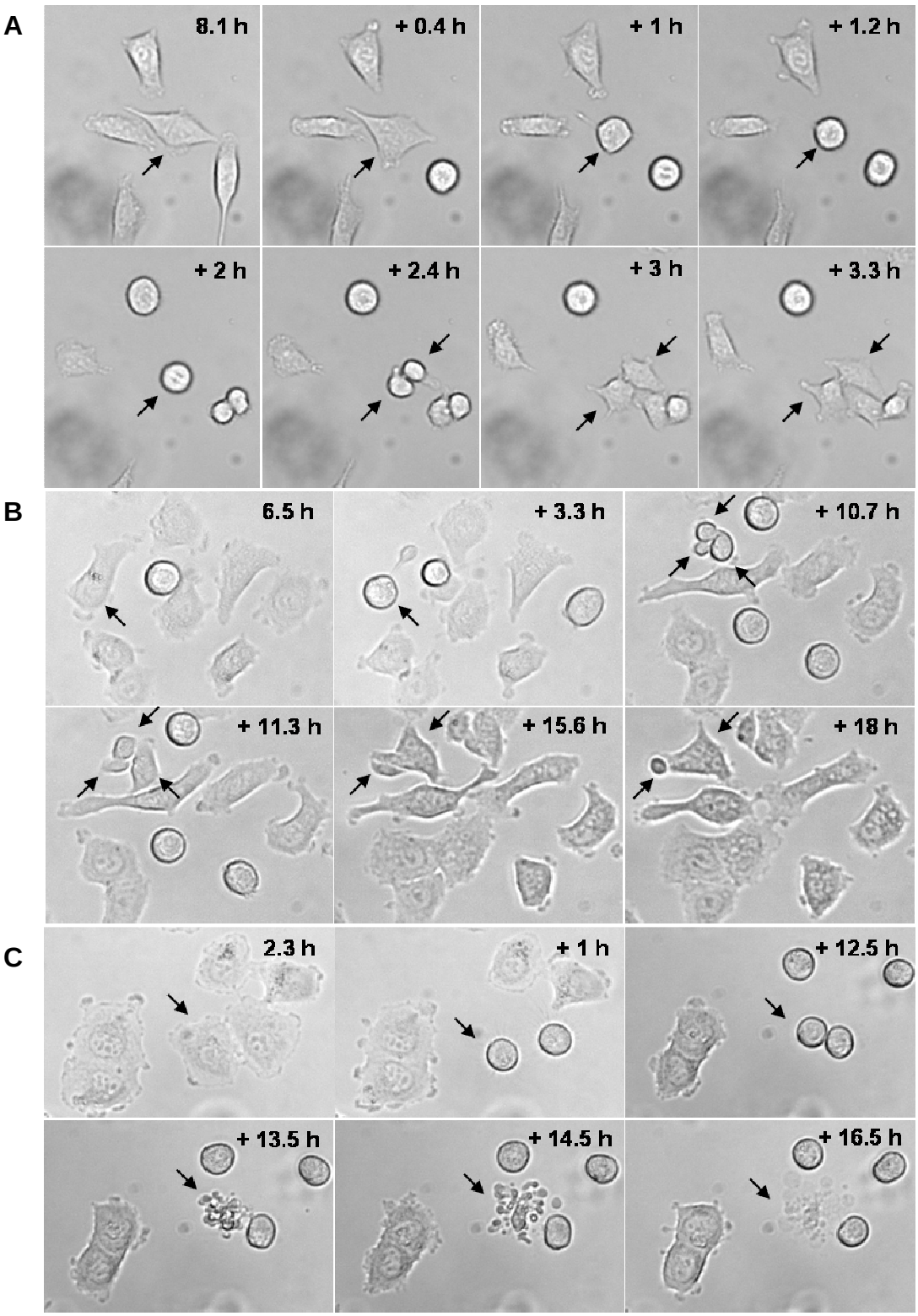

Figure 10. Live cell imaging of A549 cells treated with sagopilone. A549 cells were either **(A)** untreated or incubated with **(B)** 2.5 nM or **(C)** 40 nM sagopilone and analyzed by Nomarski interference contrast microscopy in time intervals of six minutes. The time after drug addition is given in the first image. All subsequent images display the time past until the first picture was recorded (point of drug addition t = 0 h). Arrows indicate the cells of interest.

mitosis followed by an aberrant cell division at 10.7 hours after cell rounding. Such cells seemed to divide into three daughter cells of different sizes. The two larger descendants eventually fused with each other. The smaller descendant did not participate in the fusion process and remained as single cell at 15.6 hours after cell rounding (Figure 10 B). In contrast to the untreated A549 cells, the cells that have arisen through unequal cell division were not found to reattempt cell division in the observed time period. A549 cells treated with 40 nM sagopilone displayed normal cell rounding, but in contrast to the untreated control cells they were arrested in mitosis for about 11.5 hours without showing any signs of cell division (Figure 10 C). However, 13.5 hours after drug addition apoptosis was observed. Many apoptotic blebs were visible outside of the plasma membrane and subsequently appeared scattered in close proximity to the former cell. One larger apoptotic body remained at the center surrounded by numerous blebs.

4.3.2 Aberrant cell division of A549 cells induced by low concentration of sagopilone

Confocal laser scanning microscopy of A549 cells treated with 2.5 nM sagopilone was used to investigate the observations from live cell imaging further (in collaboration with Kevin Mittelstaedt, TRG Oncology, Bayer Schering Pharma). Immunofluorescent staining of α-tubulin and chromosomal DNA was performed. Figure 11 A shows an untreated A549 cell in the metaphase of mitosis. It showed normal bipolar spindles with concentrated microtubules (K-fibers) reaching out towards the kinetochores of the chromosomes and isolated astral microtubules. Only rarely were any structures of the interphase microtubule network observable after its disassembly at the beginning of mitosis. The chromosomes appeared congressed and were aligned at the metaphase plate. At 2.5 nM sagopilone, mitotic A549 cells exhibited an abnormal spindle organization with multiple spindle poles, resulting in the formation of several plates of congressed chromosomes during metaphase (Figure 11 B). Quantitative analysis revealed that multipolar spindles were present in more than 90% of all mitotic cells after 18-hour incubation with 2.5 nM sagopilone.

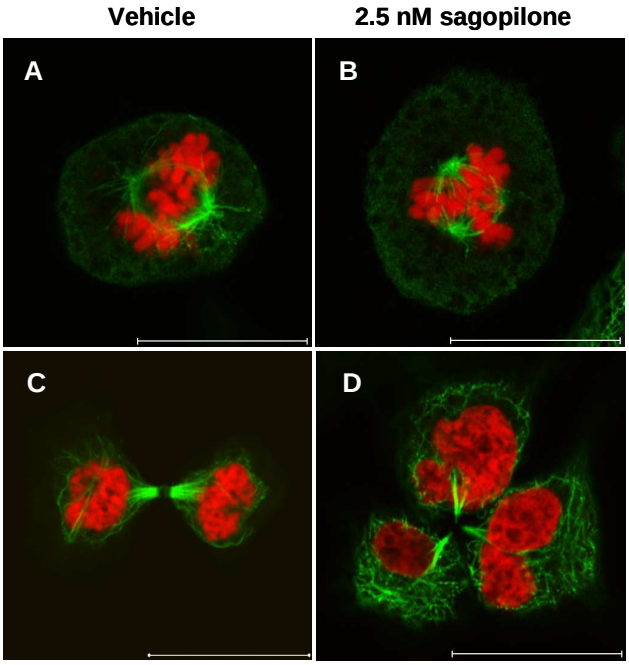

Figure 11. Sagopilone induces aberrant cell division at low concentration. A549 cells were treated either with **(A, C)** vehicle or with **(B, D)** 2.5 nM sagopilone for 18 hours, fixed and stained for α-tubulin and DNA. Fluorescence analysis was performed by confocal laser scanning microscopy. Scale bar, 20 µm.

Figure 11 C shows untreated A549 lung carcinoma cells in the late telophase where cytokinesis is almost complete and the midbodies persisting between the daughter cells. This structure remains as a tether for some time before finally breaking to complete cytokinesis. The daughter cells have similar size and DNA content indicating a proper cell division. A549 cells incubated with 2.5 nM sagopilone seemed to retain the ability to perform chromosome segregation and produced separate daughter cells (Figure 11 B). However, the process of cell division often appeared to occur in an aberrant manner, suggesting the formation of three or more daughter cells of different size and DNA content (Figure 11 D). The midbody structures in between the daughter cells suggest that they have arisen from a common progenitor.

4.3.3 Immunofluorescence staining of MDA MB 231 cells after sagopilone treatment

The effects of sagopilone on the cellular morphology of the breast cancer cell line MDA MB 231 cells were investigated following continuous incubation with the agent for 20 hours. The cell were subjected to immunofluorescence staining of α-tubulin and chromosomal DNA and analyzed by confocal laser scanning microscopy (in collaboration with Kevin Mittelstaedt, TRG Oncology, Bayer Schering Pharma). An untreated population is shown in Figure 12 A. Most of the cells possessed comparable size and DNA content. The majority of the cells were in the interphase of the cell cycle. At larger magnification the cells exhibited a well ramified microtubule network which reached into the protrusions of the cell (Figure 12 D). The nucleus revealed the normal size and shape of untreated cells containing decondensed chromosomes. Untreated mitotic cells (Figure 12 G) showed a normal bipolar spindle and the congressed chromosomes were aligned at the metaphase plate.

Figure 12 B shows MDA MB 231 cells treated with 3 nM sagopilone. Almost no differences could be observed at this magnification. A larger magnification is shown in Figure 12 H. The tubulin cytoskeleton appeared denser and less ramified at the cellular periphery as compared to the vehicle-treated cells (Figure 12 D). The nucleus exhibited multinucleation. At 3 nM sagopilone, mitotic cells exhibited an abnormal spindle organization with multiple spindle poles (>3) and several plates of congressed chromosomes (Figure 12 E).

Figure 12 C shows a population of MDA MB 231 cells treated with 40 nM sagopilone. This resulted in tubulin polymerization in interphase cells, manifested as marked microtubule bundling (Figure 12 F), in contrast to untreated cells, which exhibited a normal microtubule spread (Figure 12 D). The cell depicted in Figure 12 I showed irregular chromosomal alignment. Similarly, multipolar spindles were induced at 40 nM sagopilone. In contrast to low-concentration treatment, single chromosomes or sets of chromosomes were found to be hindered from congressing to the metaphase plate(s).

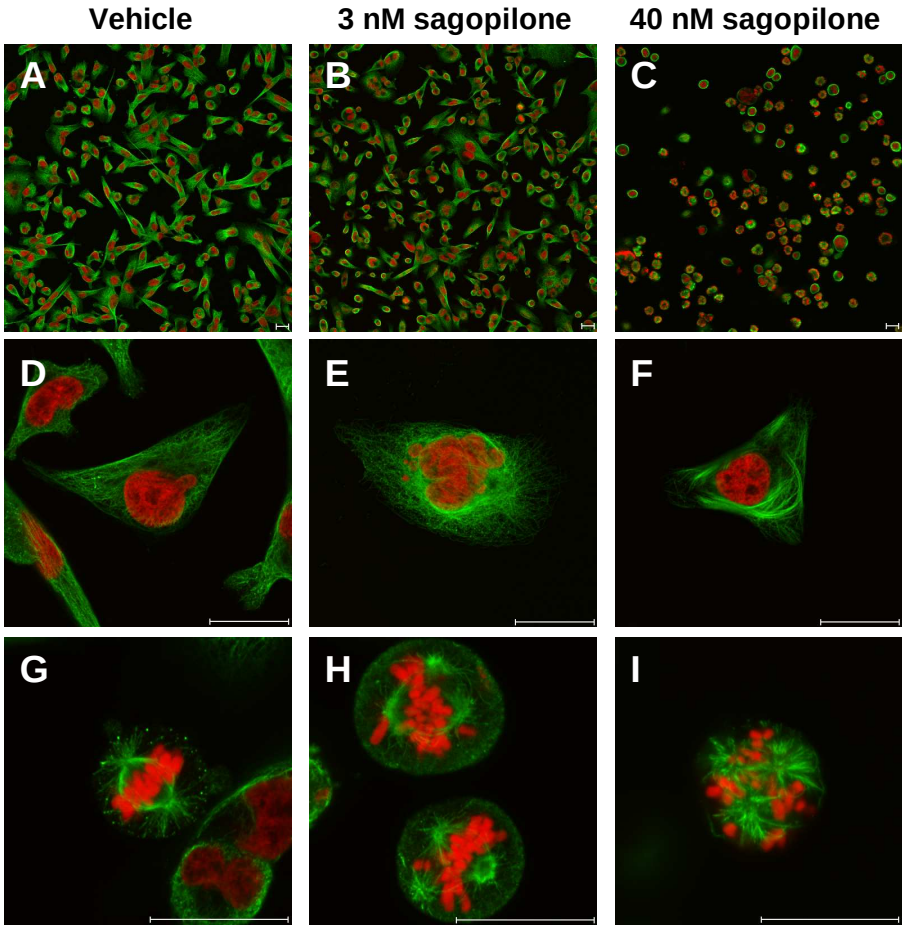

Figure 12. Immunofluorescence analysis of MDA MB 231 breast cancer cells treated with sagopilone. MDA MB 231 cells were incubated with the indicated concentrations of sagopilone for 20 hours. Afterwards, cells were fixed, stained for α-tubulin and DNA, and analyzed by confocal laser scanning microscopy. Scale bar, 20 µm.

4.4 Induction of apoptosis in A549 cells after treatment with sagopilone

In order to analyze long term effects of sagopilone, A549 cells were treated continuously with low concentration (2.5 nM) or high concentration (40 nM) sagopilone for up to 96 hours followed by cell cycle analysis. As depicted in Figure 13, the vehicle-treated A549 cells did not show changes in the cell cycle after 96 hours. In contrast, the low concentration treatment resulted in a decrease of G0/G1 cells and concomitantly in the formation of an aneuploid cell population most apparent after 18 hours. Furthermore, the number of G2/M cells was found to be

elevated after 18 hour treatment. Prolonged incubation times up to 96 hours revealed only minor changes in the cell cycle distribution. The amounts of G0/G1, G2/M and aneuploid cells were nearly constant at these time points. Only a small increase of apoptotic cells with a very low DNA content was observed, noticeable as a peak close to the y-axis. In contrast, cells incubated with 40 nM sagopilone showed a decrease in the G2/M population and underwent massive induction of apoptosis after 96 hours.

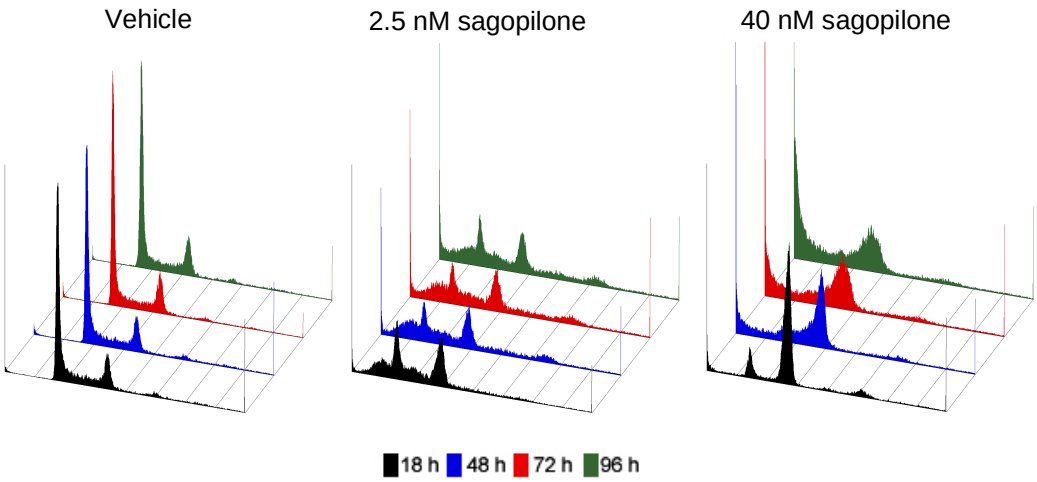

Figure 13. Time course of cell cycle distribution of A549 cells. Cells were incubated with vehicle, 2.5 nM sagopilone or 40 nM sagopilone for the indicated time, fixed and stained with propidium iodide and analyzed by flow cytometry.

Similar results were obtained from an apoptosis assay (Figure 14), which measured the loss of the mitochondrial membrane potential ($\Delta \Psi_m$) and the plasma membrane rupture as markers for programmed cell death. Again, the treatment with low concentrations of sagopilone (2.5, 5, 10 nM) caused only a minor induction of apoptosis of 19.3 % ± 4.6, 22.3 % ± 2.4 and 27.0 % ± 2.6 of cells, respectively, whereas the high concentration treatments (40 and 100 nM) led to pronounced induction of apoptosis in A549 cells (64.1 % ± 1.3 and 59.4 % ± 2.4 of cells, respectively).

In summary, low concentration treatments of A549 cells resulted only in marginal induction of apoptosis whereas high-concentration treatments caused a massive induction of apoptosis.

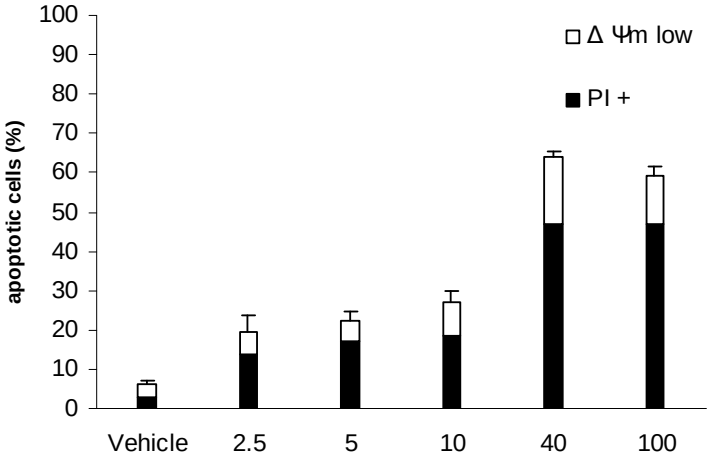

Figure 14. Apoptosis induction of A549 cells. A549 cell were incubated with growth medium containing either 0 to 100 nM sagopilone for 72 hours. The cells were harvested, stained with DiOC6(3) and propidium iodide for cytometer based detection of apoptosis-associated mitochondrial membrane potential dissipation (Δ Ψm low) and plasma membrane rupture (PI +).White and black bars indicate the mean percentage of cells (n = 3) characterized by Δ Ψm loss alone and in combination with plasma membrane breakdown (PI+), respectively. White and black bars indicate the mean percentage of cells (n = 3) characterized by Δ Ψm loss alone and in combination with plasma membrane breakdown (PI+), respectively.

4.5 Genome-wide gene expression study of A549 cells treated with sagopilone and paclitaxel

4.5.1 Objective of the gene expression study

In order to analyze the effects of the microtubule-stabilizing drugs sagopilone and paclitaxel, a gene expression profiling study was performed. The objectives of the study were to define and to compare the gene regulation patterns induced by high and low concentration sagopilone or paclitaxel. One focus of interest was on signal transduction pathways activated in response to either agent and their possible involvement in resistance to chemotherapy. The study was performed in collaboration with Dr. Anette Sommer, Target Research Berlin, Bayer Schering Pharma AG.

The study was conducted in the human non-small cell lung cancer (NSCLC) cell line A549 cell, which had been thoroughly analyzed in previous experiments. Based on those data two concentrations of either drug were chosen. One corresponds to the concentration that induces an aneuploid cell population, i.e. 2.5 nM sagopilone and 4

nM paclitaxel, and the other represents the concentration that induces a mitotic arrest, i.e. 40 nM sagopilone and 40 nM paclitaxel. RNA was isolated from 5 biological replicate plates after 18 hours treatment and the RNA was transcribed into cRNA and hybridized onto Affymetrix GeneChip HG-U133Plus2.0 arrays. The probe intensities on each array were summarized with the MAS5.0 summarization algorithm and the refined and summarized data were loaded into the CoBi database (Genedata, Basel, Switzerland). Analysis of the probeset-specific signal intensities was performed with the Expressionist Pro 4.0 Analyst software (Genedata). The data set was Lowess (locally weighted scatter plot smoothing) normalized. The Genedata software was used for principal component analysis, 2D-hierarchical clustering and statistical tests. Pathway analyses were performed with the GeneGo Metacore database and software tools.

4.5.2 Unsupervised Analysis

The principle component analysis (PCA) depicts the variance in gene expression profiles among samples. In the three-dimensional representation, the distance between two plotted spheres is inversely proportional to the degree of similarity between the gene expression profiles of the two groups using all probe sets on the Affymetrix GeneChips.

The PCA revealed two main clusters. Untreated, vehicle-treated and low concentration paclitaxel and sagopilone treatment groups clustered together. Distinct from that cluster, high concentration paclitaxel and sagopilone treatment groups formed a separate cluster (Figure 15), indicating that treatment with low drug concentration induced only relatively small gene expression changes as compared to the untreated samples, whereas a high drug concentration induced stronger gene expression changes.

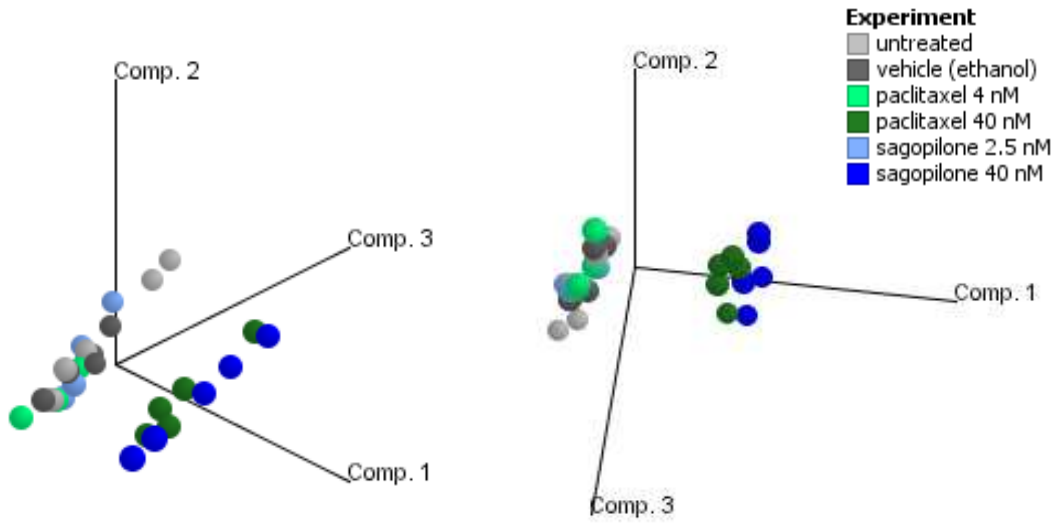

Figure 15. Principle Component Analysis (PCA) of A549 cell expression profiles. Views from two different angles are shown to better indicate the nature of the clustering. Samples are colored according to treatment with the microtubule-stabilizing drugs. Each plotted sphere represents the expression profile of an individual sample based on the projection of the data on the first three principal components, accounting for most of the variability in the data (labeled axes). Ethanol treatment was used as vehicle control.

4.5.3 Volcano plot

In order to investigate changes in gene expression of A549 cells treated for 18 hours either with 2.5 or 40 nM sagopilone, or 4 or 40 nM paclitaxel, T-tests comparing each treatment group with the vehicle-treated group were performed. The results are shown in a Volcano plot (Figure 16) depicting the significance as a function of the fold change. The p-value and the fold change parameters of the high and low concentration treatments of both compounds are given in Table 8 together with the total number and the number of up- and down-regulated genes obtained with the specific parameters from the Volcano plot.

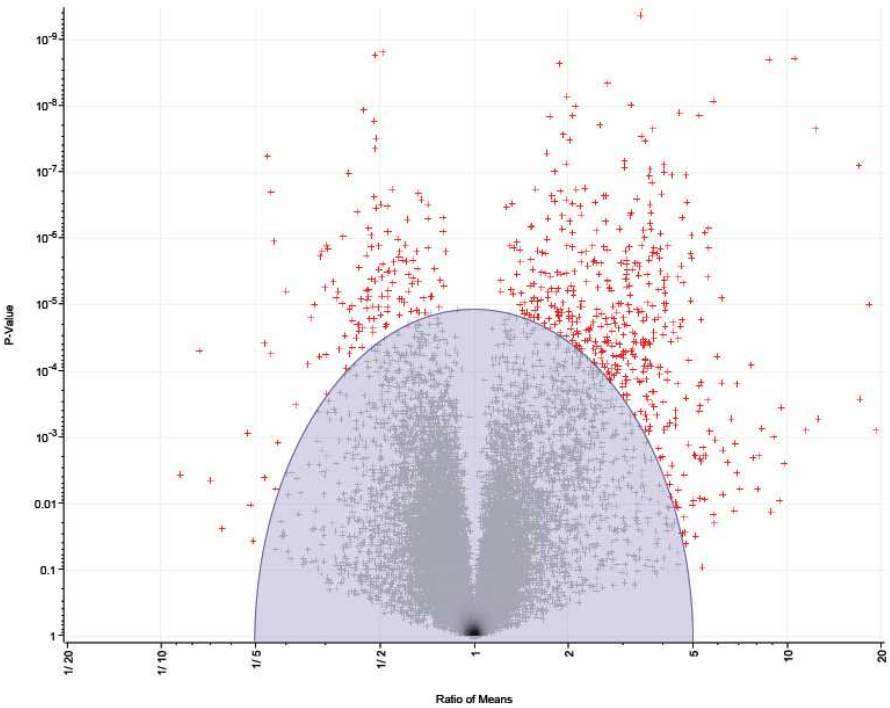

Figure 16. Volcano plot from T-test of 40 nM sagopilone vs. vehicle (threshold: >5-fold change, p-value <1x10^{-5}). The Volcano plot depicts the significance as a function of the fold change. Thus, highly significant genes with a low fold change as well as genes which possess a high fold change and a relatively low significance were indicated in red. Thresholds for the Volcano plots were defined as ellipse with >5-fold change and p-value <1x10^{-5} from T-test for 40 nM sagopilone and paclitaxel and for 2.5 nM sagopilone and 4 nM paclitaxel as ellipse with >3-fold change and p-value <5x10^{-3}.

Table 8. Gene regulation. Shown is the number of genes that were either up- or down-regulated obtained from Volcano plots (similar to the one shown in Figure 16) using specific parameters for p-value and fold change.

treatment	p-value	fold change	regulated genes	up-regulated	down-regulated
4 nM pac vs. vehicle	≤ 5x10^{-3}	≥ 3	158	83	75
2.5 nM sag vs. vehicle	≤ 5x10^{-3}	≥ 3	221	110	111
40 nM pac vs. vehicle	≤ 1x10^{-5}	≥ 5	503	403	100
40 nM sag vs. vehicle	≤ 1x10^{-5}	≥ 5	593	455	138

4.5.4 Supervised analysis

Gene lists from statistical tests were compared using Venn diagrams (Figure 17). Gene lists originate from Volcano plots (Figure 16) using the software Expressionist (Genedata). More genes are regulated by high concentration than low concentration treatment of paclitaxel or sagopilone. The overlap between high concentration

sagopilone versus vehicle and low concentration sagopilone versus vehicle accounted for 41 genes and the overlap between high concentration paclitaxel versus vehicle and low concentration paclitaxel accounted for only 9 genes, indicating that high and low concentration treatment induced and repressed completely different gene sets (Figure 17 A, B). Comparing the low concentration treatment of sagopilone with the one of paclitaxel, only 30 genes exhibited the same pattern of regulation. This implies a different gene regulation at low concentration drug treatment (Figure 17 C). In contrast, high concentration incubation led to an overlap of 391 genes (Figure 17 D), indicating a very similar mechanism of action at high concentration for both microtubule-stabilizing compounds.

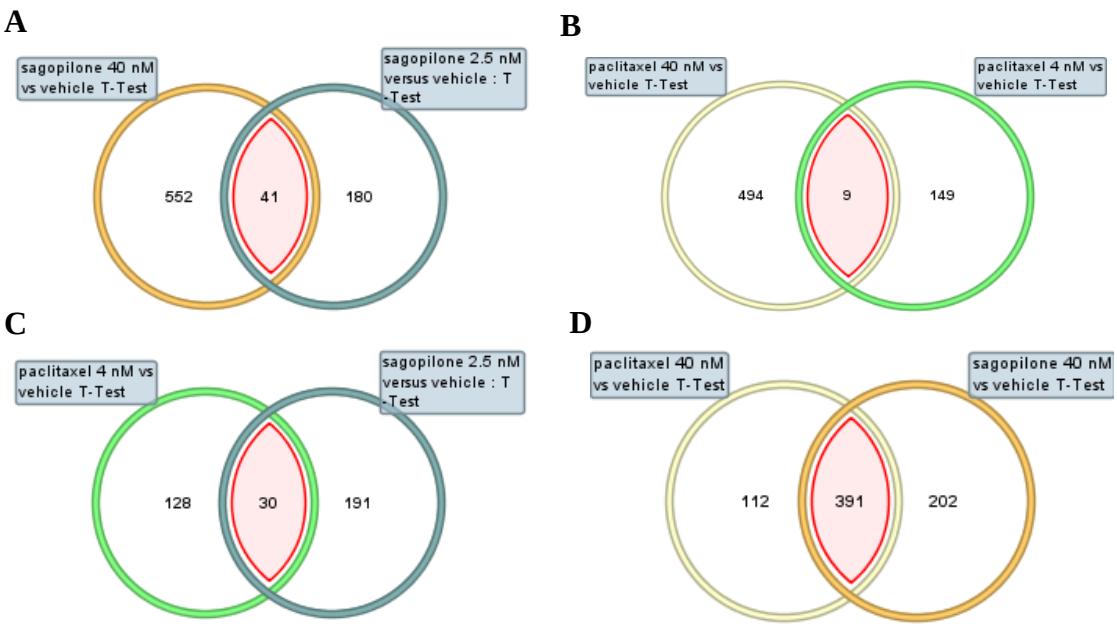

Figure 17. **Analysis of A549 cells expression differences between sagopilone and paclitaxel at low and high concentration treatments.** Circles in the Venn diagram correspond to differences at the specified treatment and overlapping regions indicate genes collectively regulated by the corresponding treatment. The indicated genes were previously found to be significantly regulated in a Volcano plot (Figure 16).

4.5.5 Two-Dimensional hierarchical clustering

In order to visualize the differential gene expression pattern of A549 cells treated for 18 hours either with 2.5 or 40 nM sagopilone, or 4 or 40 nM paclitaxel, T-tests

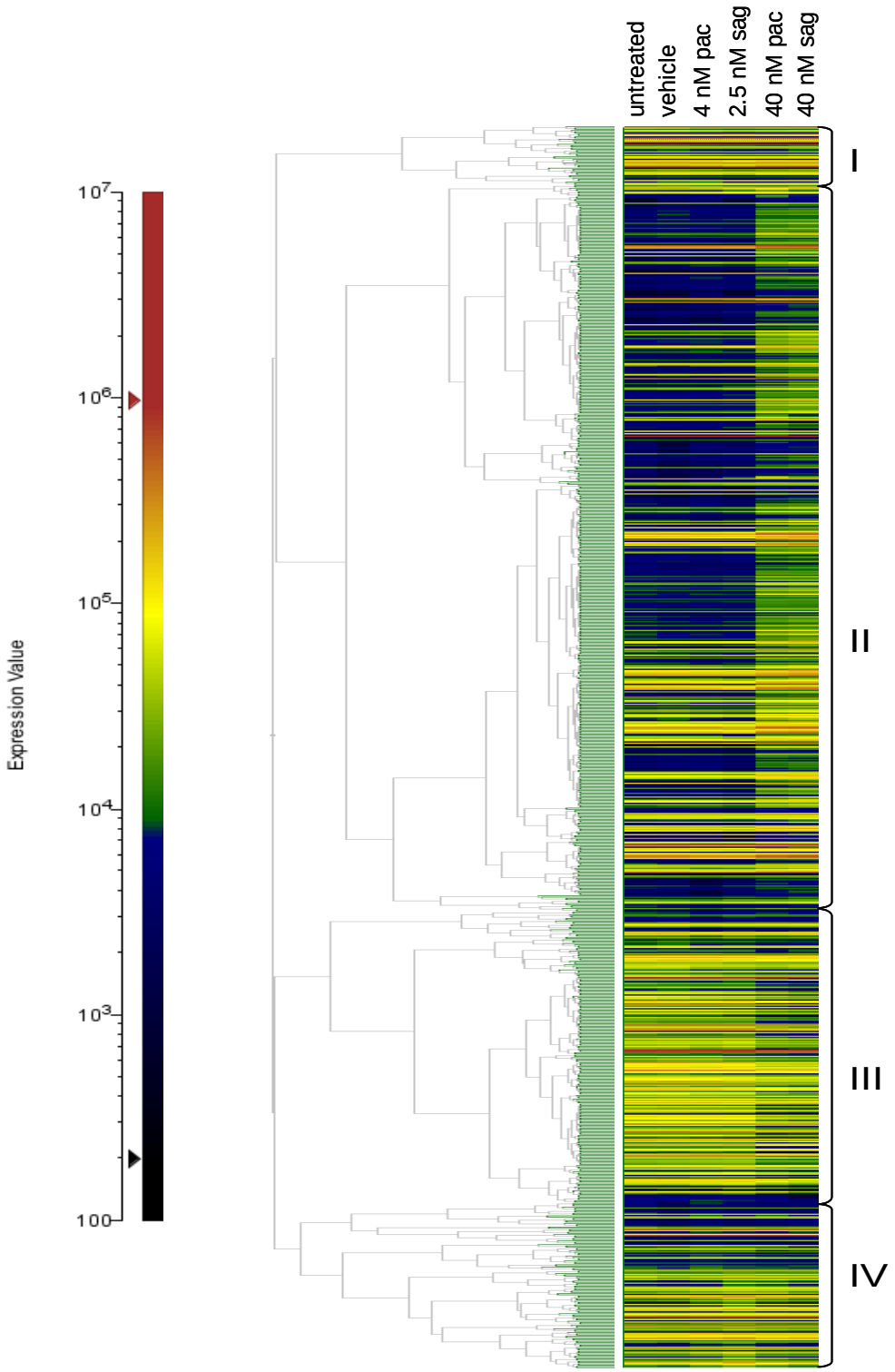

Figure 18. 2D Hierarchical clustering analysis. Hierarchical clustering analysis was performed on the combined list of 990 genes significantly regulated by sagopilone (sag) and paclitaxel (pac) (Volcano plot: >5x-fold change and p-value $<1x10^{-5}$ from T-test for 40 nM sag and pac; for 2.5 nM sag and 4 nM pac >3-fold change and p-value $<5x10^{-3}$). Each row represents a single gene, and each column represents the average of five independent experiments. Expression values are indicated by different colors. Black squares represent low gene expression. Gene expression increases from blue to red as depicted in the scale bar. The tree branches indicate the correlation between genes based on their expression data.

comparing each treatment group with the vehicle-treated group were performed (Table 8). The four different gene lists were united and subjected to clustering analysis. The combined list comprises 990 significantly regulated genes. To identify clusters of similarly regulated genes for sagopilone and paclitaxel, two-dimensional hierarchical clustering analysis was performed using gene expression data based on pairwise comparisons (treatment versus vehicle) (Figure 18). The dendrogram split into four main branches. Cluster I comprised 47 genes that were up-regulated by vehicle. In the next clusters genes were found that were either markedly increased (cluster area II) or substantially decreased (cluster area III) after high concentration sagopilone and paclitaxel. Cluster II and III accounted for 811 of 990 genes, confirming the previously reported observation that high concentration of both compounds induced strong gene expression changes (Figure 18). 132 genes that were up-regulated by 4 nM paclitaxel and 2.5 nM sagopilone formed Cluster IV. To summarize, the differentially expressed genes fell into 4 main clusters when using 2D hierarchical clustering on all samples.

4.5.6 Pathway analysis of genes regulated by paclitaxel and sagopilone

Differentially regulated genes obtained from Volcano plots (Figure 16 and Table 8) were subjected to GeneGo pathway analysis. Figure 19 A shows the pathway map "G2/M phase and mitosis". Interestingly, genes involved in G2/M phase transition and mitosis, like Cyclin A, Cyclin B, Nek2A and Securin (Sullivan and Morgan, 2007; Nigg, 2001) were up-regulated after treatment with high concentration sagopilone and paclitaxel (experiment 3, 4).

A

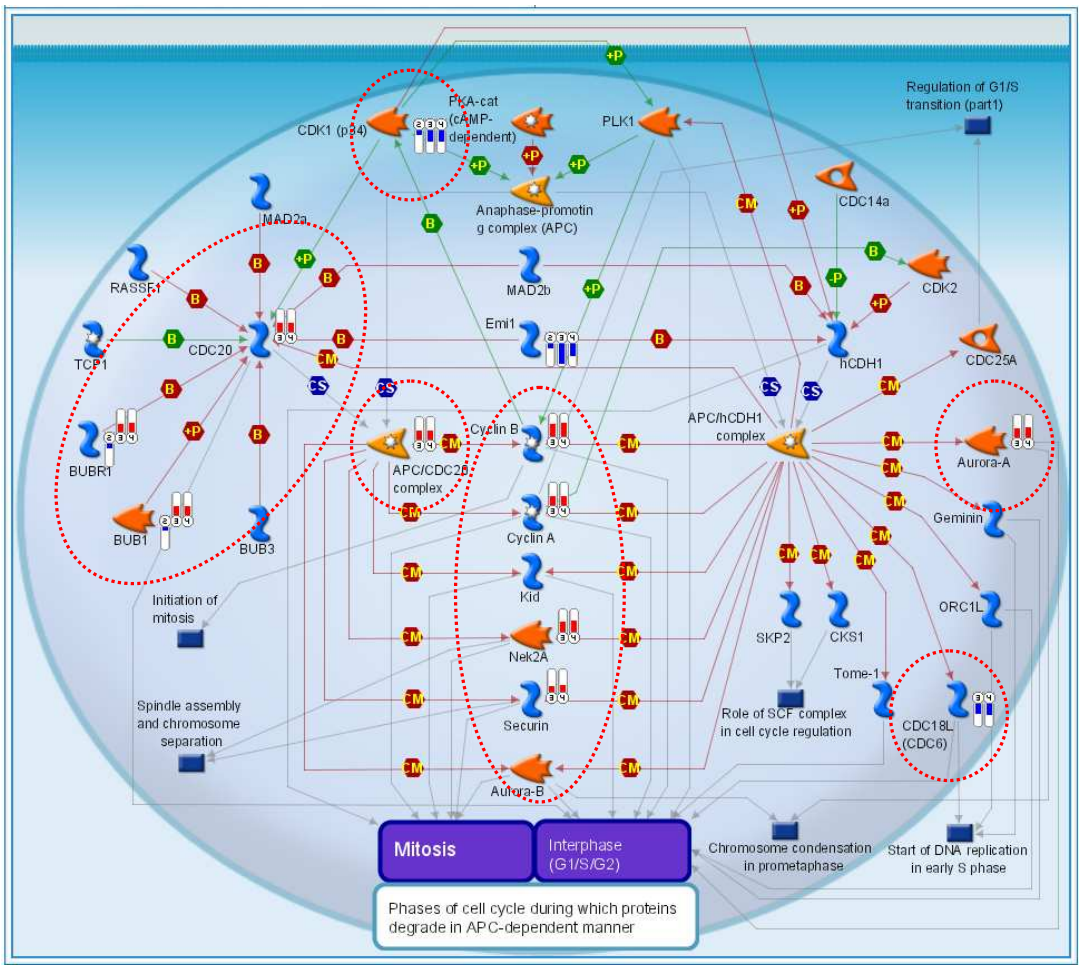

B

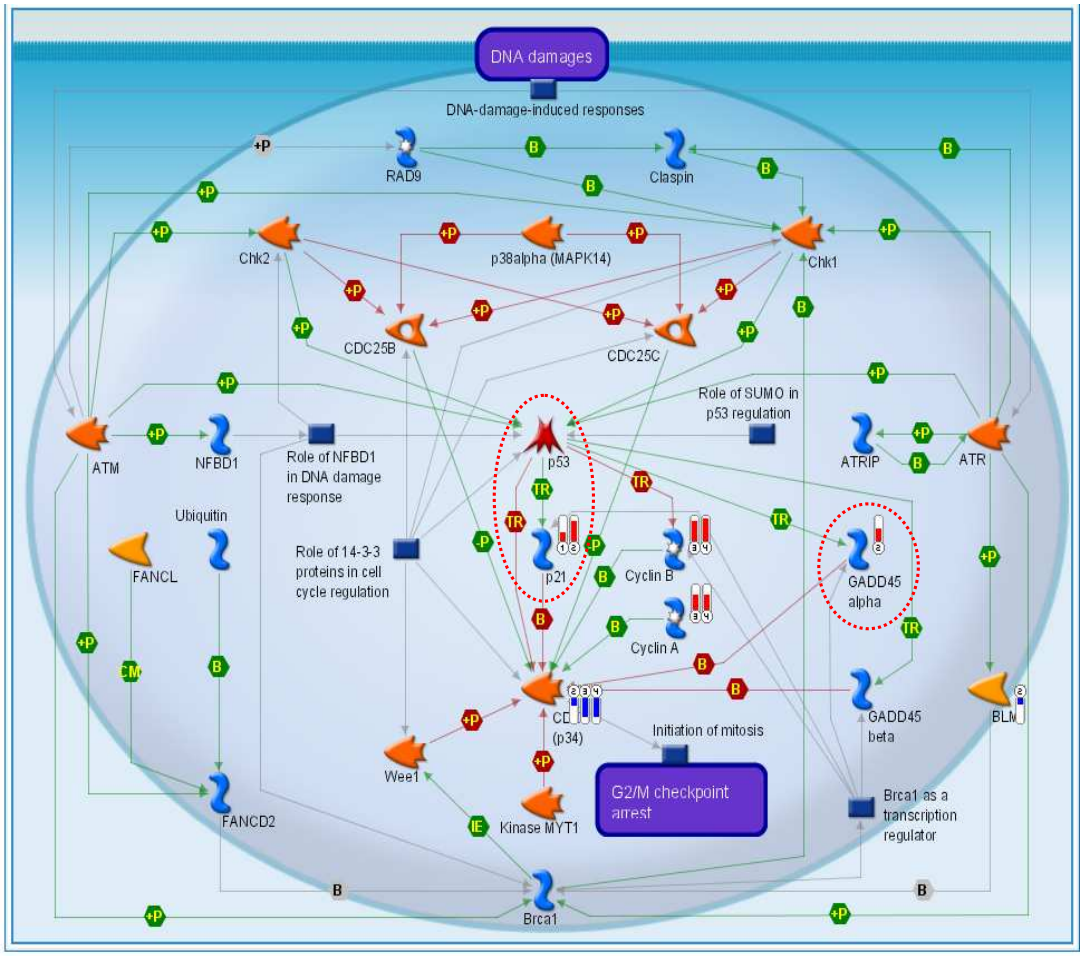

Figure 19. MetaCore pathway analysis. Influences of sagopilone and paclitaxel on genes related to **(A)** G2/M Phase and Mitosis and **(B)** ATM/ATR regulation of G2/M checkpoint were analyzed via MetaCore pathway analysis tool. Red and blue bars represent fold changes of gene expression levels significantly up- or down-regulated, respectively (Volcano plot: >5-fold change and p-value $<1x10^{-5}$ from T-test for 40 nM sagopilone and paclitaxel; for 2.5 nM sagopilone and 4 nM paclitaxel >3-fold change and p-value $<5x10^{-3}$). The number below the red and blue bars indicated the order of experiments, (1) 4 nM paclitaxel; (2) 2.5 nM sagopilone; (3) 40 nM paclitaxel; (4) 40 nM sagopilone.

CDK1, which is essential for G1/S and G2/M phase transitions of eukaryotic cells, is down-regulated in the high concentration sagopilone and paclitaxel treatment groups and slightly decreased after incubation with 2.5 nM sagopilone. Additionally, genes such as BUB1, BUBR1 and CDC20, which are components of the spindle assembly checkpoint (SAC) (Musacchio and Salmon, 2007), were up-regulated upon incubation with high concentration of both microtubule-stabilizing agents (Figure 19 A). In contrast, sagopilone low concentration treatment showed a slight down regulation of

BUB1 and BUBR1. Table 9 displays a list of regulated genes in response to high concentration sagopilone and paclitaxel. Statistically significant genes were chosen according to their involvement in G2/M phase transition and mitosis (for criteria of selection see explanation Table 9).

Table 9. Gene expression in response to high concentration treatment of sagopilone and paclitaxel. Expression data (Affymetrix) of genes, involved in G2/M transition and mitosis, significantly up- or down-regulated in A549 cells after incubation with 40 nM sagopilone (sag) or 40 nM paclitaxel (pac). Statistical significance was assessed by pairwise comparisons of treatment versus vehicle and was depicted in a Volcano plot (>5-fold change, p-value $<1x10^{-5}$). Genes which meet the criteria were further selected according to their Gene Ontology classification cell cycle, mitosis or cytokinesis. Statistical significance level $p<0.001$. n.c. = no change.

Identifier	Gene Name	Gene Symbol	Fold Change 40 nM sag	Fold Change 40 nM pac
232588_at	stromal antigen 1	STAG1	12.50	11.37
207331_at	centromere protein F, 350/400ka (mitosin)	CENPF	5.59	5.25
232466_at	Cullin 4A	CUL4A	4.90	4.66
1556339_a_at	Ubiquitin-activating enzyme E1C (UBA3 homolog, yeast)	UBE1C	4.03	3.89
215623_x_at	SMC4 structural maintenance of chromosomes 4-like 1 (yeast)	SMC4L1	3.97	3.75
244427_at	Kinesin family member 23	KIF23	3.92	3.33
233940_at	Echinoderm microtubule associated protein like 4	EML4	3.51	3.20
242362_at	Cullin 3	CUL3	2.74	n.c.
228729_at	cyclin B1	CCNB1	2.52	2.35
204641_at	NIMA (never in mitosis gene a)-related kinase 2	NEK2	2.25	2.09
221258_s_at	kinesin family member 18A	KIF18A	n.c.	2.09
218755_at	kinesin family member 20A	KIF20A	2.09	1.93
236974_at	Cyclin I	CCNI	2.01	n.c.
209408_at	kinesin family member 2C	KIF2C	1.97	1.84
208079_s_at	serine/threonine kinase 6 (aurora kinase A)	STK6	1.96	1.86
209642_at	BUB1 budding uninhibited by benzimidazoles 1 homolog	BUB1	1.92	1.69
202870_s_at	CDC20 cell division cycle 20 homolog (S. cerevisiae)	CDC20	1.91	1.79
203755_at	BUB1 budding uninhibited by benzimidazoles 1 homolog beta	BUB1B	1.91	1.69
204170_s_at	CDC28 protein kinase regulatory subunit 2	CKS2	1.86	1.81
203418_at	cyclin A2	CCNA2	1.86	1.84
210052_s_at	TPX2, microtubule-associated protein homolog (Xenopus laevis)	TPX2	1.75	1.67
218355_at	kinesin family member 4A	KIF4A	1.71	1.57
202705_at	cyclin B2	CCNB2	1.65	1.64
203554_x_at	pituitary tumor-transforming 1 (Securin)	PTTG1	1.52	1.50
209714_s_at	cyclin-dependent kinase inhibitor 3	CDKN3	1.50	n.c.
223394_at	SERTA domain containing 1	SERTAD1	n.c.	1.35
203967_at	CDC6 cell division cycle 6 homolog (S. cerevisiae)	CDC6	0.48	0.49
213523_at	cyclin E1	CCNE1	0.46	0.44
210559_s_at	cell division cycle 2, G1 to S and G2 to M	CDC2	n.c.	0.46
203213_at	cell division cycle 2, G1 to S and G2 to M	CDC2	0.42	n.c.
202107_s_at	MCM2 minichromosome maintenance deficient 2	MCM2	0.45	0.49
201930_at	MCM6 minichromosome maintenance deficient 6	MCM6	0.44	0.45
205296_at	retinoblastoma-like 1 (p107)	RBL1	0.36	0.40
205034_at	cyclin E2	CCNE2	0.22	0.24

Most of the up- and down regulated genes exhibited a very similar pattern of regulation by sagopilone and paclitaxel, indicating a similar mechanism of action after high concentration incubation. In summary, the gene regulation mirrors the state of mitotic arrest, with an activated SAC and up-regulated genes involved in G2/M phase transition and mitosis after treatment with high concentration sagopilone and paclitaxel.

The pathway “ATM (ataxia telangiectasia mutated)/ATR (ataxia telangiectasia and Rad3 related) regulation of G2/M checkpoint” is displayed in Figure 19 B. Genes, such as p21 (CDKN1A), which arrest the cell cycle at the G1 phase and GADD45A, which mediates the activation of the p38/JNK pathway, were found to be up-regulated after incubation with low concentration paclitaxel and sagopilone (experiment 1, 2). Furthermore, numerous genes which are direct transcriptional targets of p53 (Riley et al., 2008) displayed up-regulation after incubation with low concentration of both agents (Table 10). However, A549 cells treated with 2.5 nM sagopilone showed a more pronounced up-regulation of p53 target genes compared to cells treated with 4 nM paclitaxel. In detail, the antiproliferative gene BTG2, the apoptosis-inducing Fas receptors (CD95), as well as Bax, the proapoptotic member of the Bcl-2 family, were found to be up regulated by low concentration sagopilone and paclitaxel. In summary, the gene regulations observed after low concentration sagopilone and paclitaxel treatment indicate a p53 transactivation.

Table 10. Gene expression in response to low concentration treatment of sagopilone and paclitaxel. Table shows gene expression data (Affymetrix) of p53 target genes significantly up-regulated in A549 cells after incubation with 2.5 nM sagopilone (sag) or 4 nM paclitaxel (pac). Statistical significance was assessed by pairwise comparisons of treatment versus vehicle and was depicted in a Volcano plot (>3-fold change, p-value $<5x10^{-3}$). Genes, which meet the criteria, were further selected according to their transcriptional activation by p53 (Riley et. al., 2008). Statistical significance level $p<0.05$. n.c. = no change.

Identifier	Gene Name	Gene Symbol	Fold Change 2.5 nM sag	Fold Change 4 nM pac
225912_at	tumor protein p53 inducible nuclear protein 1	TP53INP1	2.82	1.90
217373_x_at	Mdm2, transformed 3T3 cell double minute 2	MDM2	2.47	n.c.
202284_s_at	cyclin-dependent kinase inhibitor 1A (p21, Cip1)	CDKN1A	2.30	1.44
215719_x_at	Fas (TNF receptor superfamily, member 6)	FAS	2.20	1.32
201236_s_at	BTG family, member 2	BTG2	2.18	n.c.
207813_s_at	ferredoxin reductase	FDXR	1.79	1.34
203725_at	growth arrest and DNA-damage-inducible, alpha	GADD45A	1.64	n.c.
227345_at	tumor necrosis factor receptor superfamily, member 10d	TNFRSF10D	1.57	n.c.
219628_at	p53 target zinc finger protein	WIG1	1.51	n.c.
223342_at	ribonucleotide reductase M2 B (TP53 inducible)	RRM2B	1.47	n.c.
208478_s_at	BCL2-associated X protein	BAX	n.c.	1.29
203409_at	damage-specific DNA binding protein 2, 48kDa	DDB2	1.29	1.30
209295_at	tumor necrosis factor receptor superfamily, member 10b	TNFRSF10B	1.28	n.c.
1563016_at	Acetyl-Coenzyme A carboxylase alpha	ACACA	0.21	0.70

4.5.7 DNA damage genes regulated in response to sagopilone and paclitaxel

Interestingly, genes involved in DNA damage response pathways were found to be up regulated after incubation with high concentration sagopilone and paclitaxel (Table 11). Genes, such as the human DNA Polymerase epsilon (POLE), which is implicated in DNA replication, recombination and repair (Popanda and Thielmann, 1992) or G22P1 (XRCC6) and XRCC5, which both form a nuclear complex involved in the repair of non-homologous DNA ends resulting from double-strand breaks, transpositions, and V(D)J recombination (Jin and Weaver, 1997), were found to be up-regulated by high concentration treatment of both agents. In contrast, low concentration incubation with sagopilone mostly down-regulated genes involved in DNA damage repair. Again, treatment with 4 nM paclitaxel showed a less distinctive gene regulation than 2.5 nM sagopilone. Four DNA damage response genes were identified as being up-regulated by 2.5 nM sagopilone, with two of them (BTG2, GADD45A) turning out to be transcriptional targets of p53 (Table 10). These results indicate that high concentration treatment of A549 cells with sagopilone or paclitaxel led to strong activation of genes involved in response to DNA damage.

Table 11. Expression of DNA damage response genes after incubation with sagopilone and paclitaxel. Genes significantly up- or down-regulated in A549 cells after incubation with **(A)** 40 nM sagopilone (sag) and 40 nM paclitaxel (pac) or **(B)** 2.5 nM sag and 4 nM pac (Table 8) were further selected using the search phrases “DNA damage”, “double strand breaks”, “DNA repair” and “excision repair” in their Gene Ontology classification. Statistical significance level $p<0.01$. n.c. = no change.

A

Identifier	Gene Name	Gene Symbol	Fold Change 40 nM sag	Fold Change 40 nM pac
1560509_at	Polymerase (DNA directed), epsilon	POLE	5.88	4.24
237133_at	Sterile alpha motif and leucine zipper containing kinase AZK	ZAK	3.88	4.38
215308_at	Thyroid autoantigen 70kDa (Ku antigen)	G22P1	3.37	3.16
232633_at	X-ray repair complementing defective repair in Chinese hamster cells 5	XRCC5	3.02	2.82
207746_at	polymerase (DNA directed), theta	POLQ	2.66	2.43
204317_at	G-2 and S-phase expressed 1	GTSE1	2.18	n.c.
211040_x_at	G-2 and S-phase expressed 1	GTSE1	n.c.	1.99
203554_x_at	pituitary tumor-transforming 1	PTTG1	1.52	1.50
208808_s_at	high-mobility group box 2	HMGB2	1.51	n.c.
204767_s_at	flap structure-specific endonuclease 1	FEN1	n.c.	0.59
205698_s_at	mitogen-activated protein kinase kinase 6	MAP2K6	0.48	0.52

B

Identifier	Gene Name	Gene Symbol	Fold Change 2.5 nM sag	Fold Change 4 nM pac
218346_s_at	sestrin 1	SESN1	2.32	1.43
201236_s_at	BTG family, member 2	BTG2	2.18	n.c.
203725_at	growth arrest and DNA-damage-inducible, alpha	GADD45A	1.64	n.c.
203409_at	damage-specific DNA binding protein 2, 48kDa	DDB2	1.29	1.30
214426_x_at	chromatin assembly factor 1, subunit A (p150)	CHAF1A	0.87	n.c.
201589_at	SMC1 structural maintenance of chromosomes 1-like 1 (yeast)	SMC1L1	n.c.	0.89
205909_at	polymerase (DNA directed), epsilon 2 (p59 subunit)	POLE2	0.82	n.c.
205733_at	Bloom syndrome	BLM	0.77	n.c.
204603_at	exonuclease 1	EXO1	0.73	n.c.
204558_at	RAD54-like (S. cerevisiae)	RAD54L	0.71	n.c.
221703_at	BRCA1 interacting protein C-terminal helicase 1	BRIP1	0.67	n.c.
235478_at	DNA cross-link repair 1C (PSO2 homolog, S. cerevisiae)	DCLRE1C	n.c.	1.94
204767_s_at	flap structure-specific endonuclease 1	FEN1	0.76	n.c.

4.6 Validation of Affymetrix gene expression study results

4.6.1 Validation of genes differentially expressed at low concentration sagopilone and paclitaxel

Figure 20 display gene expression analysis conducted by real time PCR from A549 cells treated with various concentrations of sagopilone and paclitaxel for 18 hours. The genes chosen for validation (p21, FAS, GADD45A, MDM2 and p53) are transcriptional targets of p53 and p53 itself. At 5 nM sagopilone the p21 gene expression reached the maximum of 2.7 ± 0.2 fold induction versus vehicle (Figure 20 A). The treatment with paclitaxel resulted in a similar curve shape. However, it appeared shifted towards higher concentrations, indicating the lower potency of paclitaxel. 10 nM paclitaxel induced the maximal p21 gene expression (3.2 ± 0.4 fold). The analysis of gene expression of p53 revealed no significant changes after treatment with sagopilone or paclitaxel at the transcript level (Figure 20 B). Figure 20 C showed increased protein expression levels of p53 after treatment with 1 to 10 nM sagopilone, with maximal levels at 5 and 10 nM sagopilone. The p21 protein expression was found to be elevated at the same concentrations. Paclitaxel treatment resulted in elevated expression levels of p53 at 2.5 to 20 nM with a maximal level at 10 nM.

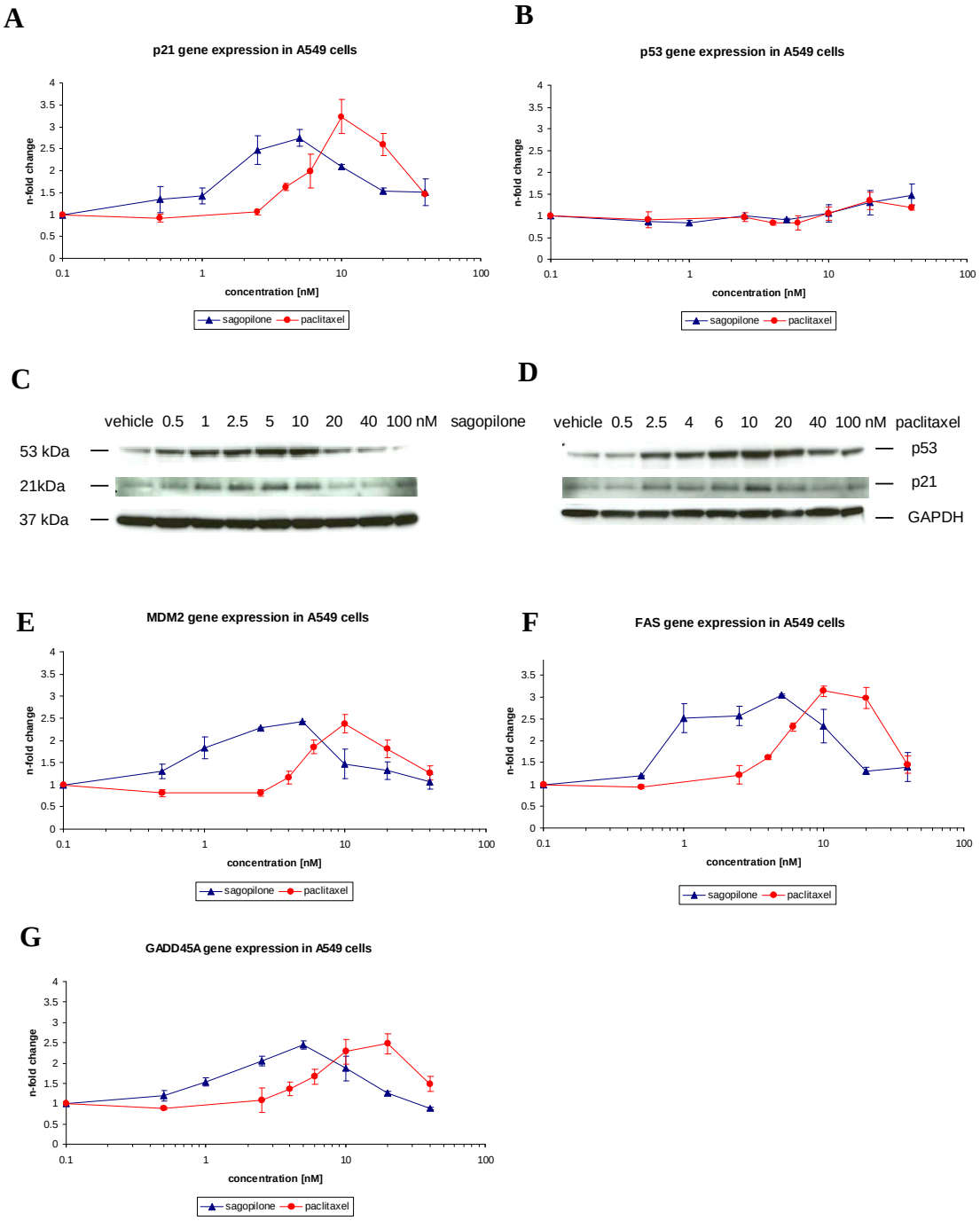

Figure 20. Regulation of p53 target genes by sagopilone and paclitaxel. A549 cells were incubated continuously with medium containing increasing concentrations of either drug for 18 hours and were subjected to RNA and protein extraction. Expression of **(A)** p21 ,**(B)** p53, **(E)** MDM2, **(F)** FAS and **(G)** GADD45A was determined by real time PCR (TaqMan). Shown is the average of three independent experiments and standard deviations. A549 cells, incubated with **(C)** sagopilone and **(D)** paclitaxel were subjected to protein extraction. Isolated protein was separated using SDS polyacrylamide gel electrophoresis, transferred to a PVDF membrane and probed with antibodies recognizing p53, p21 and GAPDH, respectively.

The p21 protein levels displayed an increase at similar concentrations of paclitaxel (Figure 20 D). Gene expression of MDM2, FAS and GADD45A in response to sagopilone and paclitaxel are depicted in Figure 20 E, F and G. The gene expression values showed a significant increase in the range of the low-concentration (1-10 nM), whereas concentrations exceeding 10 nM sagopilone resulted in lower induction of MDM2, FAS and GADD45A expression. Similar results were obtained for paclitaxel, but at higher concentrations.

4.6.2 Validation of genes differentially expressed at high concentration sagopilone and paclitaxel

High concentration treatment (40 nM) of sagopilone and paclitaxel led to mitotic arrest in the majority of the cells. Therefore the expression levels of genes involved in mitosis were analyzed. Figure 21 shows that high concentrations of both drugs markedly up-regulated gene expression and protein expression of Cyclin B1 and BUBR1.

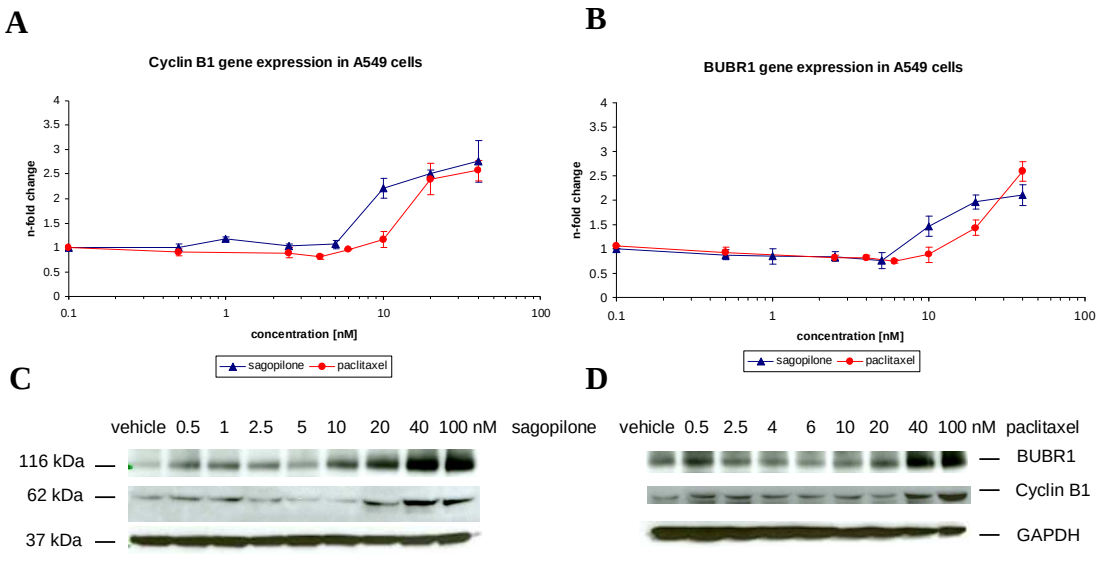

Figure 21. Regulation of Cyclin B1 and BUBR1 by sagopilone and paclitaxel. A549 cells were incubated continuously with medium containing increasing concentrations of both agents for 18 hours and were subjected to RNA extraction. After performing a reverse transcription the cDNA was subjected to real time PCR (TaqMan) of **(A)** Cyclin B1 and **(B)** BUBR1. Shown is the average of three independent experiments and standard deviations. A549 cells, incubated with **(C)** sagopilone and **(D)** paclitaxel were subjected to protein extraction. Isolated protein was separated using SDS polyacrylamide gel electrophoresis, transferred to a PVDF membrane and probed with antibodies recognizing Cyclin B1 and BUBR1, respectively. GAPDH severed as loading control.

Low concentrations did not significantly alter the expression levels of both genes. The results revealed that high concentration incubation of A549 cells with sagopilone and paclitaxel led to an up-regulation of genes and proteins involved in mitosis. These effects are very likely to be based on the blockage of mitotic progression.

4.7 In vivo *tumor xenograft model A549*

4.7.1 Response of A549 tumor xenograft to sagopilone

Sagopilone is highly effective in a variety of human tumor xenograft models including paclitaxel-resistant tumors, as determined by T/C ratios (tumor area of treated versus untreated xenograft control) (Hoffmann et al., 2008). Indeed, T/C ratios of <0.5 were observed in the majority of xenografts treated with this drug. However, the A549 tumor is one of the very few xenograft models that only showed a minor response to the sagopilone treatment. As documented in Figure 22 the growth of the A549 tumor xenograft was found to be only marginally reduced by the sagopilone treatment, and the difference compared to the control group did not achieve statistical significance. The *in vivo* tumor xenograft model A549 exhibited a T/C ratio of 0.75.

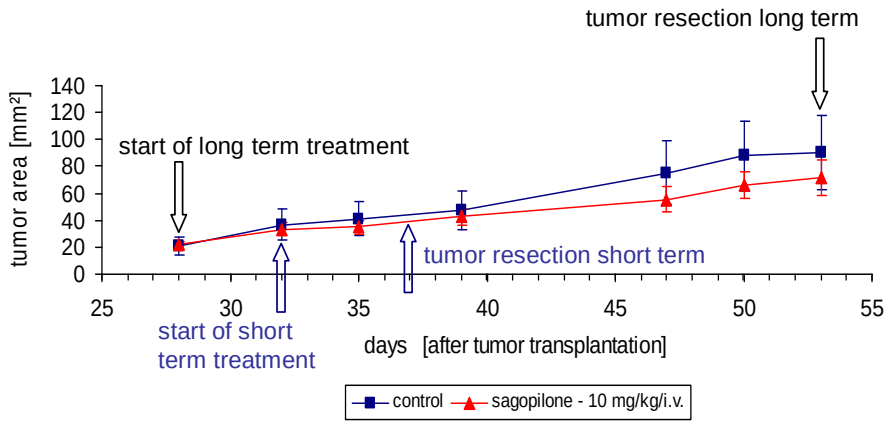

Figure 22. *In vivo* tumor xenograft model A549. Nude mice bearing A549 tumor xenografts were treated intravenously either with vehicle or 10 mg/kg sagopilone at the indicated days. Two different treatment periods were applied. Long term treatment was started from an average tumor area of 20 mm^2 and lasted for 25 days whereas short term treatment started at around 40 mm^2 and lasted for 5 days. The tumor area was measured twice weekly. Afterwards, mice were sacrificed; the tumors were taken out and immediately deep-frozen in liquid nitrogen.

Based on the expression data of the *in vitro* analysis of A549 cell it was therefore of interest to examine the gene expression profile obtained after sagopilone treatment. To address this, nude mice bearing A549 tumor xenografts were treated once with 10 mg/kg sagopilone and tumors were harvested either after 5 days (short term treatment) or 25 days (long term treatment). The tumors were subjected to gene expression analysis.

4.7.2 Gene expression analysis of A549 *in vivo* xenograft model

Figure 23 depicts gene expression analysis by real time PCR (TaqMan) of A549 xenograft tumors treated for 5 days with sagopilone. The genes were selected according to their regulation in the gene expression analysis conducted in A549 cells *in vitro* (chapter 4.6). Selected genes represent either the low concentration sagopilone gene signature (p21, FAS, GADD45A) or the high concentration sagopilone gene signature (Cyclin B1, BUBR1).

The vehicle-treated tumors (V1-V8) showed only a marginal variation of p21, FAS and GADD45A gene expression. In contrast, tumors from mice treated once with 10 mg/kg sagopilone (S1-S8) revealed a highly significant increase of p21 ($p=0.0003$), FAS ($p=0.0006$) and GADD45A ($p=0.001$) gene expression. Two other genes previously found to be up-regulated after a high concentration sagopilone treatment (Cyclin B1 and BUBR1) were not found to be changed in A549 tumors originating from mice treated with sagopilone. Thus, the gene regulation observed after a 5 day treatment indicates a p53 transactivation.

Figure 24 depicts the expression of the 5 selected genes in A549 xenografts 25 days post treatment with vehicle or sagopilone. No differences in the gene expression between vehicle- and sagopilone-treated tumors could be observed at this time point.

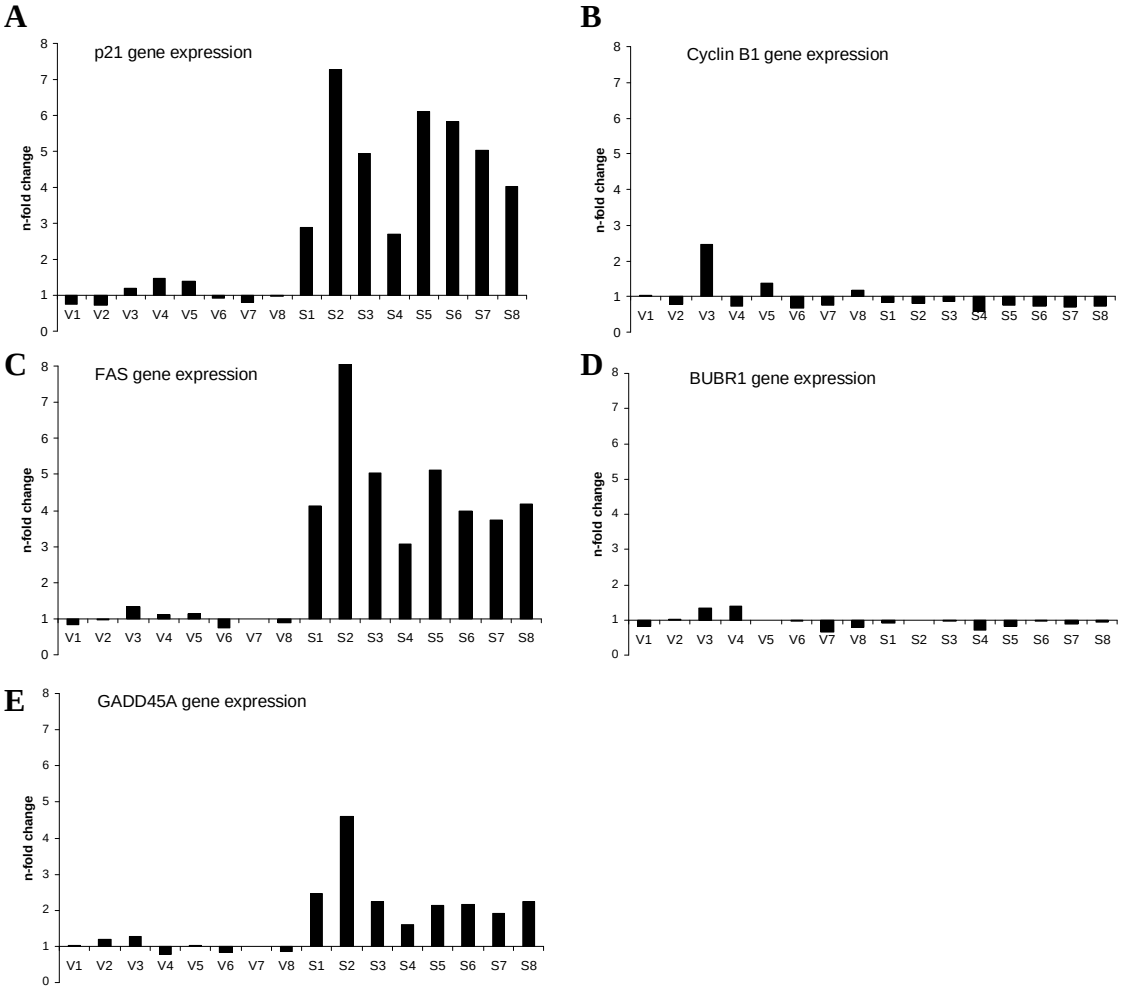

Figure 23. Gene expression of short term treated A549 *in vivo* tumor xenografts. Nude mice bearing A549 tumor xenografts were treated either with vehicle or 10 mg/kg sagopilone and were sacrificed 5 days post treatment. RNA was extracted from A549 xenografts and a reverse transcription was performed. Real time PCR was conducted with specific primers recognizing **(A)** p21, **(C)** FAS, **(E)** GADD45A, **(B)** Cyclin B1 and **(D)** BUBR1 genes, respectively. V1-V8 representing vehicle-treated samples and S1-S8 representing 10 mg/kg sagopilone-treated samples. All samples were normalized to the average expression level of the vehicle-treated samples.

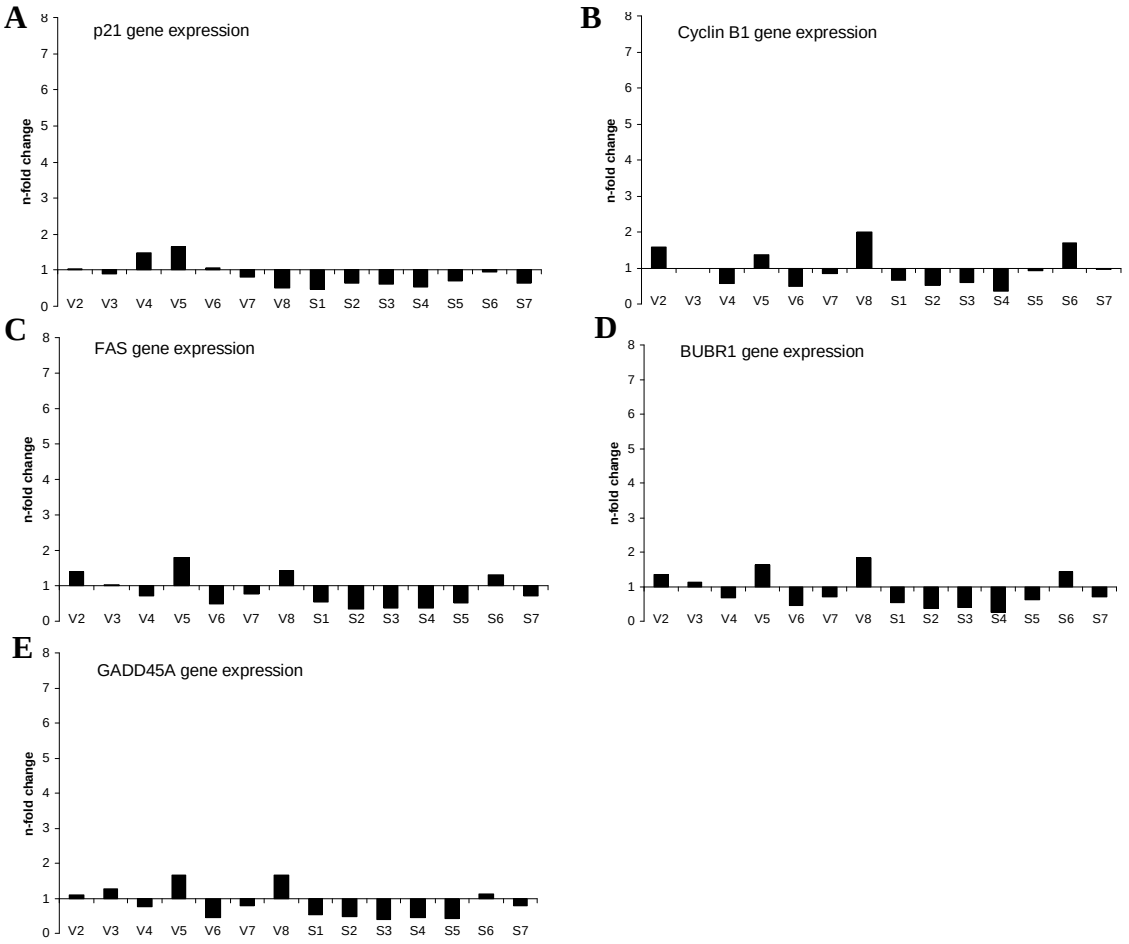

Figure 24. Gene expression of long term treated A549 *in vivo* tumor xenografts. Nude mice bearing A549 tumor xenografts were treated either with vehicle or 10 mg/kg sagopilone and were sacrificed 25 days post treatment. RNA was extracted from A549 xenografts and reverse transcription was performed. Real time PCR was conducted with specific primers recognizing **(A)** p21, **(C)** FAS, **(E)** GADD45A, **(B)** Cyclin B1 and **(D)** BUBR1 genes, respectively. V2-V8 representing vehicle-treated samples and S1-S7 representing 10 mg/kg sagopilone-treated samples. All samples were normalized to the average expression level of the vehicle-treated samples.

4.8 Contribution of the p53 status to the response to sagopilone

4.8.1 Changes in p21 gene expression in response to sagopilone treatment of p53 wild type and p53 mutated cell lines

The expression of p21 in response to sagopilone was measured in p53 wild-type (wt) and p53 mutated cell lines (mut) cell lines to assess whether the transcriptional activation of p53 is a general phenomenon among p53 wild-type cell lines (Figure

25). Therefore p21 up-regulation was used as a marker for p53 transcription activation. The p53 mutations are mostly characterized by point mutation of single base pairs located in the DNA-binding domain (chapter 3.20 p53 mutations in cell lines). The cell lines were chosen according to their p53 mutational status. As depicted in the panel A, the four p53 wt cell lines we analyzed responded with increased p21 gene expression following sagopilone treatment in the range of 1 to 10 nM. The extent of stimulation strongly varied among the different cell lines. In contrast, no p21 gene induction was observed in the four p53 mutated cell lines tested (Figure 25 B). These data demonstrate a p21 up-regulation to occur in response to sagopilone in p53 wt, but not mutated cell lines, suggesting a transcriptional activation of p53.

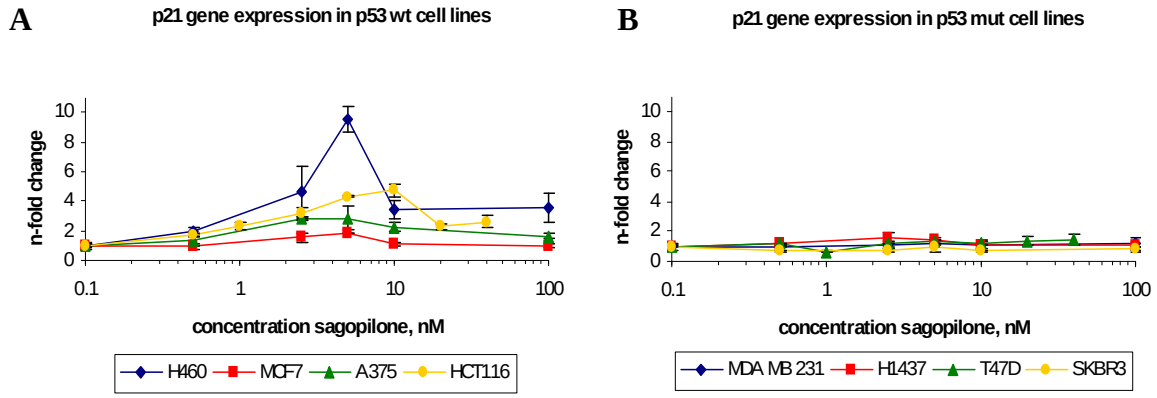

Figure 25. p21 gene expression in response to sagopilone in p53 wild type (wt) and p53 mutated (mut) cell lines. (A) p53 wt (HCT116, H460, A375, MCF7) **(B)** p53 mut (MDA MB 231, H1437, T47D and SKBR3) cell lines were incubated continuously with medium containing 0 to 100 nM of sagopilone for 18 hours and were subjected to RNA extraction. After performing reverse transcription the cDNA was subjected to real time PCR (TaqMan) with specific primers for p21. The fold change of mRNA expression versus an endogenous control (hHPRT) was calculated by the delta delta ct method and normalized to the expression value of vehicle-treated cells (fold change = 1). The average of two independent experiments and standard deviation is shown.

4.8.2 Apoptosis induction of p53 wild type and p53 mutated cell lines

An apoptosis assay was applied to analyze the contribution of the activation of p53 to the extent of cell death measured after sagopilone treatment. The p53 wt cell lines A549, H460, HCT116 and MCF7 (Figure 26 A) and the p53 mutated cell lines

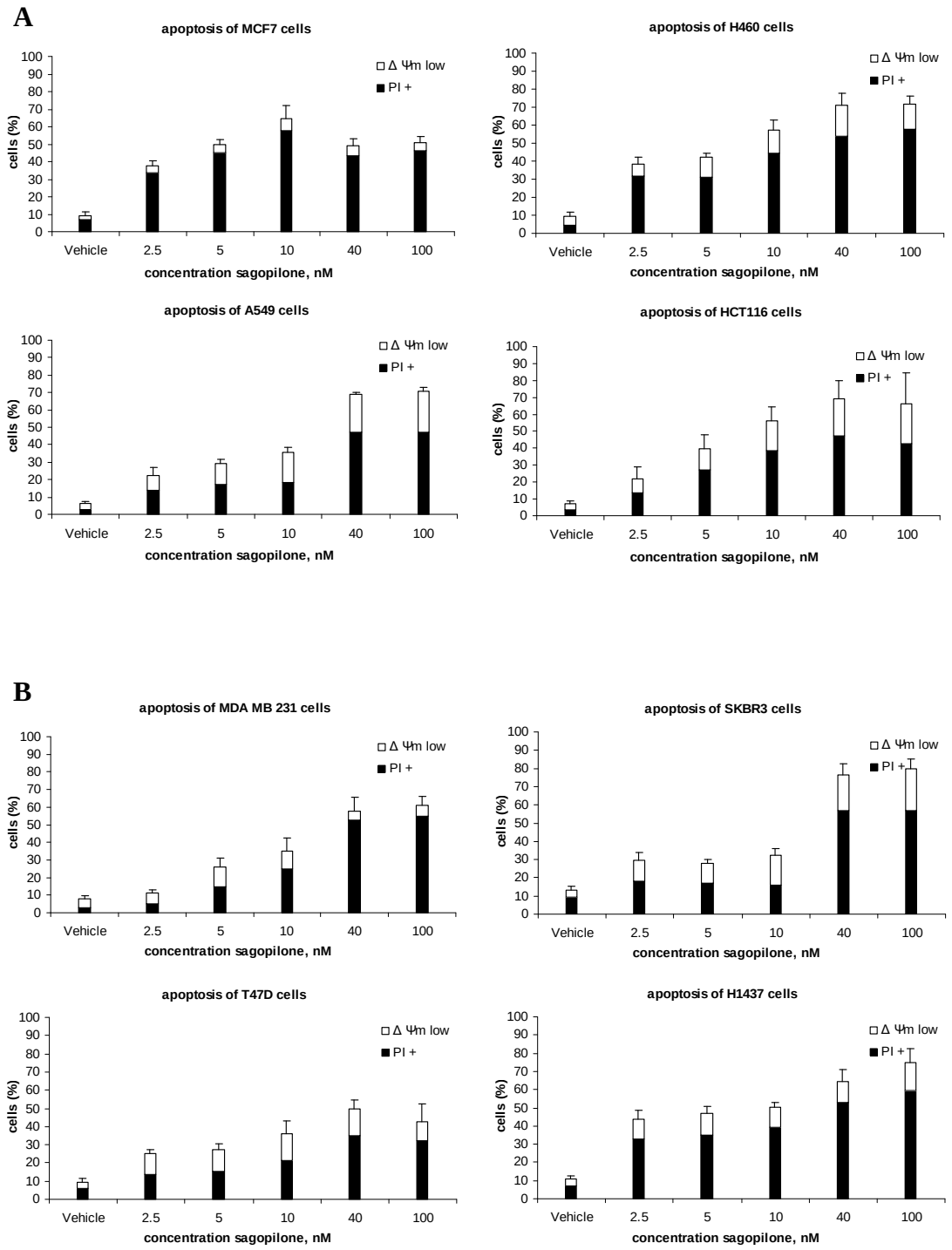

Figure 26. Apoptosis induction of p53 wild type (wt) and p53 mutated (mut) cell lines. (A) A549, H460, HCT116 and MCF7 and **(B)** MDA MB 231, SKBR3, T47D and H1437 cells were treated continuously for 72 hours with medium containing 0 to 100 nM sagopilone. Afterwards the cells were stained with DiOC6(3) and propidium iodide for cytofluorimetric detection of apoptosis-associated mitochondrial membrane potential dissipation (Δ Ψm low) and plasma membrane rupture (PI +). White and black bars indicate the mean percentage of cells (n = 2) characterized by Δ Ψm loss alone and in combination with plasma membrane breakdown (PI+), respectively.

MDA MB 231, SKBR3, T47D and H1437 (Figure 26 B) were continuously incubated with various concentrations of sagopilone for 72 hours and analyzed for apoptotic events. The extent of apoptosis induction at low and high concentration sagopilone varied among the different cell lines. The results revealed no clear correlation between the p53 mutational status and induction of apoptosis after sagopilone treatment.

4.9 Knock-down of p53 in A549 cells

4.9.1 Stable short hairpin RNA knock-down of p53 in A549 cells

To further elucidate the role of p53 (TP53) activation in response to sagopilone, A549 cells were stably transfected with expression plasmids containing short hairpin RNAs (shRNA) targeting the mRNA of p53. Figure 27 A depicts the degree of knock-down obtained in three different A549 sub-clones containing p53 sh RNAs (shp53_3, shp53_4, shp53_5) and in two A549 sub-clones containing non-targeting control shRNAs (shDh2, shQia). Real time PCR analysis confirmed the reduction of p53 mRNA levels in all sub-clones containing p53 sh RNAs to a level below 10 % compared to the non-targeting control shRNAs. Substantially diminished protein expression levels of p53 were obtained in the p53 shRNA knock-down cell lines compared to control A549 cells (Figure 27 B). Furthermore the transcriptional activation of p21 was markedly diminished in the p53 shRNA knock-down cell lines treated with sagopilone, compared to the control A549 cell lines, where p21 was found to be elevated in the expected manner after incubation with sagopilone for 18 hours (Figure 27 C).

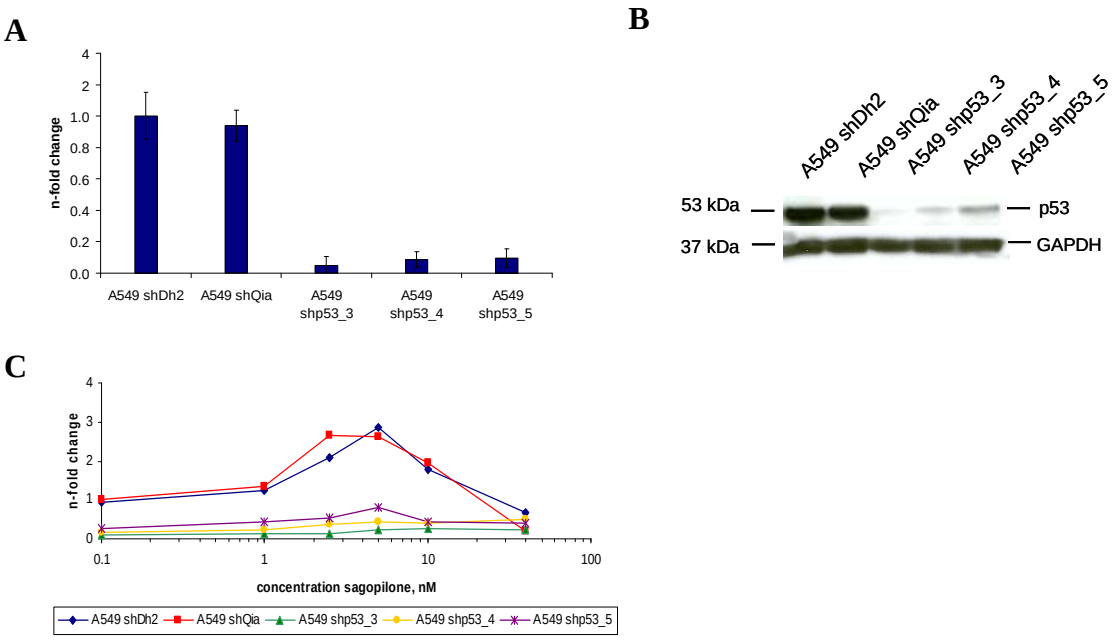

Figure 27. p53 shRNA knock-down in A549 cells. A549 cell were stably transfected with short hairpin (sh) RNA targeting the mRNA of p53 or control shRNA. **(A)** p53 gene expression of A549 shRNA controls and p53 shRNA cell lines. Shown is the average of three independent experiments and standard deviations. **(B)** Proteins from A549 p53 shRNA knock-down and shRNA control cell lines were extracted and separated using SDS polyacrylamide gel electrophoresis, transferred onto a PVDF membrane and probed with antibodies recognizing p53 and GAPDH, respectively. **(C)** p21 gene expression in response to sagopilone treatment for 18 hours of A549 p53 shRNA knock-down and control cell lines. Shown is the one representative experiment.

4.9.2 Cell cycle analysis of p53 shRNA knock-down cell lines

Figure 28 shows the cell cycle distribution of A549 cells stably transfected with p53 shRNA or control shRNA after incubation with 0 to 100 nM sagopilone for 18 hours. No significant changes in the cell cycle distribution were observed after 18 hours of treatment with sagopilone (Figure 28 A). However, a 72 hour incubation with the same drug concentration led to considerable changes in the cell distribution between the A549 control cell lines and the p53 shRNA knock-down cell lines (Figure 28 B). The latter showed a decrease of the number of cells with a G2/M (4N) DNA content and concomitantly an increase of polyploid cell numbers with >4N DNA content. This effect was most pronounced at 5 and 10 nM sagopilone (these concentrations had previously been shown to induce p53 transcriptional activity) and was seen in all three

p53 shRNA knock-down cell lines. At higher concentrations (40, 100 nM) the same changes in the cell cycle distribution were observed, however to a lesser extent.

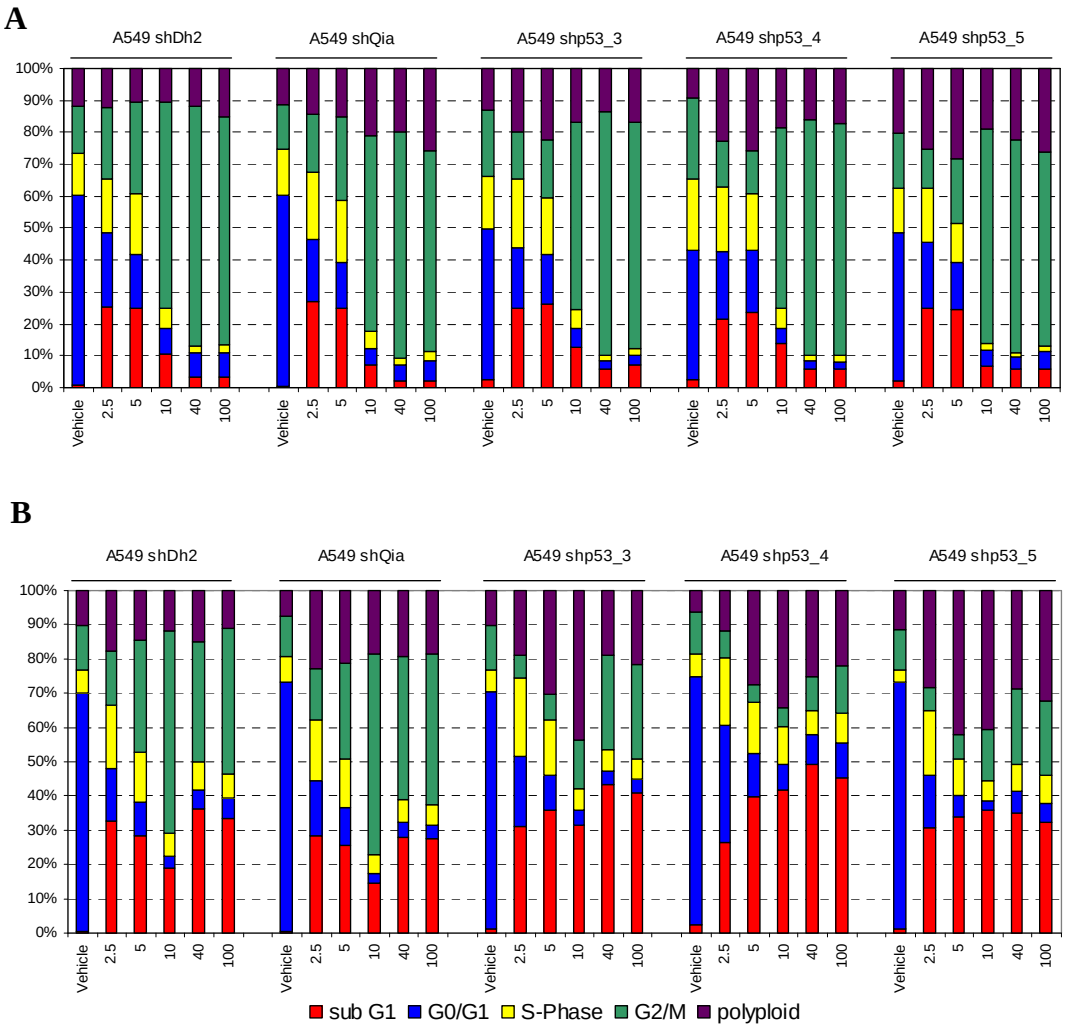

Figure 28. Overview of cell cycle analysis of p53 shRNA knock-down and control cell lines. Cells were incubated with medium containing 0 to 100 nM sagopilone for **(A)** 18 hours or **(B)** 72 hours followed by fixation and incubation with propidium iodide. DNA content was determined by flow cytometry. The amounts of cells constituting the sub G1, G0/G1, S, G2/M and polyploid populations were determined and plotted as bar charts against the drug concentration.

Figure 29 A, B shows an exemplary cell cycle distribution of A549 shDh2 and A549 shp53_3 cell lines treated with 10 nM sagopilone for 72 hours. The histograms show the decrease in cell numbers with G2/M (4N) DNA content and the concomitant increase of the number of polyploid cells in the A549 shp53_3 knock-down cell line.

Quantification of cells with G2/M (4N) DNA content and polyploid cells (> 4N) treated with various concentrations of sagopilone (Figure 29 C, D) revealed statistically significant differences between A549 shDh2 and A549 shp53_3 cell lines at concentrations of 5 and 10 nM sagopilone.

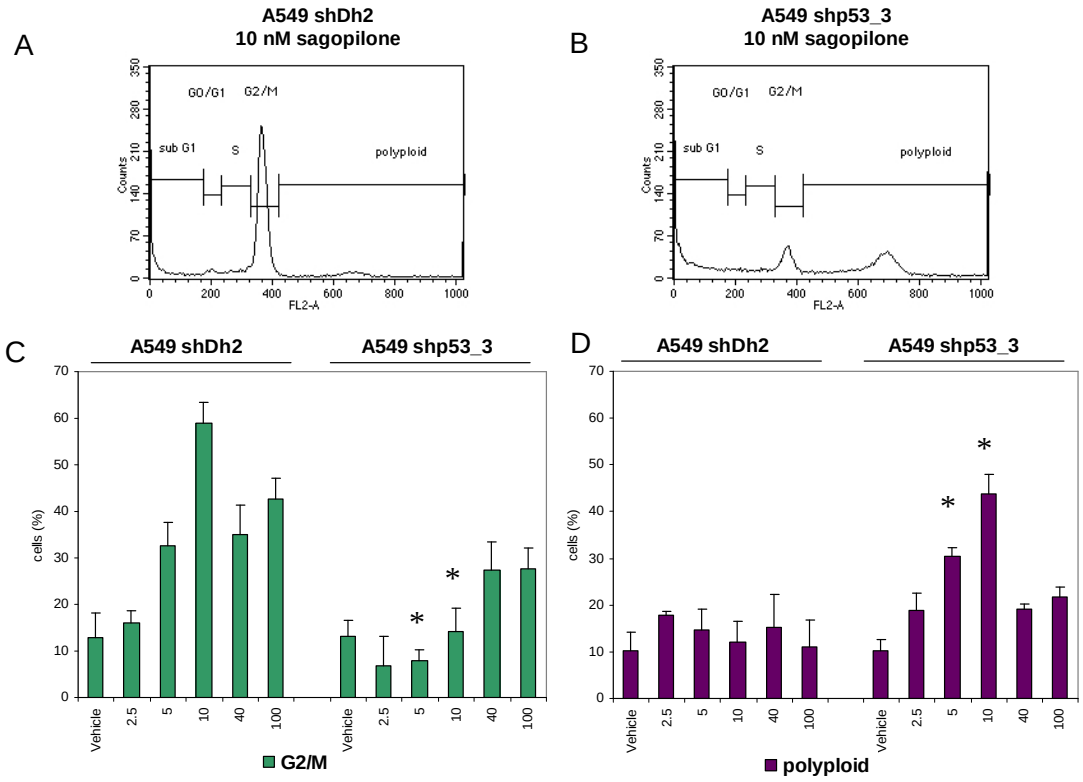

Figure 29. Cell cycle analysis of A549 shDh2 and A549 shp53_3. Both cell lines were incubated with medium containing various concentrations of sagopilone for 72 hours followed by fixation and incubation with propidium iodide. DNA content was determined by flow cytometry. **(A, B)** exemplary depiction of histograms from cell lines treated with 10 nM sagopilone. **(C, D)** quantification of G2/M and polyploid cells in both cell lines. Statistically significant differences were calculated using Student's t test ($p < 0.05$) by comparing A549 shDh2 and A549 shp53_3 cell lines treated with the same drug concentration.

4.9.3 Apoptosis induction of A549 shp53 knock-down cells

Next, the impact of the p53 knock-down on the sagopilone-induced apoptosis was measured. After treatment with different concentrations of sagopilone for 72 hours the cells were stained with DiOC6(3) and propidium iodide for cytofluorimetric detection of apoptosis-associated mitochondrial membrane potential dissipation

(Δ Ψm low) and membrane rupture (PI +). The p53 shRNA knock-down cell lines exhibited a significant increase of apoptotic cell numbers compared with the control A549 cells at 10 nM sagopilone. Additionally two out of three p53 shRNA knock-down cell lines (A549 sh RNA p53_3, A549 sh RNA p53_4) also exhibited a significant increase of apoptotic cells at 5 nM sagopilone. The treatment with 2.5 nM sagopilone increased the amount of apoptotic cells, but the results were not statistically significant. High concentration incubation with sagopilone (40 and 100 nM) led only to marginally elevated induction of apoptosis in p53 shRNA knock-down cell lines compared to control cells.

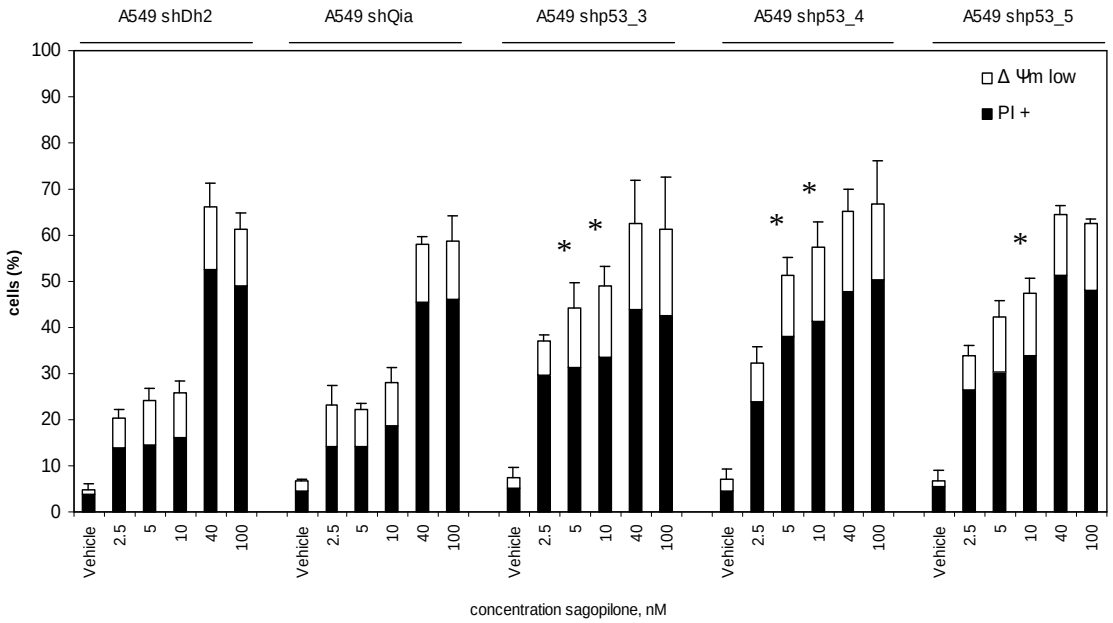

Figure 30. Apoptosis induction by sagopilone after 72 hours. A549 sh RNA control (A549 shDH2, A549 shQia) and p53 shRNA knock-down cell lines (A549 shp53_3, A549 shp53_4, shp53_5) were treated continuously for 72 hours with medium containing 0 to 100 nM sagopilone. Afterwards the cells were stained with DiOC6(3) and propidium iodide for cytofluorimetric detection of apoptosis-associated mitochondrial membrane potential dissipation (Δ Ψm low) and plasma membrane rupture (PI +). White and black bars indicate the mean percentage of cells (n = 3) characterized by Δ Ψm loss alone and in combination with plasma membrane breakdown (PI+), respectively. Statistically significant differences were calculated using Student's t test ($p < 0.05$) by comparing the response to sagopilone of control A549 cells and p53 shRNA knock-down cells treated with the same drung concentration.

4.10 Knock-down of p21 in A549 cells

4.10.1 Stable short hairpin RNA knock-down of p21 in A549 cells

Figure 31 A shows the expression level of p21 (CDKN1A) in A549 cells which were either stably transfected with expression plasmids containing shRNAs targeting p21 or non-targeting control shRNAs. The gene expression data confirmed a sufficient knock-down only in two out of four p21 shRNA knock-down cell lines, namely shp21_1 and shp21_3. Therefore only these two cell lines were chosen for further experiments. Decreased p21 protein expression levels were observed in the p21 shRNA knock-down cell lines compared to control A549 cells (Figure 31 B). Additionally, the increase in p21 mRNA levels after sagopilone treatment was diminished in the p21 shRNA knock-down cell lines compared to the control cell lines, where p21 mRNA was found to be induced by sagopilone in the typical fashion (Figure 31 C).

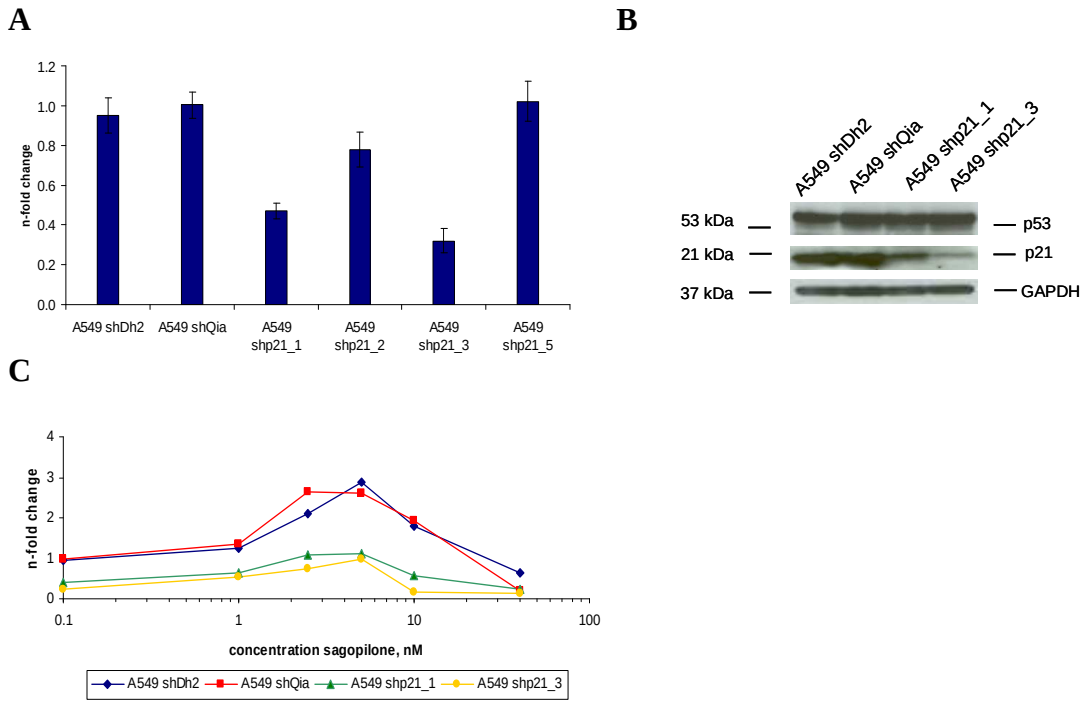

Figure 31. p21 shRNA knock-down in A549 cells. A549 cell were stably transfected with short hairpin (sh) RNA targeting the mRNA of p21 or control shRNA. **(A)** p21 gene expression of A549 shRNA controls and p21 shRNA cell lines. Shown is the average of three independent experiments and standard deviations. **(B)** Proteins from A549 p21 shRNA knock-down and shRNA control cell lines were extracted and separated using SDS polyacrylamide gel electrophoresis, transferred onto a PVDF membrane and probed with antibodies recognizing p53, p21 and GAPDH, respectively. **(C)** p21 gene expression in response to sagopilone treatment for 18 hours of A549 p21 shRNA knock-down and control cell lines. Shown is the one representative experiment.

4.10.2 Cell cycle analysis of A549 shp21 knock-down cells

The cell cycle analysis of A549 p21 shRNA knock-down cell lines and A549 control shRNA cell lines after 72 hours continuous drug incubation revealed some differences (Figure 32). The amount of cells with a DNA content of 4N (G2/M) were found to be reduced in the A549 shp21 knock-down cell lines compared to the control cell lines after treatment with 5 and 10 nM sagopilone. Concomitantly, the amount of polyploid cells (DNA content >4N) was elevated in A549 shp21_3 knock-down cell lines compared to control cell lines at the same concentrations. The number of polyploid A549 shp21_1 cells was not changed compared to the control cell lines after treatment with sagopilone.

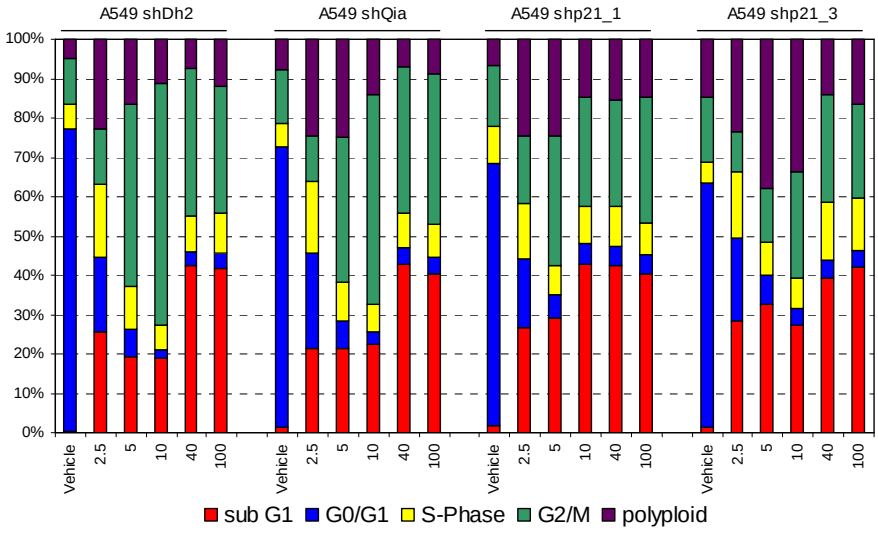

Figure 32. Overview of cell cycle analysis of A549 p21 shRNA and control cell lines. Cells were incubated with medium containing 0 to 100 nM sagopilone for 72 hours followed by fixation and incubation with propidium iodide. DNA content was determined by flow cytometry. The amounts of cells constituting the sub G1, G0/G1, S, G2/M and polyploid populations were determined and plotted as bar charts against the drug concentration.

Figure 33 A, B shows the cell cycle distribution of A549 shDh2 and A549 shp21_3 cell lines treated with 10 nM sagopilone for 72 hours. The histograms elucidate the decrease of cells with G2/M (4N) DNA content and the concomitant increase of polyploid cells in the A549 shp21_3 knock-down cell line compared to the A549 shDh2 control. Quantification of cells with G2/M (4N) DNA content and polyploid cells (>4N) treated with various concentrations of sagopilone (Figure 33 C, D)

revealed statistically significant differences between A549 shDh2 and A549 shp21_3 cell lines at concentrations of 5 and 10 nM sagopilone.

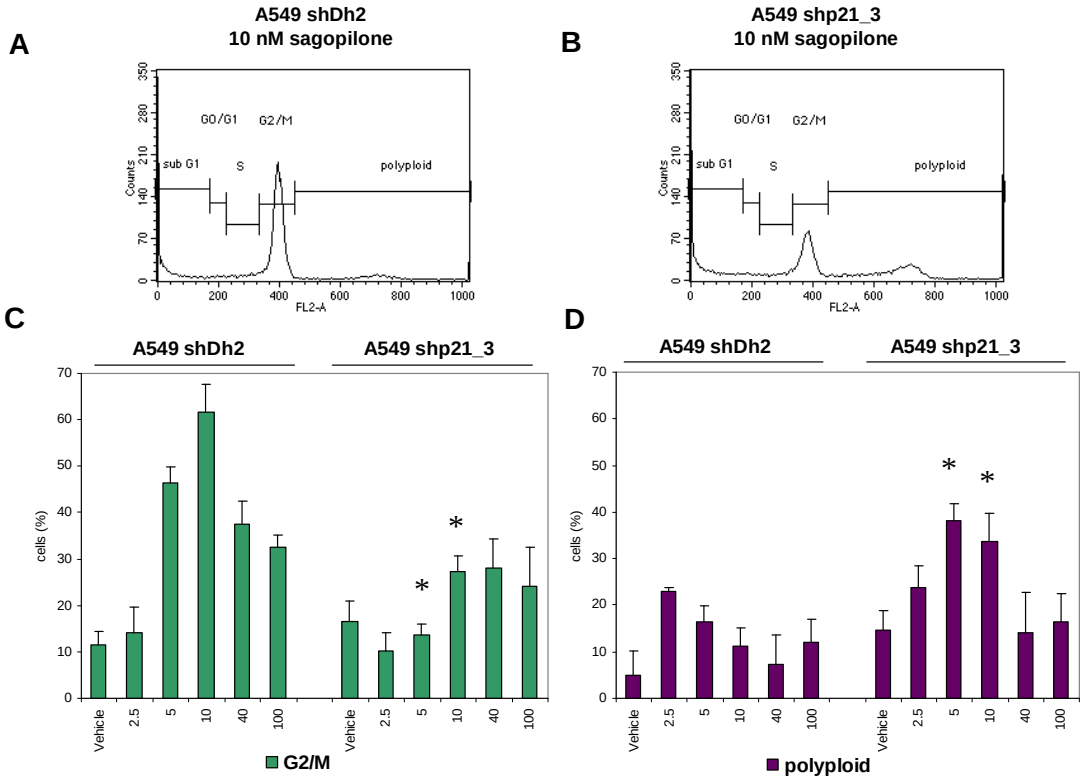

Figure 33. Cell cycle analysis of A549 shDh2 and A549 shp21_3. Both cell lines were incubated with medium containing various concentrations sagopilone for 72 hours followed by fixation and incubation with propidium iodide. DNA content was determined by flow cytometry. **(A, B)** exemplary depiction of histograms from cell lines treated with 10 nM sagopilone. **(C, D)** quantification of G2/M and polyploid cells in both cell lines. Statistically significant differences were calculated using Student's t test ($p < 0.05$) by comparing A549 shDh2 and A549 shp21_3 cell lines treated with the same drug concentration.

4.10.3 Apoptosis induction of A549 shp21 knock-down cells

An apoptosis assay was applied to determine the consequences of the p21 knock-down in A549 cells (Figure 34). After treatment with different concentrations of sagopilone the cells were stained with DiOC6(3) and propidium iodide and analyzed by flow cytometry. The results demonstrate in the A549 p21 shRNA knock-down cell lines an increase of apoptotic cell number compared to their control shRNA harboring counterparts. The effect was most prominent in the range of 2.5 to 10 nM sagopilone. Statistically significant (Student's t test, $p<0.05$) differences were observed in the 10 nM sagopilone-treated A549 cells. At higher sagopilone concentration only marginally elevated amounts of apoptotic cells were observed in the p21 shRNA A549 cell compared to the control cell lines.

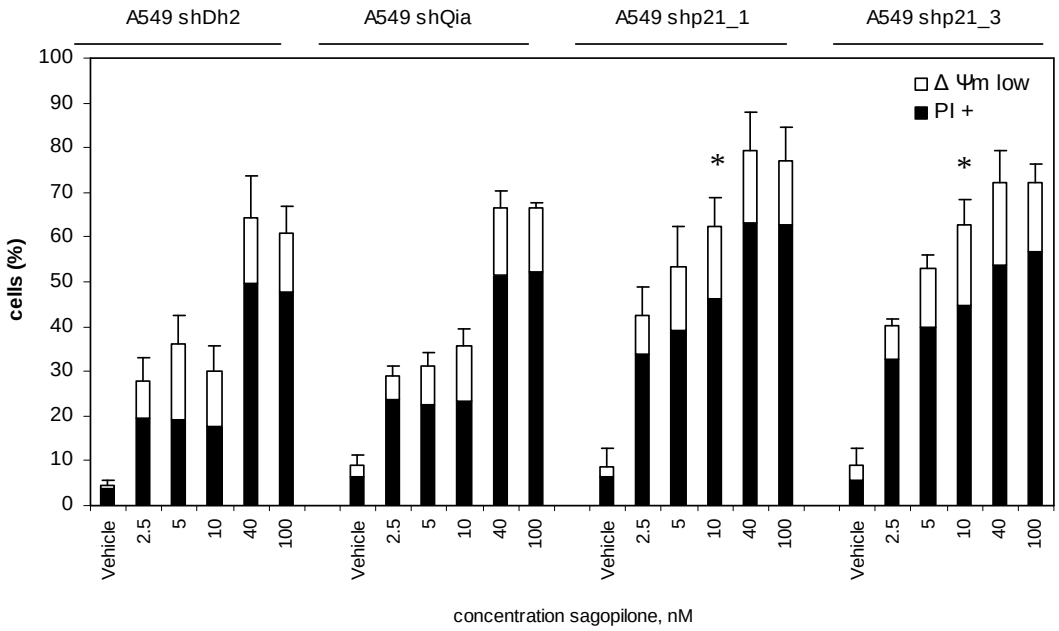

Figure 34. Apoptosis induction by sagopilone. A549 shRNA control (A549 shDh2, A549 shQia) and p21 A549 knock-down cell lines (A549 shp21_1, A549 shp21_3) were treated continuously for 72 hours with medium containing 0 to 100 nM sagopilone. Afterwards the cells were stained with DiOC6(3) and propidium iodide for cytofluorimetric detection of apoptosis-associated mitochondrial membrane potential dissipation (Δ Ψm low) and plasma membrane rupture (PI +).White and black bars indicate the mean percentage of cells (n = 3) characterized by Δ Ψm loss alone and in combination with plasma membrane breakdown (PI+), respectively. Statistically significant differences were calculated using Student's t test ($p < 0.05$) by comparing the response to sagopilone of control A549 cells and p21 shRNA knock-down cell lines treated with the same concentration of drug.

4.11 Induction of DNA damage in A549 cells after treatment with sagopilone?

The genome-wide gene expression study of A549 cells treated with high concentration sagopilone and paclitaxel revealed an up-regulation of genes involved in DNA damage repair. It was therefore of interest to determine whether the sagopilone treatment caused DNA double strand breaks (DSBs). Following this kind of DNA damage histone H2AX becomes phosphorylated and can therefore be used as marker for DNA damage. Figure 35 displays Western blot results of A549 cell lysates treated with different concentrations of sagopilone for 18 hours. γH2AX antibody incubation showed only a signal in the high concentration sagopilone-treated samples (40, 100 nM), whereas no staining was found in the low concentration treatment group (2.5 nM), and only a very slight staining was observed in the 10 nM treatment lane.

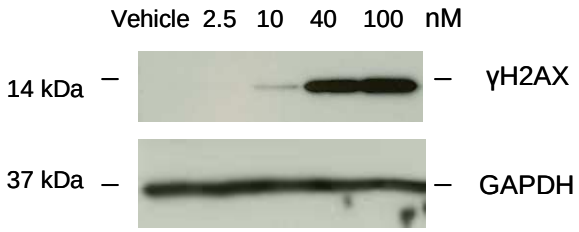

Figure 35. γH2AX as marker for DNA double strand breaks and apoptosis. A549 cell were treated with increasing concentrations of sagopilone for 18 hours and subjected to western blot analysis. γH2AX antibody staining is shown. GAPDH served as loading control.

It was further investigated, whether this H2AX phosphorylation indicated DNA damage in the absence of apoptosis or signs of DNA fragmentation as part of programmed cell death. To address this question apoptosis was inhibited by co-treatment with pan-caspase inhibitor ZVAD.fmk. Figure 36 A displays a cell cycle analysis of A549 cells incubated with 40 nM sagopilone in the absence or presence of ZVAD.fmk for various incubation periods. After 14 hours of treatment with 40 nM sagopilone the majority of cells were in the G2/M phase of the cell cycle. After 42 hours of treatment with sagopilone 36.7% ± 4.6 of the cells were found in the sub-G1

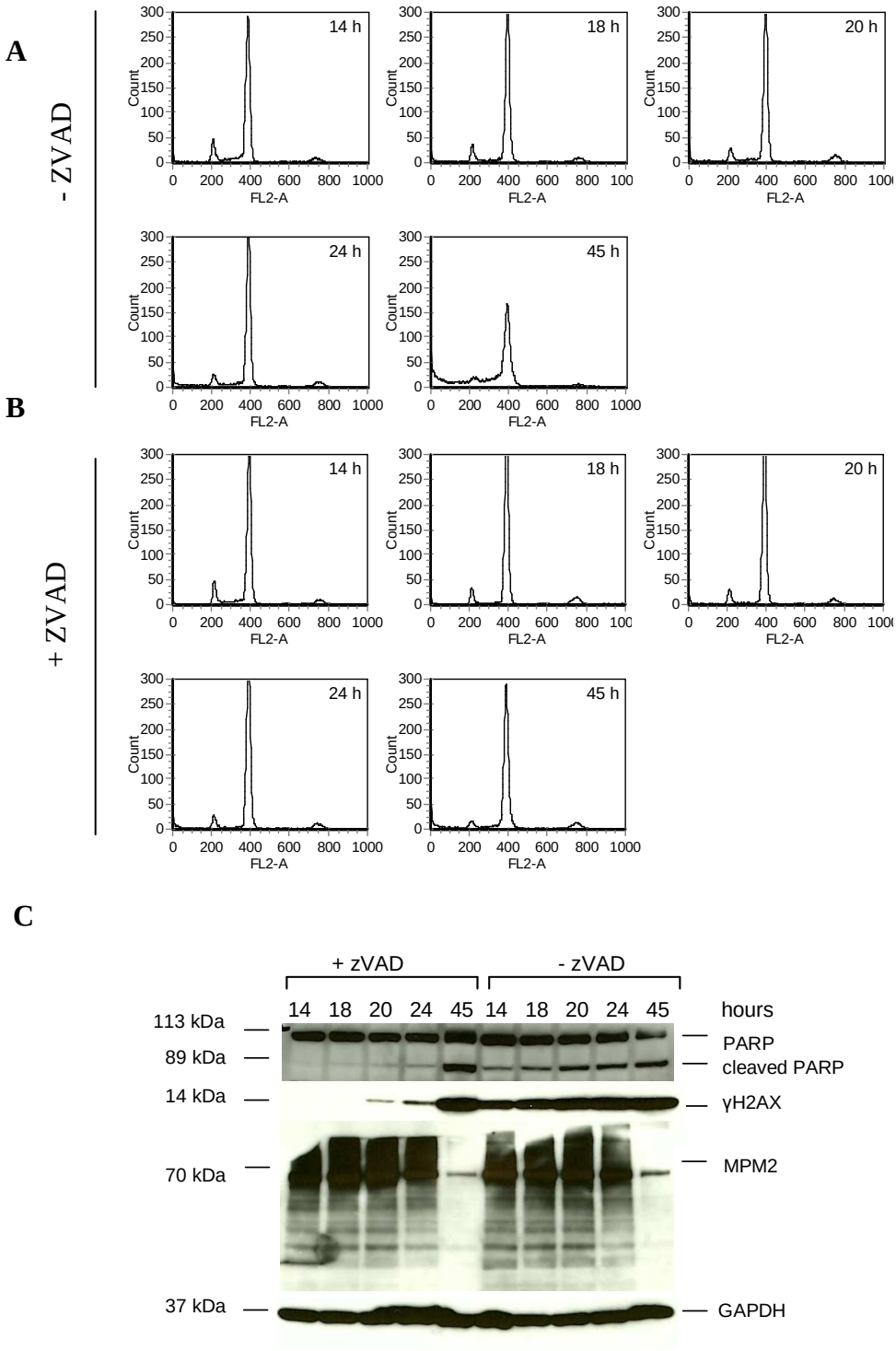

Figure 36. γH2AX as marker for DNA double strand breaks and apoptosis. (A) A549 cell were treated with increasing concentrations of sagopilone for 18 hours and subjected to western blot analysis. γH2AX antibody staining is shown. **(B)** Cell cycle analysis of A549 cells treated with 40 nM sagopilone for different time periods. The lower panel was co-treated with the pan-caspase inhibitor ZVAD.fmk. **(C)** Western blot analysis of A549 cells treated with 40 nM sagopilone for different times in the presence (+zVAD) or absence of ZVAD.fmk (-zVAD) and probed with antibodies detecting PARP, γH2AX, MPM2, respectively. GAPDH served as loading control.

population compared to 6.6 % ± 2.6 in the ZVAD.fmk co-treated cells. The data confirmed that co-treatment with the pan-caspase inhibitor ZVAD.fmk circumvents apoptosis triggered by high concentration sagopilone. During apoptosis, PARP is cleaved by caspase 3 from a 113 kDa protein into 89 kDa and 24 kDa fragments. PARP cleavage is therefore considered to be a marker of apoptosis. For this reason cell lysates were taken in parallel to the cell cycle analysis samples and subjected to gel electrophoresis. Figure 36 C displays Western blot analysis of A549 cells treated with 40 nM sagopilone at different time points in the presence or absence of ZVAD.fmk. The blot was probed with a Poly (ADP-ribose) polymerase (PARP) antibody as shown in Figure 36 C, upper panel. Co-treatment with ZVAD.fmk markedly inhibited PARP cleavage compared to the sagopilone-treated A549 cells (-ZVAD) in the time period of 14 to 24 hours. More importantly, ZVAD.fmk co-treatment inhibited histone H2AX phosphorylation in the same time frame. Figure 36 C, third panel, shows a MPM2 immunoblot. The MPM2 antibody binds to phospho amino acid-containing epitopes present on many proteins of mitotic eukaryotic cells and is therefore used as a maker of mitosis. Independently of co-treatment with ZVAD.fmk, the cells were arrested in mitosis in both treatment groups in the time period of 14 to 24 hours. At 45 hours after drug addition the A549 cells were no longer in mitosis. In the ZVAD.fmk co-treated cells presumably mitotic slippage resulted, because these cells did not possess any signs of DNA fragmentation (Figure 36 B). The sagopilone only treated A549 cells showed massive apoptosis.

5 Discussion

5.1 Sagopilone inhibits tumor cell proliferation in vitro

One of the most important functions of microtubules is the ability to form the mitotic spindle apparatus, a key component of the cell division machinery. Microtubule-stabilizing drugs like sagopilone and paclitaxel alter the rapid polymerization dynamics of the spindle microtubules and block mitosis at the metaphase/anaphase transition. The high rate of cell division renders tumors cells selectively sensitive to these kinds of drugs, because they frequently pass through a state of vulnerability to mitotic poisons.

The reasons for the higher antiproliferative activity of sagopilone compared to paclitaxel in a 72 hours proliferation assay were found in the higher ability of sagopilone to induce an accelerated tubulin polymerization *in vitro*. Further more, the intracellular uptake of sagopilone was higher compared to paclitaxel (Hoffmann et al., 2008). Sagopilone was exclusively localized to the cytoskeleton fraction, whereas paclitaxel was mostly found in the cytoplasmatic and the membrane fraction. Higher intracellular drug concentrations of sagopilone were reached in A549 cells compared to paclitaxel (Hoffmann et al., 2008).

One of the main mechanisms of resistances to paclitaxel and other chemotherapeutic drugs is the over-expression of the MDR1 (multi drug resistance) drug transporter (Sikic et al., 1997; Yabuki et al., 2007). This efflux mechanism reduces the cellular drug concentration when over-expressed and renders the cells resistant to chemotherapeutics, which are substrates of the MDR1 drug transporter. Sagopilone is not a target of MDR1 drug transporter and is therefore not affected by this kind of drug resistance (Klar et al., 2006). Thus higher intracellular drug levels can be reached which result in a higher potency of sagopilone in the MDR1 over-expressing cells. This was demonstrated on cell lines known to over-express MDR1 (chemoresistant cells) in comparison to their drug-sensitive counterparts (chemosensitive cells). Sagopilone showed activity in both drug sensitive cell lines and multidrug resistant sub-clones, while paclitaxel failed to inhibit proliferation of the MDR1 over-expressing sub-clones. The activity of paclitaxel was restored by

transfection of small hairpin (sh) RNA targeting the MDR1 gene. This indicates that the resistance of paclitaxel is based on the over-expression of MDR1 in these cell lines.

The antiproliferative activity of sagopilone was higher than that seen with paclitaxel or ixabepilone treatment as tested on several breast cancer cell lines. A retrospective analysis of patient-derived breast cancer tissues indicates that ER-positive tumors were more resistant to 6 anticancer agents than ER-negative tumors. Ixabepilone response has been associated with low levels of ER expression (Maehara et al 1990; Pusztai, 2007). The reason for the resistance of ER-positive tumors to paclitaxel was found in the ER-mediated expression of anti-apoptotic Bcl-2 protein shortly after treatment of ER-positive cell lines with estrogen (Tabuchi et al., 2009). In contrast, increased levels of Bcl-2 were not detected in ER-negative cell lines (Tabuchi et al., 2009). In this study, it has been shown that sagopilone potently inhibited tumor cell proliferation in all ER-positive cell lines. Comparable antiproliferative effects were observed with sagopilone treatment of ER-negative tumor cells suggesting that sagopilone may represent a therapeutic option for ER-positive tumors, especially in an adjuvant setting or if the tumors have become refractory to anti-hormone treatment.

5.2 Sagopilone treatment of cells results in two concentration-dependent phenotypes

In the past microtubule-targeting drugs were believed to cause mitotic arrest but more detailed studies have identified two concentration-dependent cellular phenotypes (Torres and Horwitz, 1998; Chen et al., 2002). Here it was shown that this is also true for sagopilone in A549 lung carcinoma cells. At low concentrations (2.5 nM), sagopilone affects spindle morphology without causing mitotic arrest. Functional multipolar spindles were formed that allow the passage of the spindle assembly checkpoint (SAC). The cell cycle analysis and live cell imaging data of A549 cells revealed that a prolonged mitosis was followed by an abnormal (asymmetric) cell division, resulting in aneuploid cells with <2N and >2N DNA content. Interestingly, half-maximal induction of aneuploidy in A549 cells was already observed at concentrations <0.5 nM, which was approximately equivalent to the IC50 measured in

in vitro proliferation assays. Thus, induction of aneuploidy at very low concentrations is the cause for the high anti-proliferative activity of sagopilone. Obviously, the massive loss or gain of chromosomes induced growth arrest. This is consistent with the recent observation by Weaver and Cleveland that induction of aneuploidy leads to tumor growth suppression (Weaver and Cleveland, 2007). In addition, we were also able to show that these aneuploid A549 cells became senescent after long term incubation with low concentrations of sagopilone (Michael Drosch, Bayer Schering Pharma AG, unpublished results). The fate of these aneuploid cells in terms of apoptosis induction is discussed in chapter 5.6.

A different phenotype appeared to be induced at higher sagopilone concentrations (40 nM), with progressively more perturbed microtubule (MT) dynamics, formation of MT bundles and activation of the SAC leading to an arrest in mitosis. Obviously, the strong perturbation of MT dynamics at this drug concentration prevented metaphase plate arrangement of chromosomes. Finally this resulted in induction of apoptosis. Results from live cell imaging of A549 cells suggest that induction of apoptosis directly occurred from mitosis, whereas other groups have observed an exit from mitosis to G1 prior to apoptotic cell death after treatment with microtubule-stabilizing drugs (Mollinedo and Gajate, 2003).

Associated EC50 values for mitotic arrest varied among the tested cell lines, thus confirming differences in the ability to undergo mitotic arrest between cell lines after high concentration sagopilone treatment, but the maximal percentages of cells with mitotic arrest reached 70-80 % for all cell lines. Shi et al. confirmed the relatively small variation in the maximal mitotic arrest response among cell lines treated with antimitotic drugs (Shi et al., 2008).

Comparison of the cell cycle analysis of A549 cells treated with paclitaxel or sagopilone revealed a similar concentration-dependent phenotype, indicating a similar mechanism of action of these microtubule-stabilizing drugs. However, the induction of aneuploid cells after paclitaxel treatment occurred at higher concentrations compared to sagopilone. This might be due to the high affinity of sagopilone to microtubules (Hoffmann et al., 2008). The mechanism of mitotic arrest seems to be identical for both compounds as indicated by the similar EC50 calculated for mitotic arrest by sagopilone and paclitaxel in A549 cells.

5.3 Sagopilone-induced phenotypes differ in their gene expression profiles

To explore the molecular mode of action, gene expression profiles of A549 cells treated with low- and high-concentration sagopilone and paclitaxel were analyzed. Similar gene expression profiles were observed in A549 cells treated with sagopilone and paclitaxel. On the other hand, high and low concentration gene expression profiles of both compounds were considerably different. Chen and colleagues reported comparable results with paclitaxel and the naturally occurring epothilone B (Chen et al., 2003).

High concentration treatment of A549 cell with the two drugs for 18 hours revealed identical gene expression profiles. This might be due to the fact that the majority of the cells were arrested in prometaphase at that time. The observed gene expression patterns mainly showed upregulation of components of the SAC and genes involved in mitosis (Musacchio and Salmon, 2007) compared to untreated samples. To confirm mRNA expression data, it could be shown that protein levels of Cyclin B1 and BUBR1 were upregulated after high concentration treatment. This indicates that the SAC is active and that the cells have not yet undergone progression to telophase, where Cyclin B1 is degraded. BUBR1 is a component of the SAC, which prevents separation of sister chromatids until all spindle microtubules are properly attached to the kinetochores (Musacchio and Salmon, 2007). Elevated BUBR1 protein levels indicate an active SAC.

The gene expression profiles obtained from low concentration sagopilone and paclitaxel-treated A549 cells differentiate from each other. One common feature was the transactivation of p53 and corresponding upregulation of p53 target genes which occurred after low concentration treatment of both drugs, however the effect was more pronounced after sagopilone treatment. This might be due to the fact that the concentration of paclitaxel, chosen according to the maximal induction of aneuploidy, was not equivalent to that of sagopilone. In addition to the upregulation of transcriptional targets of p53, genes involved in SAC or mitosis were down regulated. The outcome of p53 transcriptional activation, e.g. up-regulation of p21 or GADD45A, mostly activates pathways involved in cell cycle arrest (Riley et al.,

2008). This allows repair processes to take place and the cells to survive. However, the gene expression profiles also revealed the FAS receptor to be upregulated and low concentration paclitaxel treatment slightly upregulated pro-apoptotic BAX. Thus, besides the cell cycle arrest pathways proapoptotic pathways are also activated. The weak apoptosis induction after low concentration sagopilone treatment in A549 cells observed using FACS analysis leads to the conclusion that cell cycle arrest pathways are the most relevant for the cellular phenotype.

5.4 How does p53 get activated in A549 cells after treatment with low concentration sagopilone?

Low concentration treatment of A549 cells with sagopilone and paclitaxel resulted in stabilization and transcriptional activation of p53. The question remains which mechanisms trigger this response?

Induction of aneuploidy by sagopilone through unequal cell division is preceded by prolonged mitosis (4.3.1). Exit from mitosis as well as duration of mitosis is controlled by the SAC (Rieder and Maiato, 2004). This control mechanism prevents the activation of the anaphase–promoting complex (APC) via various checkpoint proteins present on unattached kinetochores (Zhou et al., 2002). The presented data (4.6.1) demonstrated an accumulation of p53 in the range of 0.5 to 5 nM sagopilone, where aneuploidy was observed. Surprisingly, an accumulation of p53 was also evident at 10 nM sagopilone, where 80% of the cells were in the G2/M state (4N DNA content) after 18 hours and no aneuploid cells were observed.

This leads to the assumption that by increasing the sagopilone concentration, unequal cell division was transformed to mitotic slippage into a tetraploid G1 state without cell division, thus eliminating the aneuploid cells. This could explain the strong p53 accumulation, despite the absence of aneuploid cells at 10 nM sagopilone (4.2.1; 4.6.1). Slippage from mitosis to G1 without cell division is a strong activator of p53 thereby preventing cells from endoreduplication and further polyploidization (Lanni et al., 1998; Vogel et al., 2004). In addition, Ha et al. have demonstrated that p53 activation, in response to mitotic spindle damage, requires signaling via mitotic checkpoint kinase BUBR1 (Ha et al., 2007). This supports the idea that a sustained

activation of the SAC could activate p53. At concentrations >10 nM sagopilone the cells were arrested in mitosis without further division or mitotic slippage and died from apoptosis.

MDM2 targets p53 for degradation, thus keeping low levels of p53 (Haupt et al., 1997). During mitosis, when transcription is absent, the level of MDM2 decreases through fast degradation of the relatively short-lived MDM2 mRNA, while the translation of the long-lived p53 mRNA proceeds, thus leading to an accumulation of p53 (Blagosklonny, 2007). Through this mechanism, p53 could measure the duration of mitosis and accumulate in case of a prolonged mitosis which indicates issues to satisfy SAC function (Blagosklonny, 2006). The prolonged duration of mitosis after low concentration sagopilone treatment might be the cause for p53 accumulation (Demidenko et al., 2008).

However, 40 nM sagopilone completely inhibited cell division and caused apoptosis. Despite the fact that mitosis (which preceded apoptosis) lasted even longer than at 2.5 nM sagopilone (4.3.1), no p53 accumulation were observed. The reason for this might be that the decision to undergo apoptosis had already been made in early mitosis. 40 nM sagopilone caused DNA damage in mitosis (assessed by phosphorylation of histone H2AX), whereas 10 nM sagopilone did not induce DNA damage and accumulated p53, likely after mitotic slippage. Apparently, the onset of apoptosis inhibited accumulation of p53.

5.5 Transactivation of p53 inhibits sagopilone-induced apoptosis in A549 cells

Incubation with high concentrations of sagopilone resulted in marked induction of mitochondrial apoptosis mediated by members of the Bcl-2 family proteins and was substantially similar to that seen with paclitaxel and other epothilones (Hoffmann et al., 2008). In contrast, low concentrations sagopilone treatment only moderately induced cell death in A549 cells. The induction of several p53 target genes involved in anti-apoptotic events (e.g. p21) and absence of regulation p53 pro-apoptotic target genes (e.g. Bax or PUMA) after low concentrations sagopilone treatment indicate the anti-apoptotic side of p53 to overweigh in these conditions.

After unequal cell division or mitotic slippage the cells finally arrest in the G1 state due to a postmitotic checkpoint that is dependent on p53 (Blagosklonny, 2006). p53 mediates G1 arrest mainly by increasing protein levels of the cyclin-dependent kinase (CDK) inhibitor p21 (CDKN1A) which binds to and inhibits the activity of cyclin-CDK2 or -CDK4 complexes. This leads to dephosphorylation of the Rb (Retinoblastoma) protein, which then acts as suppressor of E2F transcription factors whose activities are essential to initiate the S phase (Sherr and Roberts, 1999). These antiproliferative effects are assisted by binding of p21 to PCNA (proliferating cell nuclear antigen) which in turn blocks DNA synthesis required for the S phase (Child and Mann, 2006).

In this work, an increase of p21 gene expression and protein levels was observed upon low concentration sagopilone treatment. There are numerous reports in the literature about the antiapoptotic function of p21. p21 protects cells from apoptosis via binding and inhibition of CDKs, which are essential for activation of the mitochondrial caspase cascade (Janicke et al., 2007). Furthermore the antiapoptotic function of p21 is determined by its subcellular localization, which depends on differential phosphorylation (Janicke et al., 2007). p21 induced by low concentration paclitaxel treatment is targeted to the cytoplasm through Akt-dependent phosphorylation (Heliez et al., 2003). Phosphorylation of p21 on threonine 145 by the survival kinase Akt results in its accumulation and translocation from the nucleus into the cytoplasm (Child and Mann, 2006). There it is exposed to different binding partners. Cytoplasmatic p21 can bind to and inactivate procaspase 3, thereby blocking FAS-mediated apoptosis (Suzuki et al., 1998; Suzuki et al., 1999). In addition, cytoplasmatic p21 inhibits the activation of the initiator caspase 8 and 10 in death receptor-induced apoptosis (Xu et al., 2000). In addition, p21 can directly bind to and inhibit the pro-apopototic kinase ASK1 (Huang et al., 2003).

The p53-dependent p21 activation was coincident with resistance to low concentration sagopilone-induced apoptosis in A549 cells. Thus, this activation might be responsible for the apoptosis resistance of A549 cells *in vitro* after treatment with low concentration sagopilone.

5.6 p53 transactivation in A549 xenograft tumors is associated with resistance to sagopilone

The absence of p21 results in enhanced chemosensitivity to DNA-damaging compounds *in vitro* (Waldman et al., 1996) and *in vivo* (Waldman et al., 1997). However, the effect of p53 or p21 on microtubule-targeting drugs remains controversial. Here it was shown that the *in vivo* A549 xenograft model only moderately responded to sagopilone. Gene expression analysis of these xenograft tumors revealed an upregulation of p53 target genes, including p21. A comparison of genes induced after single *in vivo* treatment with sagopilone (10 mg/kg) with the genes regulated by sagopilone in A549 cells showed a correlation of the *in vivo* genes with the low concentration gene expression pattern. This *in vitro* phenotype was however accompanied by resistance to sagopilone-induced apoptosis.

It has been previously shown that p53-dependent p21 induction is connected with resistance to chemotherapeutic drugs in *in vivo* tumor models. Introduction of the Bax gene which contains several strong p53 responsive elements in A2780 ovarian cell line significantly increased responsiveness to paclitaxel in xenograft mouse models through a shift from p21 induction to BAX-induced apoptosis (De Feudis et al., 2000). Wouters et al. showed that colorectal cancer xenograft tumor models deficient for p21 were more sensitive to radiation compared to their p21 proficient counterparts (Wouters et al., 1997). Heliez and colleagues have shown that upon paclitaxel treatment of RPMI-2650 cells, p21 relocates to the cytoplasm where it prevents the G1 4N arrest, enabling these cells to escape from antiproliferative effects and may increase their survival (Heliez et al., 2003). Indeed cytosolic localization of p21 in breast cancer is associated with decreased overall and relapsed-free survival (Winters et al., 2003). Higher levels of p21 have been linked with poor prognosis in breast cancer patients treated with CMF (cyclophosphamide, methotrexate and 5FU) (Yang et al., 2003). Thus, the induction of p21 might be the reason for the sagopilone resistance of A549 tumor xenografts. In addition, p53 mutated human lung carcinomas showed a better response to sagopilone compared to p53 wt lung carcinoma models in *in vivo* xenograft mouse models (Stefanie Hammer, Bayer Schering Pharma, TRG Oncology, AACR Poster, 2009).

5.7 Knock-down of p21 in A549 cells increases apoptosis after low concentration sagopilone treatment

When the G1-S checkpoint is abrogated by knock-down of p21, one explanation might be that aneuploid cells with variations in 2N DNA content are able to progress through a second cell cycle and probably die during mitosis due to improper chromosome segregation.

Another explanation could be that at 5 nM and 10 nM sagopilone where very little aneuploidy was observed, shRNA-mediated knock-down of p21 influenced cells which have slipped out of mitosis without cell division. The shRNA knock-down of p21 might then lead to a loss of the G1-S checkpoint function and induce endoreduplication to an 8N population. These cells have likely grossly deformed nuclei and die through apoptosis. Similar results were observed with other microtubule inhibitors (MTI), e.g. paclitaxel. Stewart et al. reported the occurrence of an 8 N population of HCT116 p21 -/- cells after treatment with 25 nM paclitaxel and a concentration-dependent increased sensitivity to MTI compared to their p21 proficient counterparts *in vitro* as well as in xenograft tumors (Stewart et al., 1999). Furthermore, they showed that induction of ectopic p21 protein in p53-deficient cells significantly reduced MTI-induced apoptosis (Stewart et al., 1999). Stewart and colleagues even observed an increase of apoptosis of HCT116 p21 -/- cells compared to HCT116 p21 +/+ cells at 100 nM paclitaxel (Stewart et al., 1999). Treatment with 40 or 100 nM sagopilone induced per se high rates of apoptosis. The knock-down of p21 did not further increase the rate of apoptosis after treatment with high concentration sagopilone.

The increase of apoptosis after treatment of A549 p21 knock-down cells with low concentration sagopilone compared to control cells indicates effects on aneuploid cells arisen from aberrant cell division and effect on polyploid cells with 4N DNA content emerged from mitotic slippage.

5.8 Knock-down of p53 in A549 cells increases apoptosis after low concentration sagopilone treatment

To date the role of p53 in the sensitivity of cancer cells to MTI is contested. Some groups reported no correlation between p53 status and sensitivity to paclitaxel (O'Connor et al., 1997; Fan et al., 1998). Other reported that high levels of stathmin were observed in p53 mutated cells. Overexpression of stathmin was associated with decreased polymerization of microtubules and resistance to paclitaxel in breast cancer cells (Alli et al., 2002).

On the other hand, many groups reported that cells lacking wild type p53 displayed increased sensitivity to paclitaxel (Hawkins et al., 1996; Blagosklonny and Fojo, 1999; Cassinelli et al., 2001). Additionally, transcriptionally silent p53 was associated with an increase of microtubule associated protein 4 (MAP4), which stabilized polymerized microtubules. This led to an increased binding of paclitaxel which culminated in higher sensitivity to this drug (Zhang et al., 1998). Sensitization of p53 wild type (wt) cells to low concentration paclitaxel was achieved by combination with subtoxic concentrations of cyclic pifithrin-alpha, an inhibitor of p53 transcription (Zuco et al., 2008). The same effect was observed by siRNA-mediated knock-down of p53 in H460 cells (Zuco et al., 2008).

Here it was shown that the expression knock-down of p53 reduced the p21 induction after low concentration sagopilone treatment in A549 cells. This led to G1-S checkpoint abrogation, further progression through the cell cycle and increased apoptosis after treatment with low concentration sagopilone. These effects in A549 p53 knock-down cells were mostly based on abrogation of p53-mediated transcription at low concentration of sagopilone. The levels of p53 were significantly reduced but there were still residual p53 protein levels. This could exert transcriptional dependent and more importantly transcriptional independent effects. A number of studies suggest that p53 exerts an apoptotic function in the cytosol by association with several members of the Bcl-2 family of proteins or directly at the mitochondria by facilitating the release of apoptogenic factors (Cory and Adams, 2002; Tomita et al., 2006; Wolff et al., 2008).

About half of all cancers have mutations in p53 (Soussi and Lozano, 2005). In this study, no correlation between the p53 mutational status of 8 cell lines and the apoptotic response to sagopilone treatment was observed. It is likely that p53 could be one of many factor among which determine the response to sagopilone. Shi et al. reported that the variations in the extent of apoptosis among breast cancer cells after MTI treatment (e.g. high concentration paclitaxel) could be explained by differences in the apoptotic signaling rather than by differences in mitotic arrest (Shi et al., 2008). These findings underline the importance of the apoptotic machinery and could possibly explain the differences of apoptosis induction after sagopilone treatment which overlay effects mediated by the p53 mutational status only.

The question remains whether p53 mutated cell lines could have a higher probability to respond to sagopilone. Here, a mechanism was presented that confers resistance to sagopilone. Further analysis of the p53 knock-down cells in xenograft mouse models may confirm the obtained *in vitro* data. A more comprehensive *in vivo* and *in vitro* analysis of p53 wild type and mutated cell lines and tumors may answer the question whether patients with p53 mutated tumors might benefit more from sagopilone treatment compared to patients with p53 wt tumors.

5.9 High concentration sagopilone upregulates DNA damage response genes and induces apoptosis

DNA damage repair genes were found to be upregulated after high concentration sagopilone and paclitaxel. Furthermore, H2AX phosphorylation was observed. To elucidate whether the DNA damage was mediated mechanistically by sagopilone or caused by apoptosis induced by sagopilone treatment further experiments were carried out. Pretreatment with the pan-caspase inhibitor ZVAD.fmk led to inhibition of the H2AX phosphorylation and the cleavage of PARP which suggests that the observed DNA damage is a sign of apoptosis. However, the role of the DNA repair genes remained unclear. In addition, the type of cell death in A549 cells treated with 40 nM sagopilone seemed directly to occur out of mitosis (observation from live cell imaging). Some groups also reported this kind of cells death (DeLuca et al., 2002; Burns et al., 2003) whereas others described that MTI-induced apoptosis occurred

after mitosis in G1 (Mollinedo and Gajate, 2003). However, detailed analyses of mitotic cell death are rarely found in the literature. Niikura et al. reported a mechanism of cell death during early mitosis in BUB1-deficient cells (Niikura et al., 2007). Here, this mitotic cell death was independent of caspase activation and rather depended on p73, AIF and endonuclease G (Niikura et al., 2007). We found DNA damage induced by high concentration sagopilone in A549 cells to be caspase dependent. This DNA damage was observed as early as 14 hours after drug administration. At that time most of the cells were still arrested in mitosis. The role of the DNA damage response genes, Ku70 (XRCC6) and Ku80 (XRCC5), which were upregulated after high concentration sagopilone treatment, is unclear. First indications were obtained that a functional DNA damage response plays a role in the mode of action of sagopilone (unpublished results, VTT, Technical Research Centre, Finland). Further experiments are needed to elucidate the role of DNA damage induced by sagopilone during early mitosis.

6 References

Alli, E., Bash-Babula, J., Yang, J. M. & Hait, W. N. Effect of stathmin on the sensitivity to antimicrotubule drugs in human breast cancer. *Cancer Res* **62**, 6864-9 (2002).

Anand, S., Penrhyn-Lowe, S. & Venkitaraman, A. R. AURORA-A amplification overrides the mitotic spindle assembly checkpoint, inducing resistance to Taxol. *Cancer Cell* **3**, 51-62 (2003).

Bamford, S. et al. The COSMIC (Catalogue of Somatic Mutations in Cancer) database and website. *Br J Cancer* **91**, 355-8 (2004).

Bartek, J., Iggo, R., Gannon, J. & Lane, D. P. Genetic and immunochemical analysis of mutant p53 in human breast cancer cell lines. *Oncogene* **5**, 893-9 (1990).

Bensaad, K. & Vousden, K. H. Savior and slayer: the two faces of p53. *Nat Med* **11**, 1278-9 (2005).

Berrieman, H. K., Lind, M. J. & Cawkwell, L. Do beta-tubulin mutations have a role in resistance to chemotherapy? *Lancet Oncol* **5**, 158-64 (2004).

Bhat, K. M. & Setaluri, V. Microtubule-associated proteins as targets in cancer chemotherapy. *Clin Cancer Res* **13**, 2849-54 (2007).

Blagosklonny, M. V. Prolonged mitosis versus tetraploid checkpoint: how p53 measures the duration of mitosis. *Cell Cycle* **5**, 971-5 (2006).

Blagosklonny, M. V. Mitotic arrest and cell fate: why and how mitotic inhibition of transcription drives mutually exclusive events. *Cell Cycle* **6**, 70-4 (2007).

Blagosklonny, M. V. & Fojo, T. Molecular effects of paclitaxel: myths and reality (a critical review). *Int J Cancer* **83**, 151-6 (1999).

Bollag, D. M. et al. Epothilones, a new class of microtubule-stabilizing agents with a taxol-like mechanism of action. *Cancer Res* **55**, 2325-33 (1995).

Burns, T. F., Fei, P., Scata, K. A., Dicker, D. T. & El-Deiry, W. S. Silencing of the novel p53 target gene Snk/Plk2 leads to mitotic catastrophe in paclitaxel (taxol)-exposed cells. *Mol Cell Biol* **23**, 5556-71 (2003).

Cahill, D. P. et al. Mutations of mitotic checkpoint genes in human cancers. *Nature* **392**, 300-3 (1998).

Cassinelli, G. et al. A role for loss of p53 function in sensitivity of ovarian carcinoma cells to taxanes. *Int J Cancer* **92**, 738-47 (2001).

Castedo, M. et al. Quantitation of mitochondrial alterations associated with apoptosis. *J Immunol Methods* **265**, 39-47 (2002).

Chao, C. et al. Acetylation of mouse p53 at lysine 317 negatively regulates p53 apoptotic activities after DNA damage. *Mol Cell Biol* **26**, 6859-69 (2006).

Chen, J. G. & Horwitz, S. B. Differential mitotic responses to microtubule-stabilizing and -destabilizing drugs. *Cancer Res* **62**, 1935-8 (2002).

Chen, J. G., Yang, C. P., Cammer, M. & Horwitz, S. B. Gene expression and mitotic exit induced by microtubule-stabilizing drugs. *Cancer Res* **63**, 7891-9 (2003).

Child, E. S. & Mann, D. J. The intricacies of p21 phosphorylation: protein/protein interactions, subcellular localization and stability. *Cell Cycle* **5**, 1313-9 (2006).

Concin, N. et al. Comparison of p53 mutational status with mRNA and protein expression in a panel of 24 human breast carcinoma cell lines. *Breast Cancer Res Treat* **79**, 37-46 (2003).

Cory, S. & Adams, J. M. The Bcl2 family: regulators of the cellular life-or-death switch. *Nat Rev Cancer* **2**, 647-56 (2002).

Crighton, D. et al. DRAM, a p53-induced modulator of autophagy, is critical for apoptosis. *Cell* **126**, 121-34 (2006).

Das, S., Boswell, S. A., Aaronson, S. A. & Lee, S. W. P53 promoter selection: choosing between life and death. *Cell Cycle* **7**, 154-7 (2008).

De Feudis, P. et al. Driving p53 response to Bax activation greatly enhances sensitivity to taxol by inducing massive apoptosis. *Neoplasia* **2**, 202-7 (2000).

DeLuca, J. G., Moree, B., Hickey, J. M., Kilmartin, J. V. & Salmon, E. D. hNuf2 inhibition blocks stable kinetochore-microtubule attachment and induces mitotic cell death in HeLa cells. *J Cell Biol* **159**, 549-55 (2002).

Demidenko, Z. N. et al. Mechanism of G1-like arrest by low concentrations of paclitaxel: next cell cycle p53-dependent arrest with sub G1 DNA content mediated by prolonged mitosis. *Oncogene* **27**, 4402-10 (2008).

Di Stefano, V., Soddu, S., Sacchi, A. & D'Orazi, G. HIPK2 contributes to PCAF-mediated p53 acetylation and selective transactivation of p21Waf1 after nonapoptotic DNA damage. *Oncogene* **24**, 5431-42 (2005).

Fan, S., Cherney, B., Reinhold, W., Rucker, K. & O'Connor, P. M. Disruption of p53 function in immortalized human cells does not affect survival or apoptosis after taxol or vincristine treatment. *Clin Cancer Res* **4**, 1047-54 (1998).

Forozan, F. et al. Molecular cytogenetic analysis of 11 new breast cancer cell lines. *Br J Cancer* **81**, 1328-34 (1999).

Fukasawa, K. Oncogenes and tumour suppressors take on centrosomes. *Nat Rev Cancer* **7**, 911-24 (2007).

Gan, P. P., Pasquier, E. & Kavallaris, M. Class III beta-tubulin mediates sensitivity to chemotherapeutic drugs in non small cell lung cancer. *Cancer Res* **67**, 9356-63 (2007).

Gottesman, M. M. Mechanisms of cancer drug resistance. *Annu Rev Med* **53**, 615-27 (2002).

Gu, W. & Roeder, R. G. Activation of p53 sequence-specific DNA binding by acetylation of the p53 C-terminal domain. *Cell* **90**, 595-606 (1997).

Ha, G. H. et al. p53 activation in response to mitotic spindle damage requires signaling via BubR1-mediated phosphorylation. *Cancer Res* **67**, 7155-64 (2007).

Halpain, S. & Dehmelt, L. The MAP1 family of microtubule-associated proteins. *Genome Biol* **7**, 224 (2006).

Hanahan, D. & Weinberg, R. A. The hallmarks of cancer. *Cell* **100**, 57-70 (2000).

Harrison, M. & Swanton, C. Epothilones and new analogues of the microtubule modulators in taxane-resistant disease. *Expert Opin Investig Drugs* **17**, 523-46 (2008).

Haupt, Y., Maya, R., Kazaz, A. & Oren, M. Mdm2 promotes the rapid degradation of p53. *Nature* **387**, 296-9 (1997).

Hawkins, D. S., Demers, G. W. & Galloway, D. A. Inactivation of p53 enhances sensitivity to multiple chemotherapeutic agents. *Cancer Res* **56**, 892-8 (1996).

He, L., Yang, C. P. & Horwitz, S. B. Mutations in beta-tubulin map to domains involved in regulation of microtubule stability in epothilone-resistant cell lines. *Mol Cancer Ther* **1**, 3-10 (2001).

Heliez, C., Baricault, L., Barboule, N. & Valette, A. Paclitaxel increases p21 synthesis and accumulation of its AKT-phosphorylated form in the cytoplasm of cancer cells. *Oncogene* **22**, 3260-8 (2003).

Hoffmann, J. et al. Sagopilone crosses the blood-brain barrier in vivo to inhibit brain tumor growth and metastases. *Neuro Oncol* (2008).

Hoffmann, J. et al. Improved cellular pharmacokinetics and pharmacodynamics underlie the wide anticancer activity of sagopilone. *Cancer Res* **68**, 5301-8 (2008).

Huang, S. et al. Sustained activation of the JNK cascade and rapamycin-induced apoptosis are suppressed by p53/p21(Cip1). *Mol Cell* **11**, 1491-501 (2003).

Hyman, A. A. & Karsenti, E. Morphogenetic properties of microtubules and mitotic spindle assembly. *Cell* **84**, 401-10 (1996).

Ioffe, M. L., White, E., Nelson, D. A., Dvorzhinski, D. & DiPaola, R. S. Epothilone induced cytotoxicity is dependent on p53 status in prostate cells. *Prostate* **61**, 243-7 (2004).

Janicke, R. U., Sohn, D., Essmann, F. & Schulze-Osthoff, K. The multiple battles fought by anti-apoptotic p21. *Cell Cycle* **6**, 407-13 (2007).

Janssen, K., Pohlmann, S., Janicke, R. U., Schulze-Osthoff, K. & Fischer, U. Apaf-1 and caspase-9 deficiency prevents apoptosis in a Bax-controlled pathway and promotes clonogenic survival during paclitaxel treatment. *Blood* **110**, 3662-72 (2007).

Jin, S. & Weaver, D. T. Double-strand break repair by Ku70 requires heterodimerization with Ku80 and DNA binding functions. *Embo J* **16**, 6874-85 (1997).

Kavallaris, M., Burkhart, C. A. & Horwitz, S. B. Antisense oligonucleotides to class III beta-tubulin sensitize drug-resistant cells to Taxol. *Br J Cancer* **80**, 1020-5 (1999).

Kavallaris, M. et al. Taxol-resistant epithelial ovarian tumors are associated with altered expression of specific beta-tubulin isotypes. *J Clin Invest* **100**, 1282-93 (1997).

Klar, U. et al. Total synthesis and antitumor activity of ZK-EPO: the first fully synthetic epothilone in clinical development. *Angew Chem Int Ed Engl* **45**, 7942-8 (2006).

Klar, U., Hoffmann, J. & Giurescu, M. Sagopilone (ZK-EPO): from a natural product to a fully synthetic clinical development candidate. *Expert Opin Investig Drugs* **17**, 1735-48 (2008).

Knights, C. D. et al. Distinct p53 acetylation cassettes differentially influence gene-expression patterns and cell fate. *J Cell Biol* **173**, 533-44 (2006).

Kops, G. J., Weaver, B. A. & Cleveland, D. W. On the road to cancer: aneuploidy and the mitotic checkpoint. *Nat Rev Cancer* **5**, 773-85 (2005).

Kovach, J. S. et al. Direct sequencing from touch preparations of human carcinomas: analysis of p53 mutations in breast carcinomas. *J Natl Cancer Inst* **83**, 1004-9 (1991).

Kroemer, G., Galluzzi, L. & Brenner, C. Mitochondrial membrane permeabilization in cell death. *Physiol Rev* **87**, 99-163 (2007).

Lage, H. & Dietel, M. Effect of the breast-cancer resistance protein on atypical multidrug resistance. *Lancet Oncol* **1**, 169-75 (2000).

Lage, H. & Dietel, M. Multiple mechanisms confer different drug-resistant phenotypes in pancreatic carcinoma cells. *J Cancer Res Clin Oncol* **128**, 349-57 (2002).

Lane, D. P. & Crawford, L. V. T antigen is bound to a host protein in SV40-transformed cells. *Nature* **278**, 261-3 (1979).

Lanni, J. S. & Jacks, T. Characterization of the p53-dependent postmitotic checkpoint following spindle disruption. *Mol Cell Biol* **18**, 1055-64 (1998).

Lichtner, R. B. et al. Subcellular distribution of epothilones in human tumor cells. *Proc Natl Acad Sci U S A* **98**, 11743-8 (2001).

Linzer, D. I. & Levine, A. J. Characterization of a 54K dalton cellular SV40 tumor antigen present in SV40-transformed cells and uninfected embryonal carcinoma cells. *Cell* **17**, 43-52 (1979).

Liu, L. et al. p53 sites acetylated in vitro by PCAF and p300 are acetylated in vivo in response to DNA damage. *Mol Cell Biol* **19**, 1202-9 (1999).

Maehara, Y. et al. Estrogen-receptor-negative breast cancer tissue is chemosensitive in vitro compared with estrogen-receptor-positive tissue. *Eur Surg Res* **22**, 50-5 (1990).

Makrides, V., Massie, M. R., Feinstein, S. C. & Lew, J. Evidence for two distinct binding sites for tau on microtubules. *Proc Natl Acad Sci U S A* **101**, 6746-51 (2004).

Masuda, A., Maeno, K., Nakagawa, T., Saito, H. & Takahashi, T. Association between mitotic spindle checkpoint impairment and susceptibility to the induction of apoptosis by anti-microtubule agents in human lung cancers. *Am J Pathol* **163**, 1109-16 (2003).

Matoba, S. et al. p53 regulates mitochondrial respiration. *Science* **312**, 1650-3 (2006).

McGrogan, B. T., Gilmartin, B., Carney, D. N. & McCann, A. Taxanes, microtubules and chemoresistant breast cancer. *Biochim Biophys Acta* **1785**, 96-132 (2008).

Mitsudomi, T. et al. p53 gene mutations in non-small-cell lung cancer cell lines and their correlation with the presence of ras mutations and clinical features. *Oncogene* **7**, 171-80 (1992).

Mollinedo, F. & Gajate, C. Microtubules, microtubule-interfering agents and apoptosis. *Apoptosis* **8**, 413-50 (2003).

Mozzetti, S. et al. Class III beta-tubulin overexpression is a prominent mechanism of paclitaxel resistance in ovarian cancer patients. *Clin Cancer Res* **11**, 298-305 (2005).

Murray-Zmijewski, F., Slee, E. A. & Lu, X. A complex barcode underlies the heterogeneous response of p53 to stress. *Nat Rev Mol Cell Biol* **9**, 702-12 (2008).

Musacchio, A. & Salmon, E. D. The spindle-assembly checkpoint in space and time. *Nat Rev Mol Cell Biol* **8**, 379-93 (2007).

Nettles, J. H. et al. The binding mode of epothilone A on alpha,beta-tubulin by electron crystallography. *Science* **305**, 866-9 (2004).

Nigg, E. A. Mitotic kinases as regulators of cell division and its checkpoints. *Nat Rev Mol Cell Biol* **2**, 21-32 (2001).

Nigro, J. M. et al. Mutations in the p53 gene occur in diverse human tumour types. *Nature* **342**, 705-8 (1989).

Niikura, Y., Dixit, A., Scott, R., Perkins, G. & Kitagawa, K. BUB1 mediation of caspase-independent mitotic death determines cell fate. *J Cell Biol* **178**, 283-96 (2007).

O'Connor, P. M. et al. Characterization of the p53 tumor suppressor pathway in cell lines of the National Cancer Institute anticancer drug screen and correlations with the growth-inhibitory potency of 123 anticancer agents. *Cancer Res* **57**, 4285-300 (1997).

Orr, G. A., Verdier-Pinard, P., McDaid, H. & Horwitz, S. B. Mechanisms of Taxol resistance related to microtubules. *Oncogene* **22**, 7280-95 (2003).

Panda, D., Miller, H. P., Banerjee, A., Luduena, R. F. & Wilson, L. Microtubule dynamics in vitro are regulated by the tubulin isotype composition. *Proc Natl Acad Sci U S A* **91**, 11358-62 (1994).

Penson, R. T. et al. Expression of multidrug resistance-1 protein inversely correlates with paclitaxel response and survival in ovarian cancer patients: a study in serial samples. *Gynecol Oncol* **93**, 98-106 (2004).

Pietsch, E. C., Sykes, S. M., McMahon, S. B. & Murphy, M. E. The p53 family and programmed cell death. *Oncogene* **27**, 6507-21 (2008).

Pinsky, B. A. & Biggins, S. The spindle checkpoint: tension versus attachment. *Trends Cell Biol* **15**, 486-93 (2005).

Popanda, O. & Thielmann, H. W. The function of DNA polymerases in DNA repair synthesis of ultraviolet-irradiated human fibroblasts. *Biochim Biophys Acta* **1129**, 155-60 (1992).

Pusztai, L. Markers predicting clinical benefit in breast cancer from microtubule-targeting agents. *Ann Oncol* **18 Suppl 12**, xii15-20 (2007).

Quick, Q. A. Epothilone B induces glioblastoma cell death via survivin down-regulation. *Exp Oncol* **30**, 195-201 (2008).

Reichenbach, H. & Hofle, G. Discovery and development of the epothilones : a novel class of antineoplastic drugs. *Drugs R D* **9**, 1-10 (2008).

Rieder, C. L. & Maiato, H. Stuck in division or passing through: what happens when cells cannot satisfy the spindle assembly checkpoint. *Dev Cell* **7**, 637-51 (2004).

Riley, T., Sontag, E., Chen, P. & Levine, A. Transcriptional control of human p53-regulated genes. *Nat Rev Mol Cell Biol* **9**, 402-12 (2008).

Sakaguchi, K. et al. DNA damage activates p53 through a phosphorylation-acetylation cascade. *Genes Dev* **12**, 2831-41 (1998).

Schroeder, A. et al. The RIN: an RNA integrity number for assigning integrity values to RNA measurements. *BMC Mol Biol* **7**, 3 (2006).

Sherr, C. J. & Roberts, J. M. CDK inhibitors: positive and negative regulators of G1-phase progression. *Genes Dev* **13**, 1501-12 (1999).

Shi, J., Orth, J. D. & Mitchison, T. Cell type variation in responses to antimitotic drugs that target microtubules and kinesin-5. *Cancer Res* **68**, 3269-76 (2008).

Sikic, B. I. et al. Modulation and prevention of multidrug resistance by inhibitors of P-glycoprotein. *Cancer Chemother Pharmacol* **40 Suppl**, S13-9 (1997).

Soussi, T. & Lozano, G. p53 mutation heterogeneity in cancer. *Biochem Biophys Res Commun* **331**, 834-42 (2005).

Stewart, Z. A., Mays, D. & Pietenpol, J. A. Defective G1-S cell cycle checkpoint function sensitizes cells to microtubule inhibitor-induced apoptosis. *Cancer Res* **59**, 3831-7 (1999).

Strobel, T., Kraeft, S. K., Chen, L. B. & Cannistra, S. A. BAX expression is associated with enhanced intracellular accumulation of paclitaxel: a novel role for BAX during chemotherapy-induced cell death. *Cancer Res* **58**, 4776-81 (1998).

Sudo, T., Nitta, M., Saya, H. & Ueno, N. T. Dependence of paclitaxel sensitivity on a functional spindle assembly checkpoint. *Cancer Res* **64**, 2502-8 (2004).

Sullivan, M. & Morgan, D. O. Finishing mitosis, one step at a time. *Nat Rev Mol Cell Biol* **8**, 894-903 (2007).

Suzuki, A., Tsutomi, Y., Akahane, K., Araki, T. & Miura, M. Resistance to Fas-mediated apoptosis: activation of caspase 3 is regulated by cell cycle regulator p21WAF1 and IAP gene family ILP. *Oncogene* **17**, 931-9 (1998).

Suzuki, A., Tsutomi, Y., Miura, M. & Akahane, K. Caspase 3 inactivation to suppress Fas-mediated apoptosis: identification of binding domain with p21 and ILP and inactivation machinery by p21. *Oncogene* **18**, 1239-44 (1999).

Swanton, C. et al. Regulators of mitotic arrest and ceramide metabolism are determinants of sensitivity to paclitaxel and other chemotherapeutic drugs. *Cancer Cell* **11**, 498-512 (2007).

Swanton, C., Tomlinson, I. & Downward, J. Chromosomal instability, colorectal cancer and taxane resistance. *Cell Cycle* **5**, 818-23 (2006).

Tabuchi, Y. et al. Resistance to paclitaxel therapy is related with Bcl-2 expression through an estrogen receptor mediated pathway in breast cancer. *Int J Oncol* **34**, 313-9 (2009).

Tomita, Y. et al. WT p53, but not tumor-derived mutants, bind to Bcl2 via the DNA binding domain and induce mitochondrial permeabilization. *J Biol Chem* **281**, 8600-6 (2006).

Torres, K. & Horwitz, S. B. Mechanisms of Taxol-induced cell death are concentration dependent. *Cancer Res* **58**, 3620-6 (1998).

Trivedi, M., Budihardjo, I., Loureiro, K., Reid, T. R. & Ma, J. D. Epothilones: a novel class of microtubule-stabilizing drugs for the treatment of cancer. *Future Oncol* **4**, 483-500 (2008).

Tsukamoto, F. et al. Immunohistochemical Detection of P-glycoprotein in Breast Cancer and Its Significance as a Prognostic Factor. *Breast Cancer* **4**, 259-263 (1997).

Vikhanskaya, F. et al. Inactivation of p53 in a human ovarian cancer cell line increases the sensitivity to paclitaxel by inducing G2/M arrest and apoptosis. *Exp Cell Res* **241**, 96-101 (1998).

Vogel, C., Kienitz, A., Hofmann, I., Muller, R. & Bastians, H. Crosstalk of the mitotic spindle assembly checkpoint with p53 to prevent polyploidy. *Oncogene* **23**, 6845-53 (2004).

Vousden, K. H. & Lane, D. P. p53 in health and disease. *Nat Rev Mol Cell Biol* **8**, 275-83 (2007).

Wagner, P. et al. Microtubule Associated Protein (MAP)-Tau: a novel mediator of paclitaxel sensitivity in vitro and in vivo. *Cell Cycle* **4**, 1149-52 (2005).

Waldman, T., Lengauer, C., Kinzler, K. W. & Vogelstein, B. Uncoupling of S phase and mitosis induced by anticancer agents in cells lacking p21. *Nature* **381**, 713-6 (1996).

Waldman, T. et al. Cell-cycle arrest versus cell death in cancer therapy. *Nat Med* **3**, 1034-6 (1997).

Wani, M. C., Taylor, H. L., Wall, M. E., Coggon, P. & McPhail, A. T. Plant antitumor agents. VI. The isolation and structure of taxol, a novel antileukemic and antitumor agent from Taxus brevifolia. *J Am Chem Soc* **93**, 2325-7 (1971).

Warnick, C. T., Dabbas, B., Ford, C. D. & Strait, K. A. Identification of a p53 response element in the promoter region of the hMSH2 gene required for expression in A2780 ovarian cancer cells. *J Biol Chem* **276**, 27363-70 (2001).

Weaver, B. A. & Cleveland, D. W. Aneuploidy: instigator and inhibitor of tumorigenesis. *Cancer Res* **67**, 10103-5 (2007).

Winters, Z. E., Leek, R. D., Bradburn, M. J., Norbury, C. J. & Harris, A. L. Cytoplasmic p21WAF1/CIP1 expression is correlated with HER-2/ neu in breast cancer and is an independent predictor of prognosis. *Breast Cancer Res* **5**, R242-9 (2003).

Wolff, S., Erster, S., Palacios, G. & Moll, U. M. p53's mitochondrial translocation and MOMP action is independent of Puma and Bax and severely disrupts mitochondrial membrane integrity. *Cell Res* **18**, 733-44 (2008).

Wouters, B. G., Giaccia, A. J., Denko, N. C. & Brown, J. M. Loss of p21Waf1/Cip1 sensitizes tumors to radiation by an apoptosis-independent mechanism. *Cancer Res* **57**, 4703-6 (1997).

Xu, S. Q. & El-Deiry, W. S. p21(WAF1/CIP1) inhibits initiator caspase cleavage by TRAIL death receptor DR4. *Biochem Biophys Res Commun* **269**, 179-90 (2000).

Yabuki, N. et al. Gene amplification and expression in lung cancer cells with acquired paclitaxel resistance. *Cancer Genet Cytogenet* **173**, 1-9 (2007).

Yang, C. P. et al. A highly epothilone B-resistant A549 cell line with mutations in tubulin that confer drug dependence. *Mol Cancer Ther* **4**, 987-95 (2005).

Yang, W. et al. ErbB2 overexpression in human breast carcinoma is correlated with p21Cip1 up-regulation and tyrosine-15 hyperphosphorylation of p34Cdc2: poor responsiveness to chemotherapy with cyclophoshamide methotrexate, and 5-fluorouracil is associated with Erb2 overexpression and with p21Cip1 overexpression. *Cancer* **98**, 1123-30 (2003).

Yeh, J. J., Hsu, W. H., Wang, J. J., Ho, S. T. & Kao, A. Predicting chemotherapy response to paclitaxel-based therapy in advanced non-small-cell lung cancer with P-glycoprotein expression. *Respiration* **70**, 32-5 (2003).

Yoon, D. S. et al. Variable levels of chromosomal instability and mitotic spindle checkpoint defects in breast cancer. *Am J Pathol* **161**, 391-7 (2002).

Zhang, C. C. et al. The role of MAP4 expression in the sensitivity to paclitaxel and resistance to vinca alkaloids in p53 mutant cells. *Oncogene* **16**, 1617-24 (1998).

Zhivotovsky, B. & Kroemer, G. Apoptosis and genomic instability. *Nat Rev Mol Cell Biol* **5**, 752-62 (2004).

Zhou, J., Yao, J. & Joshi, H. C. Attachment and tension in the spindle assembly checkpoint. *J Cell Sci* **115**, 3547-55 (2002).

Zuco, V. & Zunino, F. Cyclic pifithrin-alpha sensitizes wild type p53 tumor cells to antimicrotubule agent-induced apoptosis. *Neoplasia* **10**, 587-96 (2008).

7 List of Publications

Parts of this thesis were already published or presented.

Publications:

Improved cellular pharmacokinetics and pharmacodynamics underlie the wide anticancer activity of sagopilone.
Hoffmann, J., Vitale, I., Buchmann, B., Galluzzi, L., Schwede, W., Senovilla, L., Skuballa, W., Vivet, S., Lichtner, R. B., Vicencio, J. M., Panaretakis, T., Siemeister, G., Lage, H., Nanty, L., Hammer, S., Mittelstaedt, K., **Winsel, S.**, Eschenbrenner, J., Castedo, M., Demarche, C., Klar, U., and Kroemer, G.; Cancer Res, *68:* 5301-5308, 2008.

Sagopilone (ZK-EPO), a novel epothilone, induces cell cycle arrest and apoptosis, leading to tumor growth inhibition in multiple breast cancer models.
S Winsel, J Eschenbrenner, S Hammer, K Mittelstaedt, U Klar, C Sachse, M Hannus, M Seidel, B Weiss, C Merz, G Siemeister, J Hoffmann; (rejected by Cancer Research; currently under review by Molecular Cancer Therapeutics)**.**

Molecular Mode of Action and Mechanisms of Resistances of Sagopilone.
S Winsel, S Hammer, A Sommer, K Mittelstaedt, U Klar, B Buchman, W Schwede, G Siemeister, J Hoffmann; (Manuscript in preparation)**.**

Poster:

Translational oncology research results strongly support the clinical evaluation of the novel epothilone sagopilone (ZK-EPO) in breast cancer.
Sebastian Winsel, Stefanie Hammer, Kevin Mittelstaedt, Bernd Buchmann, Wolfgang Schwede, Iduna Fichtner, Werner Skuballa, Gerhard Siemeister, Ulrich Klar, Jens Hoffmann. Poster presented at the 97th Annual Meeting of the American Association for Cancer Research (AACR), April 14-18, 2007, Los Angeles, California, USA.

Subcellular distribution and cellular activity of the novel epothilone sagopilone (ZK-EPO).
S Winsel, S Hammer, J Eschenbrenner, K Mittelstaedt, B Buchmann, W Schwede, W Skuballa, U Klar, J Hoffmann. Poster presented at ECCO 14 – the European Cancer Conference. 23-27 September 2007, Barcelona, Spain.

Comparative antitumor activity and mode of action of the third-generation epothilone sagopilone (ZK-EPO) in chemoresistant tumors
S.Winsel, S. Hammer, K. Mittelstaedt, W. Schwede, W. Skuballa, G.Siemeister, U. Klar, J. Hoffmann. Poster presented at 14th International AEK Cancer Congress, 28.2.-2.3.2007 in Frankfurt/ Main, Germany.

Abbreviations

AACR	American Association for Cancer Research
ABC	ATP-binding cassette
BCA	Bicinchoninic acid
BSA	Bovine serum albumin
cDNA	Complementary deoxyribonucleic acid
CIN	Chromosomal instability
CO2	Carbon dioxide
DMEM	Dulbecco's Modified Eagle Medium
DMSO	Dimethyl sulfoxide
DNA	Deoxyribonucleic acid
DNase	Deoxyribonuclease
EC50	Half-maximal effective concentration
ECL	Enhanced chemoluminescence
EDTA	Ethylenediaminetetraacetic acid
ER	Estrogen receptor
FACS	Fluorescence-activated cell sorting
FBS	Fetal bovine serum
FDA	Food and Drug Administration, USA
GTP	Guanosine triphosphate
HATs	Histone acetyltransferases
HPRT	Hypoxanthine-guanine phosphoribosyltransferase
IC50	Half-maximal inhibitory concentration
MAPs	Microtubule associated proteins
MDR	Multi drug resistance
MIT	Microtubule inhibitors
MW	Molecular weight
NGS	Normal goat serum
PBS	Phosphate-buffered saline
PCR	Polymerase chain reaction
PI	Propidium iodide
PVDF	Polyvinylidene fluoride
qRT-PCR	Quantitative real time polymerase chain reaction
RNA	Ribonucleic acid
RNase	Ribonuclease
RPMI	Royal Park Memorial Institute
RT-PCR	Reverse transcription polymerase chain reaction
SAC	Spindle assembly checkpoint
SDS	Sodium dodecyl sulfate
shRNA	Short hairpin RNA
t	Time
U	Unit
UKCCCR	United Kingdom Coordinating Committee for Cancer Research
WHO	World Health Organization
ZVAD.fmk	Carbobenzoxy-valyl-alanyl-aspartyl-[O-methyl]- fluoromethylketone
γH2AX	Phosphorylated form of Histone 2AX

Acknowledgements

I am especially grateful to Dr. Jens Hoffmann for providing me a great opportunity to conduct my doctoral research in this company and for his constant guidance and support. Also I would like to thank Dr. Stefanie Hammer for her help. She was always available for scientific discussions and helped me with many time-saving tips. Many thanks for her very valuable comments on my thesis.

My further acknowledgements go to Dr. Bernard Heandler, who supervised my thesis as first referee and provided very helpful criticism on my thesis. Moreover, I would like to thank Prof. Dr. Petra Knaus for her willingness to coach me in her function as university professor from FU Berlin.

I also wish to thank Dr. Stefan Prechtl and Kevin Mittelstaedt for their help and advice on live cell imaging and immunofluorescence microscopy. I thank Dr. Florian Prinz and Dr. Ulrike Ulbricht for the help with lenti virus production.

I thank all my colleagues and especially the PhD students from BSP for having such a pleasant time in the company.

A big “Thank you!” goes to my parents and my sister Kirstin for their constant encouragement and support.

Thanks go also to Paymann Harirchian for correcting my thesis.